hexagon:2611.00651v1

Towards a conformal field theory of critical percolation. II. Scalar responses and null identities

Alberto Gandolfi[1,2]

[1]Division of Science, New York University Abu Dhabi,
PO Box 129188, Abu Dhabi, United Arab Emirates.

[2]NYUAD Center for Interdisciplinary Data Science & AI (CIDSAI),
NYUAD Research Institute, New York University Abu Dhabi,
PO Box 129188, Abu Dhabi, UAE.

Email: ag189@nyu.edu

17 November 2026

Abstract

We construct the scalar response to closing a small disk in critical site percolation on the triangular lattice. The response records how the obstacle changes every connection at a surrounding boundary. Its normalized cutoff error is of order $r^{11/15}$, and an open-cutset argument gives its leading fusion with the density field in the complete-record norm. We identify the signed response in a domain with six alternating boundary tips and prove the level-two null identities against finite separated density, scalar, and stress insertions. These identities determine the mixed scalar–density four-point function. Assuming Camia and Feng's asymptotic formula for one energy and two density insertions, we give their energy field a geometric interpretation as the normalized response to closing a small disk. The resulting correlation of two energies and two densities is the difference of a successive-bottleneck and an alternative-route contribution, and it changes sign. The second coefficient in the angularly averaged scalar–density collision defines a nonzero insertion Ψ of weights $(77/96, 77/96)$. Fixed stress contours and radial integrals give joint correlations of every fixed finite collection of separated Ψ insertions, with error $O_{\mathcal{D}'}(\sum_i r_i^{1/2})$ at arbitrary relative extraction radii. We compute its two-point coefficient and signed two-obstacle connection asymptotics, including the leading stress term when the scalar sources collide in a two-density correlation. These results realize the known analytic conformal blocks through specified lattice observables. The construction uses the complete-record stress estimates and finite-hole density correlations of Paper I.

Status of this version. This is a preliminary preprint. The detailed verification of the mathematical arguments and their dependencies is ongoing and is not yet complete. The manuscript is being made public to make the arguments available for scrutiny and discussion while this verification continues. Its mathematical claims should therefore be regarded as provisional.

Contents

1 Introduction **1**

2 Previous results **2**
2.1 Density correlations and percolation estimates . . . 2
2.2 The inputs from Paper I . . . 3
2.3 Analytic blocks and related field constructions . . . 3

3 Outline of the results **3**

4 Framework and main results **5**
4.1 Lattice model, domains, and density normalization . . . 5
4.2 Records, parity, and completion . . . 6
4.3 Stress insertions and the testing convention . . . 7
4.4 The scalar prescription . . . 8
4.5 Scalar rows and the correlation class . . . 8
4.6 Scalar construction and leading fusion . . . 9
4.7 Finite-tip response and null identities . . . 10
4.8 The scalar–density four-point function . . . 11
4.9 Identification with the microscopic energy . . . 12
4.10 The subleading field and its joint separated insertions . . . 13

5 Construction of the scalar response **14**
5.1 A positive quad estimate and its retained-pair summation . . . 15
5.2 From finitely many tips to the microscopic frontier . . . 16
5.3 Arbitrary finite joint insertions . . . 18
5.4 Conformal covariance and pointwise two-root correlations . . . 19
5.5 The Ward hierarchy with both stress chiralities . . . 20
5.6 The probability-weighted four-tip calibration . . . 21
5.7 The positive plane calibration . . . 22

6 Leading scalar–density fusion **23**
6.1 Odd survival is an increasing event . . . 23
6.2 A sampled open cutset screens the full partition . . . 24
6.3 Survival probabilities and signed projection . . . 26
6.4 The local scalar–density response . . . 26
6.5 Calibration at the fixed outgoing cut . . . 27

7 Identification of the six-tip signed response **28**
7.1 Finite-tip covariance and stopped exploration . . . 28
7.2 The finite surgery quotient . . . 37
7.3 Screening integrals and their differential identities . . . 37
7.4 A uniform estimate and the collision boundary data . . . 40
7.5 The differential equation for the response . . . 43
7.6 Killed uniqueness on the circular chamber . . . 44

8 The Ward identity in a marked domain **47**
8.1 Joint sources in a marked domain . . . 47
8.2 The angular source and an exact reflected map . . . 49
8.3 Transport of the scalar response . . . 50
8.4 The doubled boundary Ward operator . . . 51

9 Localization of the null identity **53**

10 The disk response and the energy field **56**
10.1 Local response and pivotality . . . 56
10.2 The microscopic pair and its annular contributions . . . 57
10.3 Comparison in a quad . . . 58
10.4 The complete outgoing record . . . 60
10.5 Logarithmic averaging and normalization . . . 61
10.6 Signed connection events . . . 62
10.7 Null identities and density fusion . . . 63

11 The mixed four-point function **64**
11.1 The differential equation for the response . . . 64
11.2 From the weak equation to conformal blocks . . . 65
11.3 The connection matrix . . . 65

12 The second odd fusion coefficient **66**
12.1 Continuity of the collision family . . . 66
12.2 A distributional Euler lemma . . . 67
12.3 The two null equations and their first angular modes . . . 68
12.4 Extraction of the scalar second coefficient . . . 69
12.5 Conformal covariance of the extracted insertion . . . 69

13 Joint construction of separated subleading insertions **71**
13.1 Local integral representatives and their topology . . . 71
13.2 Replacing the exterior Ward operator by a local contour . . . 72
13.3 A bounded representative for the first angular mode . . . 73
13.4 The coefficient representation and a uniform tail . . . 74
13.5 The local expression space and its completion . . . 76
13.6 A tensor estimate . . . 77
13.7 Joint extraction . . . 78
13.8 Covariance and Ward identities of the joint fields . . . 79
13.9 Removing the known quadratic descendant . . . 82

14 Nonvanishing and low-point normalizations **82**
14.1 A finite-point detector for the extracted field . . . 82
14.2 The two-point normalization from two disjoint collisions . . . 83
14.3 The scalar vacuum channel . . . 85
14.4 Two scalar sources approach the stress channel . . . 85

15 Two-point connections and two small obstacles **87**
15.1 The one-obstacle comparison . . . 87
15.2 The signed two-obstacle observable . . . 88
15.3 An explicit subleading connection asymptotic . . . 89

16 Conclusions **90**

A Leading projection of three density marks **91**

B A Monte Carlo comparison **93**
B.1 A comparison independent of normalization . . . 93
B.2 Sampling and results . . . 93

Use of generative AI **95**

1 Introduction

An open percolation cluster offers many routes between distant points. A small hole can usually be bypassed, but sometimes it closes the only passage that keeps two points connected. Shrinking the hole turns this sensitivity into a local observable. A pair of holes asks a further question: are the two obstructions successive bottlenecks, or can each be bypassed only by using the other route? The signed difference between these possibilities is one of the connection probabilities computed below.

We study the scalar response produced by closing a circular disk, together with the fields obtained when that disk approaches a density mark. Paper I constructs the directional response measured by a rotating ellipse and identifies it with the bulk stress tensor [29]. Here the circular source leads to a scalar field of dimension $5/4$. We construct its correlations, prove its null identities, and identify a nonzero subleading field in its fusion with the density. The formal definitions and precise statements begin in Section 4.

The first step is to keep the full information needed to complete a local experiment: which boundary sites are open, which are connected, and how the marked clusters meet them. A small disk changes this record by a signed measure. We prove convergence of the normalized measure, uniformly under bounded exterior completion. An open connected cutset then screens the interior of a cluster carrying an odd number of density marks. This gives the leading scalar–density fusion and the leading projection of three nearby density insertions.

The next step identifies a differential equation for these observables. In a domain with six alternating boundary tips, there are five possible partitions of the three open arcs. We determine all five components of the scalar response by following an interface together with the response in the domain it leaves behind. When two neighboring tips merge, a short boundary cap reduces the response to the calibrated four-tip experiment. We prove this convergence uniformly away from further tip collisions, and use the resulting boundary values in a killed-diffusion uniqueness argument. The geometric stress variation then gives a second-order cancellation. A protected exploration and an eight-arm estimate extend that cancellation to arbitrary finite separated spectators, yielding the null identities that determine the mixed four-point function.

Our scalar response also gives a geometric interpretation of the energy field defined by Camia and Feng [27]. Their construction starts from a product of two nearby cluster signs with its mean subtracted. Ours measures how distant connections change when a small disk is closed. Assuming their asymptotic formula for the correlation of one energy with two densities [27, (1.9)], Theorem 4.9 shows that these two constructions give the same field after a constant rescaling. The three-point formula fixes this constant. Within the class of correlations constructed here, either prescription can then be used at any fixed finite collection of distinct locations, together with density, scalar, and stress insertions.

To compare the two definitions, we separate configurations according to the annular scale at which the two nearby marks first join. Four-arm estimates give a common bound for these contributions, and the logarithmic normalization averages over the scales. Section 10 compares each contribution with the disk response while keeping its small four-arm probability and every outgoing connection. This local comparison gives the equality of correlations and connects the disk response with logarithmic density fusion, as described by Camia and Feng's four-point asymptotic [26, Theorem 1.1, (1.9)].

For the correlation of two energies with two densities, the disk interpretation separates two geometric contributions. Two source regions can form successive bottlenecks, or they can provide alternative routes for the same connection. The former contribution is positive and the latter negative. Our four-point formula includes both terms and changes sign; Section 10.6

compares it with the expression in [27, (3.37)], which contains only the first.

Finally, bring a scalar source toward a density mark and average over the direction of approach. After the leading density contribution is subtracted, the next scalar term has relative order $r^{3/2}$. Its coefficient defines the field Ψ. Local integral representations control this extraction uniformly when other, disjoint pairs also shrink. They yield every fixed finite collection of separated plane Ψ insertions, together with their Möbius covariance, Ward identities, and two-point normalization.

The distinction between the two estimates reflects their uses. The leading fusion is controlled against every bounded test of the complete outgoing record. The subleading construction is controlled after smooth testing in the source coordinates. Theorem 4.11 gives the latter topology and its quantitative error. The explicit low-point formulas also have pointwise continuous representatives, as stated in Theorem 4.8 and Proposition 14.1.

The four-point formula also describes two scalar obstacles approaching one another while the density marks remain distant. Its constant term cancels. The first surviving terms distinguish the direction of approach and agree, with an explicit coefficient, with the stress correlations $\langle T\Phi\Phi\rangle$ and $\langle \bar{T}\Phi\Phi\rangle$. Section 14.4 makes this comparison with the zero-central-charge structure of Paper I [29, Section 2.5].

Section 2 places these results in the literature, and Section 3 describes the proof. Section 4 introduces the formal framework and states the main results. Sections 5–6 construct the scalar response and its leading fusion. Sections 7–9 establish the finite-tip response and the null identities. Section 10 identifies the normalized energy insertion with the disk scalar. The four-point calculation in Section 11 leads to the extraction and joint construction in Sections 12–13. Sections 14–15 give the normalization and connection formulas. Appendix A gives the leading projection of three nearby density marks. Appendix B reports a finite-lattice comparison with the two-obstacle formula.

2 Previous results

2.1 Density correlations and percolation estimates

Density correlations encode the connections between marked points. In Camia's construction, each open cluster receives an independent symmetric sign; averaging products of the signs selects configurations in which every marked cluster contains an even number of marks [1, Section 1.2, (1.8)–(1.11), and Theorem 1.5]. The resulting conformally covariant field has scaling dimension $5/48$. We use the normalization in which its plane two-point function has coefficient one; it is fixed in Section 4.1.

The full percolation scaling limit and local convergence of exploration paths to SLE_6 are due to Camia and Newman [2, 3]. One-arm ratios, quasi-multiplicativity, and polychromatic arm exponents control the connection events used below [4, 5, 7]. Zhan's two-curve Green theorem gives the positive small-disk asymptotic for a selected pair of SLE_6 curves, with relative error exponent $11/15$ [12, Theorem 1.1, (1.1)–(1.3)]. Section 5 transfers this estimate to the complete signed connectivity response.

The coupling behind the leading fusion is related to the open-circuit arguments in Camia [1, Lemma 2.1] and the connected-cutset construction of Hillairet [10, Lemmas 2.1–2.3 and Section 2.5]. The extension needed here keeps the parity of every marked component and all its unmarked outgoing connections. It also keeps the survival probabilities when a signed local response is propagated through an annulus.

2.2 The inputs from Paper I

Paper I supplies the complete-record boundary-strip estimate, protected exploration, and angular stabilization used to construct the stress tensor [29, Theorems 4.3, 8.4, and 9.1]. Its finite-hole density theorem provides the fixed-radius mesh limits and the bounded exterior completions [29, Theorem 10.1 and Sections 15–16]. The holomorphic stress hierarchy and local contour operations are given in [29, Theorem 17.1 and Appendix A.3].

We use these statements on their specified record spaces and domain classes. Section 4 recalls the conventions needed here and explains how parity labels enter the completion. Section 5 then proves the scalar extension and the Ward hierarchy containing both stress chiralities. All locators for Paper I refer to the version of 15 November 2026, cited in the bibliography.

2.3 Analytic blocks and related field constructions

The screening integrals used for the six-tip calculation appear in the Coulomb-gas formulas of Flores, Kleban and Ziff [15, Section 3.1.3, (53), (55)–(56)]. We use their analytic form and prove its identification with the complete signed disk response in Section 7. The weight 77/96 occurs in the one-cluster spectrum of Jacobsen and Saleur [21, (77)], following an earlier occurrence in the candidate spectrum of Picco, Ribault and Santachiara [20, (2.7)]. The subsequent development of that spectrum is described in [21, 22]. The mixed conformal blocks and their fusing coefficients appear in [22, Section 4.1.1] and [23, Appendix A.1]. Our four-point calculation fixes their normalization for the disk-deletion observable.

Camia and Feng construct an energy field from a centered product of neighboring cluster signs and a logarithmic partner from a mesoscopic density pair [27, (1.8), (1.15), and (1.18)–(1.26)]. Theorem 4.9 uses their single-energy three-point asymptotic [27, (1.9)] to calibrate a comparison of the complete local records. The probabilistic inputs are the four-arm coupling and strong separation of Garban, Pete and Schramm [7, Proposition 3.1 and Lemma 3.3], and the sharp arm bounds of Du, Gao, Li and Zhuang [8, Theorems 1.2–1.3]. The resulting identification connects a local geometric response with the scalar appearing in logarithmic density fusion. The pivotal interpretation of such responses is also central to near-critical percolation [7, 9].

Dubédat's boundary-SLE fusion arguments give a related use of null equations and regularity to identify collision coefficients [28, Sections 4–5].

The probabilistic development of Liouville conformal field theory provides a useful comparison. Kupiainen, Rhodes and Vargas establish Ward identities, second-order BPZ equations, and a degenerate four-point formula under their stated charge restrictions [31, arXiv version, Theorems 2.1–2.3]. Baverez and Wu identify irreducible quotient modules and the vanishing of singular descendants for negative Kac charges [32, Theorem 1.2 and (1.6)]. In the present setting the vanishing identity is proved through finite-tip percolation responses and localization. Guillarmou, Kupiainen, Rhodes and Vargas subsequently establish a convergent four-point bootstrap and crossing symmetry for Liouville theory [33, Theorem 1.1 and Corollary 1.2]. This suggests further questions about compatible overlapping fusions and complete field expansions for percolation.

3 Outline of the results

A local obstacle can be studied from outside a surrounding circle. The information crossing that circle is the common thread of the construction. The following outline is informal;

Section 4 gives the definitions, hypotheses, and topologies.

From a disk to a scalar field. Closing a disk changes the law of the outgoing connections. Dividing this change by the 5/4 power of the radius produces a Cauchy family, with error exponent 11/15. The estimate survives any bounded completion of the surrounding configuration. It therefore gives joint scalar, density, and stress correlations at separated points. The same construction determines a positive scalar–two-density amplitude.

From an odd cluster to the leading fusion. An open connected cutset makes all surviving inner connections join the same outer cluster. When the inner marks have odd total parity, that cluster carries one effective odd mark. A coupling makes this screening uniform over the inner record. Applying it to a nearby scalar and density gives the leading density term; applying it to three nearby densities gives a symmetric coefficient depending on their fixed shape.

From six tips to a local null identity. Six boundary tips retain enough information to identify the scalar response and its stress variation. The five partition components are expressed by six screening integrals and a finite linear map. A stopped exploration identifies the solution of the differential equations. Configurations with more surviving tips are controlled by an eight-arm estimate, which makes their contribution to the second-order null combination vanish after localization.

From the microscopic energy to the disk response. The centered cluster-sign pair splits into first-connection events at dyadic scales and a remainder with two outgoing odd components. Four-arm estimates make the normalized remainder vanish. A coupling compares each centered annular source with the same binary connection response in a quad, uniformly over its boundary faces. Protected exploration extends this comparison to the full outgoing record. Averaging over scales leaves one coefficient, which the assumed one-energy/two-density limit fixes. This yields the joint identification with the disk scalar.

From the second coefficient to joint insertions. The null equations determine the mixed four-point function and govern the angular modes of a scalar–density collision. The second scalar coefficient defines Ψ, with conformal weights $(77/96, 77/96)$. A contour representation and two radial inverses give a local expression whose remainder is bounded after source testing. Combining these expressions in disjoint regions proves joint convergence at arbitrary relative extraction radii. The four-point function then supplies both a nonzero mixed correlation and the two-point normalization of Ψ.

Connection probabilities. For two small obstacles, inclusion–exclusion gives the probability of two successive bottlenecks minus the probability of two alternative routes. The corresponding normalized response is the mixed four-point function. Bringing one endpoint toward an obstacle reveals the same nonzero term of relative order $r^{3/2}$. Bringing the two obstacles toward each other instead reveals the directional response measured by the stress tensor.

4 Framework and main results

We now specify the local experiments and the information retained when they are joined. Each source is enclosed by a fixed region. Sampling the remaining percolation configuration then combines the sources through their boundary records.

4.1 Lattice model, domains, and density normalization

Work with critical site percolation on the triangular lattice of mesh $a > 0$, identifying a site with its hexagonal cell. Each sampled cell is independently open or closed with probability $1/2$. For a planar set K, its inner-cell approximation K^a consists of the cells contained in K. Forcing K closed means closing precisely those cells and retaining the sampled colors elsewhere. These are the conventions of [29, Section 4.1]. A marked point is represented by its nearest lattice site, with ties resolved by the real and then imaginary coordinate.

Unless a domain is indicated, correlations are in the plane. The finite-hole domains used below have the form

$$U = D_0 \setminus \bigcup_{j=1}^{m} K_j,$$

where D_0 is the plane or a bounded simply connected domain with analytic Jordan boundary, and the K_j are pairwise disjoint compact Jordan bodies with analytic boundaries, contained in D_0. Their cells and the cells outside D_0^a are forced closed. Distinct insertions have disjoint fixed source neighborhoods inside the domain before their own regulator holes are forced. These neighborhoods remain separated from the background boundary components, and density marks lie outside the unmarked source neighborhoods. At fixed positive hole sizes, uniform geometric estimates use a fixed number of marks and holes, positive lower bounds on their separations, and the analytic boundary charts and tubular neighborhoods of [29, Sections 4.1 and 10]. The exterior completion bound of [29, Theorem 10.1(iii)] is uniform as regulator holes shrink inside their fixed source neighborhoods. An admissible conformal map between these domains extends holomorphically across every analytic boundary component with nonzero derivative. At infinity we use the coordinate $1/z$ and the spherical convention of [29, Section 10]; connections are still made by finite lattice paths.

Conditional on the percolation colors, give each open cluster an independent sign taking the values $+1$ and -1 with equal probability. Let $S_a(z)$ be that sign at the marked site, and zero if the site is closed. Put

$$\pi_a = \mathbb{P}_a(0 \leftrightarrow \partial B_1(0)), \qquad \Phi_a(z) = c_\Phi \pi_a^{-1} S_a(z),$$

where $c_\Phi > 0$ is the fixed normalization for which the continuum density insertion satisfies

$$\langle \Phi(u)\Phi(v)\rangle = |u - v|^{-2x}, \qquad x = \frac{5}{48}, \quad h_\Phi = \bar{h}_\Phi = \frac{5}{96}. \tag{4.1}$$

For distinct marks, the density correlation in U is

$$\left\langle \prod_{i=1}^{n} \Phi_U(z_i) \right\rangle = \lim_{a \downarrow 0} \mathbb{E}_U^a \prod_{i=1}^{n} \Phi_a(z_i),$$

where $\mathbb{E}_U^a$ averages both the colors and the cluster signs. The cluster-sign construction and existence of these density correlations in simply connected domains are given in [1, Section 1.2, (1.8)–(1.11), and Theorem 1.5]; their finite-hole extension is [29, Theorem 10.1]. Signs are assigned independently to the clusters of each forced configuration. Averaging the signs gives

one precisely when all marked sites are open and each resulting cluster contains an even number of marks, and zero otherwise.

We write $\alpha_1^a(s,d)$ for the probability of an open arm across the annulus with radii $s<d$, and $\alpha_j^a(s,d)$ for j disjoint alternating arms when $j\geq 2$ is even. A polychromatic arm pattern is a fixed sequence containing both colors; it need not alternate. We also use the corresponding polychromatic upper bounds for such patterns. At fixed positive radii, $\alpha_j(s,d)$ denotes the continuum probability. Fixed changes of the annular radii are absorbed in the constants. The arm events, their separation estimates, and quasi-multiplicativity are used as in [7, Section 2.1 and Appendix A]; the exponents are those of [4, 5]. The Russo–Seymour–Welsh (RSW) crossing bounds are used in the form specified in [29, proof of Lemma 7.3].

4.2 Records, parity, and completion

For a fixed source region D, its frontier is the set of cells of D^a adjacent to the complement. A complete frontier record lists the color of every frontier cell, the partition of the open frontier cells according to their connections inside D^a, and the parity of the number of density marks in each open class. A frontier cell used as the endpoint of a connection is called a port. A record is realizable if it is produced by a coloring and the specified marks in the sampled region. Fixed connections supplied by an adjoining region are called its wiring. All labels are retained when regions are combined.

For a marked region, a coloring has zero weight if any marked site is closed or if an open cluster confined to the interior contains an odd number of marks. Otherwise we retain the frontier record and the parities of its open classes; each interior even class contributes one. With n density marks, the normalized marked row multiplies these weights by $(c_\Phi/\pi_a)^n$.

A row is a finite complex measure on this finite record space. If its masses are $m(s)$, its variation norm is

$$\|m\|_{\mathrm{var}}=\sum_s |m(s)| = \sup_{|F|\leq 1} |m(F)|.$$

Joining regions takes the equivalence relation generated by their open connections and adds the parities modulo two. A component that ceases to meet the outgoing frontier contributes zero if its parity is odd; an even component is erased. These rules follow directly from the cluster-sign average above. A complete exterior filling imposes even parity on every final marked cluster.

For fixed exterior data, this operation maps each local record either to one completed record or to zero. Averaging over exterior colors gives a substochastic completion kernel. Its row sums are at most one, so it contracts the variation norm. This is the completion convention of [29, Sections 4.1, 9.2, and 10], with the parity labels just specified.

Lemma 4.1 (Parity and local source bounds)**.** *An unmarked source row can be combined with any fixed realizable marked exterior record without increasing its variation norm. More generally, the row obtained by gluing finitely many disjoint marked or unmarked source regions has variation norm at most the product of their row norms. A normalized density root in a disk of radius d has row norm at most Cd^{-x} after the mesh limit.*

Proof. For a fixed marked exterior record, joining partitions and adding parities is a deterministic map, with an odd disappearing class sent to zero. The triangle inequality proves contraction. For several regions, independent local fillings give the tensor product of the local rows; its variation norm is the product of their variation norms. Exterior completion contracts this product. In a disk containing one density root, a surviving row requires an open connection from that root to the frontier. Its mass is $c_\Phi \pi_a^{-1}\mathbb{P}_a(z^a \leftrightarrow \partial B_d(z))$. The

one-arm ratio [1, (2.1)] bounds its mesh limit by Cd^{-x}. Marked composite regions are formed by this gluing procedure from disjoint root disks and unmarked source disks. □

For a common fixed cut D of scale d, a family $m = (m^a)$ of rows has upper seminorm

$$\|m\|_{D,*} = \limsup_{a \downarrow 0} \|m^a\|_{\mathrm{var}}.$$

We identify families whose difference has zero seminorm and take the Banach completion, as in [29, Section 9.2, (9.5)]. The notation $\|\cdot\|_{d,*}$ suppresses the fixed cut. When uniformity over frontier occupations is stated, the supremum over those words is taken inside the mesh upper limit. Fixed realizable exterior wirings and parities are then attached by contraction. At each fixed separated configuration, scalar and stress radii are removed in this completed space using the Cauchy estimates and finite gluing proved in Section 5; normalized density rows are mesh families in the same space. Only after these local source limits are formed do collision radii vary. A bound stated before the source limit means its mesh upper limit followed by the upper limit over the indicated positive source radii. Every difference is formed at the same mesh and on the same labeled record space.

Lemma 4.2 (A common transcript for protected sources)**.** *Fix a closed protecting disk inside a source region and perform the exploration of [29, Section 8.1], which reveals cells only outside that disk. Its transcript is the ordered record of revealed colors, traced interface segments, labels, and connections. For any collection of forced sets contained in the protecting disk, the transcript is the same. Conditional on it, the unrevealed cells have their independent fair law before forcing. The original frontier record is recovered by a common completion map of variation norm at most one.*

Proof. Each exploration decision uses only previously revealed colors outside the protecting disk. Replaying a feasible transcript fixes the revealed colors. Product independence gives the conditional law of every unrevealed cell. Joining the remaining partition to the connections stored in the transcript recovers the original record. Contraction follows from the triangle inequality, as in [29, Lemma 8.1]. Thus the same exploration applies to circles as well as to the ellipses used there. □

4.3 Stress insertions and the testing convention

The local strip estimates use strictly convex Jordan bodies with real-analytic boundary. After rescaling by the target size, their inner and outer radii are uniformly comparable, their normal neighborhoods are uniformly injective, and their analytic boundary charts have derivatives bounded above and away from zero. We call these *controlled analytic targets*; the precise bounds are those of [29, Section 4.1 and Theorem 4.3]. Disks, fixed-shape ellipses, and their sufficiently small holomorphic deformations satisfy these bounds.

Fix an ellipse parameter $0 < e < 1$. Let $K_{r,e,\phi}(w)$ have center w, semiaxes $r(1+e)$ and $r(1-e)$, and orientation ϕ. With $N_a(K)$ denoting the number of cells in K^a, the holomorphic stress regulator is

$$\tau_{a,r,e}(w) = \frac{1}{2\pi e r^2} \int_0^{2\pi} e^{-2i\phi}\, 2^{N_a(K_{r,e,\phi}(w))} \mathbf{1}_{\{K_{r,e,\phi}(w)^a \text{ closed}\}}\, d\phi.$$

This is precisely [29, (4.8)]; e is its semiaxis parameter. The limits of its correlations define T in [29, Theorem 17.1]. We use the complex-conjugate regulator for $\bar{T}$. The completed-row estimates are [29, Theorem 9.1]. Section 5 proves the joint extension containing both

chiralities and the scalar source introduced next. At a source cut of scale d, the angular row has norm at most Cd^{-2}, and its normalized Cauchy error at radius s is at most $Cd^{-2}(s/d)^{1/4}$.

A finite separated word is a product of finitely many specified insertions at pairwise distinct centers, with fixed disjoint source neighborhoods. A spectator word is such a product outside the region being studied. A local source or a product contained in one such region will also be called a local insertion. Brackets denote the joint limit of the corresponding regulated expectation, in the order specified below and in the relevant theorem.

The weights $(h, \bar{h})$ of a primary insertion mean that under an admissible conformal map f its correlation transforms with the factor $f'(z)^h \overline{f'(z)}^{\bar{h}}$ in that slot. For scalar weights this is $|f'(z)|^{2h}$. Stress and density weights are $(2, 0)$, $(0, 2)$, and $(5/96, 5/96)$, respectively. The Ward sums displayed below are plane identities. Finite-tip domains have the boundary variation terms derived in Section 8.

We use Wirtinger derivatives: for $z = u + iv$, $\partial_z = (\partial_u - i\partial_v)/2$ and $\partial_{\bar{z}} = (\partial_u + i\partial_v)/2$. Source derivatives in correlation identities are understood distributionally.

When needed, correlations are distributions in the original source coordinates. On a compact separated configuration set, the notation $F_r = O_{\mathcal{D}'}(r^\alpha)$ means that there are $C < \infty$ and an integer M such that

$$|\langle F_r, \psi \rangle| \le C r^\alpha \max_{|\beta| \le M} \|\partial^\beta \psi\|_\infty$$

for every smooth test supported there. Derivatives use the real coordinates of all tested sources. The constants and test order may depend on the fixed word and compact set. For joint auxiliary parameters we use the same finite seminorm after smooth testing in those parameters; the required uniformity is established in the proofs. This is the weak-transport convention of [29, Lemma 17.2].

4.4 The scalar prescription

Let $N_a(r, z)$ count the cells in $B_r(z)^a$, and define

$$H^a_{B_r(z)} = 2^{N_a(r,z)} \mathbf{1}_{\{B_r(z)^a \text{ is closed}\}}, \qquad E^\circ_{a,r}(z) = r^{-y}(1 - H^a_{B_r(z)}), \qquad y = \frac{5}{4}. \tag{4.2}$$

For any integrable regulated observable Y_a, with all other source supports disjoint from the disk,

$$\mathbb{E}[E^\circ_{a,r}(z) Y_a] = r^{-y}\{\mathbb{E}[Y_a] - \mathbb{E}_{\mathbb{C}\setminus B_r(z)}[Y_a]\}. \tag{4.3}$$

For a general target K, the notation H^a_K denotes the same forcing weight $2^{N_a(K)} \mathbf{1}_{\{K^a \text{ closed}\}}$. The second expectation in (4.3) uses the same exterior product law with every cell of $B_r(z)^a$ forced closed. Conditioning proves the identity at each mesh. We write E° for the continuum insertion constructed from these regulators in Theorem 4.3; its joint correlations are established in Theorem 4.4.

The mesh is removed first at fixed positive source radii. These radii then tend to zero with separated centers. A collision of centers is taken subsequently. In the endpoint asymptotic, both obstacle radii are removed at each fixed endpoint separation before that separation tends to zero.

4.5 Scalar rows and the correlation class

Let D be a fixed source disk containing no density marks. Write $\nu_0^{a,D}$ and $\nu_{B_r}^{a,D}$ for its outgoing record laws, respectively before and after forcing $B_r(z)$ closed. The cut has scale d, and z

stays a fixed positive fraction of d from it. Define

$$R_r^{a,D} = r^{-y}(\nu_0^{a,D} - \nu_{B_r}^{a,D}). \tag{4.4}$$

For a controlled analytic target K inside D, use $\nu_K^{a,D}$ for the same record law with K^a closed. For two such targets of size r separated by normal displacement δ, Paper I gives

$$\|\nu_{K'} - \nu_K\|_{d,*} \le C\alpha_4(Cr,d)\,\delta/r, \tag{4.5}$$
$$\|\nu_{B_r} - \nu_\varnothing\|_{d,*} \le C\alpha_4(Cr,d). \tag{4.6}$$

Here the notation suppresses the common cut D and the mesh-family superscript; the seminorm is that of Section 4.2. These are [29, Theorem 4.3, (4.1), and (4.6)]. The arm estimate is $\alpha_4(r,d) \le C_p(r/d)^p$ for each $p < 5/4$ [5, 7].

The term *physical row* refers to the response defined by this lattice prescription. Below we call it the scalar row. The norm is the completed-record norm of Section 4.2. Let

$$\mathscr{C}_0 = \{\text{finite separated words in } \Phi, E^\circ, T, \bar{T}\}. \tag{4.7}$$

Theorem 4.4 constructs the correlations of this class. For a fixed word, its normalized exterior completion is bounded after the independent arms from its density roots have been extracted, by Lemma 4.1 and [29, Theorem 10.1(iii)].

A *local packet* is a finite linear combination of products from $\mathscr{C}_0$ inside one source region, evaluated on the same outgoing record. When a packet contains a subtraction, its terms are kept together in variation-norm estimates.

4.6 Scalar construction and leading fusion

Theorem 4.3 (Scalar completed-record construction)**.** *For a source whose distance from its outgoing cut is comparable with d, the rows (4.4) satisfy*

$$\|E^\circ\|_{d,*} \le Cd^{-y}, \qquad \sup_{0<r\le\epsilon} \limsup_{a\downarrow 0} \|R_r^{a,D} - R_\epsilon^{a,D}\|_{\mathrm{var}} \le Cd^{-y}(\epsilon/d)^{11/15}. \tag{4.8}$$

For $R/2 \le r \le R$ the unnormalized signed scaling defect obeys

$$\limsup_{a\downarrow 0} \left\|(\nu_{B_r}^{a,D} - \nu_0^{a,D}) - (r/R)^y(\nu_{B_R}^{a,D} - \nu_0^{a,D})\right\|_{\mathrm{var}} \le C(R/d)^{119/60}. \tag{4.9}$$

The estimates are uniform over frontier occupations in this unmarked source region, with every frontier label retained. Fixed realizable exterior wirings and parity labels are attached by the completion of Lemma 4.1; the bounds hold after every common bounded exterior completion.

The exponent $11/15$ comes from Zhan's positive two-curve estimate [12, Theorem 1.1, (1.1)–(1.3)]. Section 5 transfers that estimate to the signed complete record by summing over the interface pairs and applying protected exploration.

Theorem 4.4 (Finite joint scalar, density, and stress correlations)**.** *Every finite separated word in $\mathscr{C}_0$ has a joint plane correlation after the mesh limit and arbitrary relative source-radius limits. The scalar and density slots are primary, with weights $(5/8,5/8)$ and $(5/96,5/96)$. The stress slots have weights $(2,0)$ and $(0,2)$. If $Y = \prod_j X_j(z_j)$ is such a word, the separated Ward identities are*

$$\langle T(w)Y\rangle = \sum_j \left\{ \frac{h_j}{(w-z_j)^2} + \frac{1}{w-z_j}\partial_{z_j} \right\} \langle Y\rangle, \tag{4.10}$$
$$\langle \bar{T}(w)Y\rangle = \sum_j \left\{ \frac{\bar{h}_j}{(\bar{w}-\bar{z}_j)^2} + \frac{1}{\bar{w}-\bar{z}_j}\partial_{\bar{z}_j} \right\} \langle Y\rangle.$$

The identities have central charge zero and hold in the stated distribution topology. Words with exactly two density roots and any finite number of the other sources also have pointwise continuous representatives at every separated configuration. In particular,

$$\langle E^{\circ}(z)\Phi(u)\Phi(v)\rangle = C_{\circ}\frac{|u-v|^{y-2x}}{|z-u|^{y}|z-v|^{y}}, \qquad C_{\circ}>0. \tag{4.11}$$

Section 5 derives this theorem from Theorem 4.3 and the finite-hole and stress framework of [29], including mixed $T,\bar{T}$ words and the pointwise two-root extension. Conformal covariance fixes the three-point form; the disk response calibrates its positive amplitude.

Theorem 4.5 (Leading mixed fusion in the complete record)**.** *For every $0<\gamma<x$, uniformly in the collision angle and for $r \ll d$,*

$$\|r^{y}E^{\circ}(z)\Phi(z+re^{i\theta}) - C_{\circ}\Phi(z)\|_{d,*} \le Cd^{-x}(r/d)^{\gamma}. \tag{4.12}$$

The outgoing record retains all even connections and all odd parity marks. The coefficient is the constant in (4.11)*.*

Section 6 proves this theorem by odd-parity screening and a bounded remote detector at the completion cut.

The same screening argument gives a symmetric leading coefficient for three nearby density marks. Proposition A.1, in Appendix A, states the complete-record estimate and its far-density calibration.

4.7 Finite-tip response and null identities

A finite-tip domain is a simply connected proper subdomain of $\mathbb{C}$ with finitely many cyclically ordered marked boundary prime ends and alternating open and closed boundary arcs. Its lattice approximations, separate slit banks, and marked Carathéodory convergence are those of [29, Sections 7.1–7.2 and 8.4]. A quad has four such tips. A link pattern is the noncrossing pairing of tips made by its boundary-to-boundary interfaces. We write $\mathbb{D}$ for the unit disk and $\mathbb{H}$ for the upper half-plane.

The positive constant c_E is the coefficient of the probability-weighted four-tip scalar response; its precise calibration is given in Section 5.6, equation (5.24). The plane amplitude $C_{\circ}$ is fixed by (4.11). In the unit disk, the four-tip coefficient is $c_E G_{4,\mathbb{D}}$, where

$$G_{4,\mathbb{D}}(0;\theta_1,\dots,\theta_4) = \prod_{j<k\le 4}|e^{i\theta_j}-e^{i\theta_k}|^{1/3}. \tag{4.13}$$

It multiplies the difference of the connected and separated open-arc partition states; the selecting crossing probability is included. Section 5.6 derives this formula from Cardy's formula, [12, Theorem 1.1], and [29, Lemma 6.1].

Theorem 4.6 (The signed six-tip response)**.** *In a simply connected domain with six alternating boundary tips, the scalar response is a signed row on the five partitions of its three open arcs. If a conformal map $f: D\to\mathbb{D}$ sends the source z to 0, that row is*

$$R_D(z) = |f'(z)|^{5/4}\, c_E V M^{+} K. \tag{4.14}$$

Here V and M are the finite partition maps defined in Section 7.2, M^{+} is the inverse on the complement of its kernel defined there, and K is the vector of six screening integrals in (7.14)*, evaluated at the image tips. The equality holds in every partition coordinate and after every common bounded exterior completion. The normalized row is bounded uniformly over the boundary-tip positions. Its locally uniform simple-pair limits are the corresponding four-tip responses described in Lemma 7.7.*

Section 7 gives the formulas and proves their identification with the disk response. The analytic integrals specialize [15, Section 3.1.3, (53), (55)–(56)].

For the next statement, $L_{-1}E^\circ = \partial_z E^\circ$ and $L_{-2}E^\circ$ is the contour insertion

$$\langle (L_{-2}E^\circ)(z)Y\rangle = \frac{1}{2\pi i}\oint_\Gamma \frac{\langle T(w)E^\circ(z)Y\rangle}{w-z}\,dw, \tag{4.15}$$

where the positively oriented fixed contour encloses the scalar source patch and excludes the spectator sources. The antiholomorphic descendant is defined by conjugation. These are source-coordinate distributions, using the joint Ward construction proved in Section 5 and the local contour convention of Paper I [29, Appendix A.3].

The level-two null operation and its conjugate are

$$\mathcal{N}_z E^\circ(z) = (L_{-2}E^\circ)(z) - \frac{2}{3}\partial_z^2 E^\circ(z), \qquad \mathcal{N}_{\bar z}E^\circ(z) = (\bar L_{-2}E^\circ)(z) - \frac{2}{3}\partial_{\bar z}^2 E^\circ(z). \tag{4.16}$$

Theorem 4.7 (The common-spectator null identity)**.** *For every $Y \in \mathscr{C}_0$ separated from z,*

$$\langle \mathcal{N}_z E^\circ(z)Y\rangle = 0, \qquad \langle \mathcal{N}_{\bar z}E^\circ(z)Y\rangle = 0. \tag{4.17}$$

The identities hold for the stress descendants in the source-coordinate distribution topology.

The proof combines Theorem 4.6, the reflected stress variation and eight-arm localization. The formal singular vector is classical [18].

The finite-boundary identities will also be used separately: Propositions 8.2 and 8.3 prove the Ward and level-two identities coordinatewise on the four- and six-tip boundary partitions. A common bounded exterior completion preserves these identities. Localization then gives the bulk theorem in source distributions.

4.8 The scalar–density four-point function

For the connectivity interpretation, let $p_a(u,v)$ be the probability that two lattice approximations to u, v are in the same open cluster, and let $p_a^K(u,v)$ be the probability that an open path between them exists outside K. With the arguments suppressed in the numerator, define

$$\mathcal{I}(z,w;u,v) = \lim_{\epsilon,\delta\downarrow 0}\lim_{a\downarrow 0}\frac{p_a - p_a^{B_\epsilon(z)} - p_a^{B_\delta(w)} + p_a^{B_\epsilon(z)\cup B_\delta(w)}}{p_a \epsilon^{5/4}\delta^{5/4}}. \tag{4.18}$$

The two terms in this signed inclusion–exclusion response count successive bottlenecks and alternative routes, as described in Section 15. Set

$$\eta = \frac{(z-v)(u-w)}{(z-w)(u-v)}. \tag{4.19}$$

$$\mathfrak{k} = \frac{5}{12}\left[\frac{\Gamma(1/4)}{\Gamma(3/4)}\right]^2. \tag{4.20}$$

Here Γ is the gamma function [25, 5.2.1]. The constant $\mathfrak{k}$ is fixed by the normalization of the blocks below; its evaluation follows from the Gauss connection formula in Section 11 [25, 15.10.21].

Theorem 4.8 (The mixed four-point function and two-hole response)**.** *Let*

$$F(\eta,\bar\eta) = \langle E^\circ(\infty)\Phi(1)E^\circ(\eta)\Phi(0)\rangle. \tag{4.21}$$

The field at infinity is defined in a regular spherical chart. Then

$$F(\eta,\bar\eta)=C_\circ^2(|f_0(\eta)|^2-\mathfrak{k}^2|f_1(\eta)|^2), \tag{4.22}$$

where

$$\begin{aligned} f_0(\eta)&=[\eta(1-\eta)]^{-5/8}{}_2F_1\left(-\frac{5}{4},\frac{3}{4};\frac{1}{4};\eta\right),\\ f_1(\eta)&=[\eta(1-\eta)]^{-5/8}\eta^{3/4}{}_2F_1\left(-\frac{1}{2},\frac{3}{2};\frac{7}{4};\eta\right). \end{aligned} \tag{4.23}$$

The Gauss function ${}_2F_1$ is defined by its power series and analytic continuation as in [25, 15.2.1]. The branches are fixed on $0<\eta<1$ and then continued together. For separated z,w,u,v, the limit (4.18) exists pointwise and equals $|z-w|^{-5/2}F(\eta,\bar\eta)$ with (4.19). After the mesh limit, the expression inside the outer limit in (4.18) differs from $\mathcal{I}$ by $O(\epsilon^{11/15}+\delta^{11/15})$ on fixed separated configurations, with geometry-dependent constants.

The null equation reduces the correlation to a hypergeometric equation. Leading fusion fixes the first coefficient, and single-valuedness fixes the second. The rate of convergence of the disk response is the exponent in Theorem 4.3.

4.9 Identification with the microscopic energy

The disk prescription measures how a local obstruction changes the exterior connections. The microscopic energy begins with two nearby density marks. The following comparison identifies the information that the two sources send to a fixed surrounding cut.

For $0<a<1$, choose a lattice site $z^a\to z$ and the two sites z^a-a, z^a+a. Write $p_\infty=\mathbb{P}_a(z^a-a\leftrightarrow z^a+a)$ for their full-plane connection probability. Translation and scaling of the lattice make this constant independent of z^a and a. The Camia–Feng regulator is

$$\phi_a(z^a)=\frac{S_a(z^a-a)S_a(z^a+a)-p_\infty}{a^y|\log a|},\qquad y=\frac{5}{4}, \tag{4.24}$$

as in [27, (1.8), (1.15)]. In a fixed source disk $D=B_d(z)$ containing these two marks, let σ_a^D be the outgoing row of the two unnormalized cluster signs. With the record and parity rules of Section 4.2, the row of (4.24) is

$$\mathsf{L}_a^D=\frac{\sigma_a^D-p_\infty\nu_0^{a,D}}{a^y|\log a|}. \tag{4.25}$$

The unmarked row $\nu_0^{a,D}$ is viewed on the same record space with zero parity on every open class. The comparison disk $B_\rho(z^a)$ has the same lattice center as the pair. At fixed ρ, the strip estimate (4.5) identifies its mesh limit with that of the disk centered at z.

In our density normalization, the one-energy/two-density asymptotic of [27, (1.9)] reads

$$\lim_{a\downarrow0}\mathbb{E}[\phi_a(z^a)\Phi_a(u^a)\Phi_a(v^a)]=c_\Phi^2C_2\frac{|u-v|^{y-2x}}{|z-u|^y|z-v|^y},\qquad C_2>0, \tag{4.26}$$

for distinct z,u,v. Here C_2 is their three-point coefficient and c_Φ is the density normalization from Section 4.1; in the notation of [27, (1.6)], $c_\Phi=C_1^{-1/4}$. The proof of (1.9) in [27, Section 3.1] is completed at (3.9), using Lemma 3.1, before the multi-energy argument and independently of its Step 3.

Theorem 4.9 (Identification of the energy insertion)**.** *Assume the one-energy/two-density asymptotic* (4.26) *from [27, (1.9)]. For every fixed source disk D, the microscopic energy row and the disk row satisfy*

$$\lim_{\rho\downarrow 0}\limsup_{a\downarrow 0}\left\|\mathsf{L}_a^D-\frac{c_\Phi^2C_2}{C_\circ}R_\rho^{a,D}\right\|_{\mathrm{var}}=0. \tag{4.27}$$

The comparison is uniform over frontier occupations and is preserved by every common bounded exterior completion.

Let ϕ denote the normalized energy insertion obtained by multiplying each regulator (4.24) *by $C_\circ/(c_\Phi^2C_2)$. For every fixed finite collection of separated energy sources and every spectator word $Y\in\mathscr{C}_0$ outside their source disks, its joint correlations exist and satisfy*

$$\left\langle\prod_{i=1}^m\phi(z_i)Y\right\rangle=\left\langle\prod_{i=1}^m E^\circ(z_i)Y\right\rangle. \tag{4.28}$$

The limits use the mesh and source-radius order and the source-distribution convention of Section 4.3.

Section 10 proves the comparison by localizing the sign pair into annular first-connection events, comparing their centered responses with a disk in a quad, and then completing the full outgoing record. The asymptotic (4.26) fixes the one remaining scalar coefficient. In particular, the matched normalization gives

$$\langle\phi(z)\Phi(u)\Phi(v)\rangle=\langle E^\circ(z)\Phi(u)\Phi(v)\rangle. \tag{4.29}$$

Theorem 4.9 therefore connects the local geometric response with the energy insertion from logarithmic density fusion. Its joint form transfers the null identities and mixed four-point function to this normalized energy throughout the stated class.

4.10 The subleading field and its joint separated insertions

Theorem 4.10 (One nonzero subleading odd insertion)**.** *There is a correlation insertion Ψ at one new source, against the entire class $\mathscr{C}_0$, such that for every $0<\gamma<5/48$,*

$$\begin{aligned}A_r(z)&:=\frac{r^y}{2\pi}\int_0^{2\pi}E^\circ(z)\Phi(z+re^{i\theta})\,d\theta\\&=C_\circ\Phi(z)+r^{3/2}\Psi(z)+25C_\circ r^2\partial_z\partial_{\bar z}\Phi(z)+O_{\mathcal{D}'}(r^{2+\gamma}).\end{aligned} \tag{4.30}$$

The limit defining Ψ exists through all positive radii. Its plane correlations are Möbius covariant with weights

$$h_\Psi=\bar h_\Psi=\frac{77}{96}. \tag{4.31}$$

Its separated stress action is the corresponding primary Ward action. Moreover,

$$\langle\Psi(z)E^\circ(w)\Phi(u)\rangle=-\mathfrak{k}^2C_\circ^2\frac{|w-u|^{1/4}}{|z-w|^{11/4}|z-u|^{11/24}}, \tag{4.32}$$

so Ψ is not the zero insertion.

The weight occurs in the one-cluster spectrum [21, (77)]. The coefficient agrees with the fusing data in [23, (A.3)–(A.5)], with the scalar normalization fixed by the disk response.

Theorem 4.11 (Joint construction of finitely many subleading insertions)**.** *With A_r as in (4.30), define*

$$Q_r(z) = r^{-3/2}[A_r(z) - C_\circ \Phi(z)]. \tag{4.33}$$

For every fixed $m < \infty$ and $Y \in \mathscr{C}_0$, with disjoint collision regions and all spectator sources separated, the joint limit

$$\left\langle \prod_{i=1}^{m} \Psi(z_i) Y \right\rangle = \lim_{r_1,\dots,r_m \downarrow 0} \left\langle \prod_{i=1}^{m} Q_{r_i}(z_i) Y \right\rangle \tag{4.34}$$

exists in source distributions, at arbitrary relative rates of the positive radii. On every compact separated configuration set,

$$\left\langle \prod_{i=1}^{m} Q_{r_i}(z_i) Y \right\rangle = \left\langle \prod_{i=1}^{m} \Psi(z_i) Y \right\rangle + O_{\mathcal{D}'}\left(\sum_{i=1}^{m} r_i^{1/2} \right). \tag{4.35}$$

The mesh and all scalar, density, and stress source regulators are removed at each fixed positive collision-radius tuple before this joint limit. The result agrees with the one-slot insertion, is symmetric in the new slots, is independent of auxiliary source regions, contours, radial averaging windows, and integral approximations, and agrees with every iterated limit of these disjoint collisions. Constants and test seminorms may depend on m, Y, and the compact separation geometry.

For every $0 < \gamma < 5/48$, the descendant-subtracted regulators

$$\widehat{Q}_r(z) = Q_r(z) - 25 C_\circ r^{1/2} \partial_z \partial_{\bar{z}} \Phi(z) \tag{4.36}$$

give the same joint limit with error $O_{\mathcal{D}'}(\sum_i r_i^{1/2+\gamma})$.

Section 13 uses a fixed stress contour and two Euler inverses to obtain a bounded local representative after source testing, with an integrable tail. Gluing disjoint regions then proves the joint theorem. The inputs are the leading complete-record estimate and the null identity on $\mathscr{C}_0$.

Write

$$\mathscr{C}_1 = \{\text{finite separated words in } \Phi, E^\circ, T, \bar{T}, \Psi\}. \tag{4.37}$$

Corollary 13.5, in Section 13.8, gives its Möbius covariance, Ward identities, scalar null identities, and parity rule. The two-point normalization is proved in Proposition 14.1; the endpoint connection asymptotic is Corollary 15.3.

5 Construction of the scalar response

A shrinking disk changes a distant connection only when it blocks an essential passage. We compare the full connection record before and after closing the disk, and then attach the other observations outside a fixed cut. This gives the scalar response and its joint correlations in Theorems 4.3 and 4.4. The geometric inputs are the retained-pair surgery, count-weighted arm bound and protected exploration of [29, Sections 7–9]. The positive local asymptotic is Zhan's two-curve Green theorem [12, Theorem 1.1].

Write

$$y = \frac{5}{4}, \qquad \beta = \frac{11}{15}, \qquad \lambda = y + \beta = \frac{119}{60}. \tag{5.1}$$

For a common lattice cut $D = B(c, d)$ and a source z a fixed positive fraction of d from its boundary, let $\nu_K^{a,D}$ be the law of the outgoing record when K is forced closed. Every frontier

occupation and every identification of open frontier vertices is retained. For the scalar source set

$$R_r^{a,D} = r^{-y}(\nu_{\varnothing}^{a,D} - \nu_{B_r(z)}^{a,D}). \tag{5.2}$$

The variation norm is the full sum of absolute masses. All comparisons below use the same finite-mesh record space, followed by the mesh-first upper limits specified in Section 4. The forcing identity is (4.3); complete records and the norm-one action of exterior completion are defined as in [29, Sections 4.1, 8.1, and 9.2].

5.1 A positive quad estimate and its retained-pair summation

In a simply connected conditional quad Ω, let $H_\Omega(r)$ be the probability, under its normalized two-SLE$_6$ law, that both selected curves meet $B_r(z)$. Put $S = \operatorname{dist}(z, \partial\Omega)$. Zhan's theorem gives

$$H_\Omega(r) = c_* \mathcal{G}_\Omega(z) r^y \left\{1 + O((r/S)^\beta)\right\}, \qquad c_* > 0, \tag{5.3}$$

with an error constant independent of the four marked prime ends. Choose a fixed sufficiently small $c_0 > 0$. If $\ell \le S < 2\ell$ and $r < c_0\ell/2$, then, uniformly in $b \in [1/2, 1]$,

$$\left|H_\Omega(r) - b^{-y} H_\Omega(br)\right| \le C(r/\ell)^\lambda H_\Omega(c_0\ell). \tag{5.4}$$

Indeed, the two leading terms in (5.3) cancel. The remainder is at most $C\mathcal{G}_\Omega(z) r^y (r/\ell)^\beta$, whereas the same positive asymptotic, at the fixed fraction $c_0\ell$, gives $H_\Omega(c_0\ell) \ge c\mathcal{G}_\Omega(z)\ell^y$. Equation (5.3), including its uniform relative error, is [12, Theorem 1.1, (1.1)–(1.3)] at $\kappa = 6$. Equation (5.4) follows by an unnormalized comparable-scale comparison of these positive quantities.

Begin with a fixed finite family of alternating boundary arcs. Write α for the link pattern of the boundary-to-boundary interfaces, p_α for its probability, and s_α for the associated open boundary partition. If a connected target meets exactly two boundary chords i, j, deletion changes the partition to a deterministic $s_{\alpha,ij}$. Set

$$J_{\alpha,ij} = \delta_{s_\alpha} - \delta_{s_{\alpha,ij}}, \qquad \|J_{\alpha,ij}\|_{\mathrm{var}} \le 2.$$

A target meeting at most one boundary chord changes no boundary partition. Interior loops carry no outer labels. These facts identify the whole partition change. The finite planar surgery is proved in [29, Lemma 7.1 and Section 7.1]. Its sign agrees with the unforced-minus-deleted prescription (5.2).

Use one common buffer radius $R_0 \in [Mr, 2Mr]$, with M a fixed large constant, for both B_r and B_{br}. Conditional on α, retain the marginal $\mu_{\alpha,ij}$ of all interfaces other than i, j. If the selected pair lies in one complementary component containing z, its conditional law is the normalized two-SLE$_6$ law in the resulting quad Ω_{ij}; otherwise its contribution is zero. Set $S_{ij} = \operatorname{dist}(z, \partial\Omega_{ij})$. If N_R denotes the number of original boundary chords meeting $B_R(z)$, the surgery identity gives

$$\begin{aligned} D_{r,b}^D &:= (\nu_{\varnothing}^D - \nu_{B_r}^D) - b^{-y}(\nu_{\varnothing}^D - \nu_{B_{br}}^D) \\ &= \sum_\alpha p_\alpha \sum_{i<j} J_{\alpha,ij} \int \mathbf{1}_{\{S_{ij} > R_0\}} [H_{\Omega_{ij}}(r) - b^{-y} H_{\Omega_{ij}}(br)]\, d\mu_{\alpha,ij} + \mathcal{E}_{r,b}, \end{aligned} \tag{5.5}$$

$$\|\mathcal{E}_{r,b}\|_{\mathrm{var}} \le C\mathbb{P}(N_{R_0} \ge 3). \tag{5.6}$$

Here the continuum expression initially refers only to finitely many marked arcs and their finite partition space. At the lattice level the same decomposition is made before taking the

limit. When at most two chords enter the buffer, there is at most one selected pair that can change the record. When three or more enter, the exceptional contribution is bounded by the probability in (5.6). The pattern probabilities p_α and retained marginals $\mu_{\alpha,ij}$ weight every term. The conditional pair law and weighted decomposition are constructed in [29, Lemmas 7.3–7.4 and Section 7.2], using the multiple-SLE resampling of [13]. Here the scalar coefficients $1, -b^{-y}$ replace the angular coefficients.

Consider a dyadic shell $\ell \le S_{ij} < 2\ell$ with $2\ell < cd$. Another retained boundary chord then comes within 2ℓ of z. If the two selected chords both hit $B_{c_0\ell}(z)$, at least three original chords hit $B_{2\ell}(z)$. Conditional expectation followed by summation over the original weights gives

$$\sum_\alpha p_\alpha \sum_{i<j} \int \mathbf{1}_{\{\ell \le S_{ij} < 2\ell\}} H_{\Omega_{ij}}(c_0\ell)\, d\mu_{\alpha,ij} \le \mathbb{E}[N_{2\ell}^2 \mathbf{1}_{\{N_{2\ell}\ge 3\}}] \le C_\eta (\ell/d)^{35/12-\eta}. \tag{5.7}$$

The final inequality is the count-weighted six-arm estimate. It combines the ordinary six-arm bound with the exponential tail for the number of traversing chords. It is taken in the unconditioned law, so its constant does not depend on α or the number of initial boundary arcs. For the macroscopic shell the corresponding second moment is bounded by a constant. The count estimate is [29, Lemma 7.5 and Section 7.3]. Its exponent $35/12$ is from [5, Theorem 4]; the RSW and separated-arm inputs are discussed in [7]. Applying the tower identity preserves all connections in the record.

Applying (5.4) inside (5.5) and using (5.7) bounds a shell by

$$C_\eta (r/\ell)^{119/60} (\ell/d)^{35/12-\eta} = C_\eta (r/d)^{119/60} (\ell/d)^{14/15-\eta}. \tag{5.8}$$

Choose $0 < \eta < 14/15$. The dyadic shell sum is finite, with a constant independent of its number of shells. The macroscopic shell contributes $C(r/d)^{119/60}$, and the buffer error has the higher power $35/12 - \eta$. This proves the finite-marked-boundary version of the defect estimate. Here absolute values are taken after the probability-weighted decomposition, so the positive conditional bound controls the signed row.

5.2 From finitely many tips to the microscopic frontier

Protect $B_R(z)$, with R a fixed small fraction of d, and run the source-independent exploration of [29, Theorem 8.4 and Section 8]. Since it queries no site in the protecting disk, the transcript has the same law for the unforced experiment and for both deleted disks. The remaining source component contains $B_{R-O(a)}(z)$ and has alternating active tips. A deterministic completion of norm at most one restores every original frontier label and every outer identification.

Restrict first to transcripts with at most M_0 active tips and separation at least δ, keeping $r, R, M_0, \delta > 0$ fixed. The continuity needed to pass the finite-boundary estimate to these transcripts concerns curves and targets in the protected interior. The passage to the limit uses the following continuity properties.

Take any sequence of meshes tending to zero and of such transcript values, allowing also the comparison factors $b \in [1/2, 1]$ to vary. Translate the source to zero. By [29, Lemma 8.3 and Theorem 8.4(iii)], a subsequence has a fixed number and cyclic order of tips, a limiting factor b, and marked Carathéodory convergence to a domain containing $B_R(0)$. The limiting prime ends are distinct. The conditional color law in each domain is the ordinary percolation law with these alternating boundary colors. Therefore [29, Theorem 7.2, Lemma 7.3, and Proposition 8.5] give convergence of its labelled interface tuple in disk coordinates, together with its link-pattern labels.

To pass the buffer tests to the limit, choose $L < R/2$ larger than all buffer radii. If f_n and f are the normalized disk maps, the functions

$$\min\{L, |f_n^{-1}(\zeta)|\}, \qquad \min\{L, |f^{-1}(\zeta)|\},$$

extended by L to the unit circle, converge uniformly on the closed disk. Indeed, their nonconstant parts lie in a common compact subset of the disk, since the source domains contain $B_{R/2}(0)$, and the inverse maps converge locally uniformly there. The minimum of a continuous function along a curve is continuous in the uniform curve metric modulo reparametrization. There are finitely many limiting curves, so choose the buffer radius outside the countable union of atoms of their minimum-distance laws. The buffer-avoidance indicators and buffer counts then converge jointly. This buffer may be chosen for the limiting law of the sequence; the estimates above are uniform throughout its allowed fixed-factor range.

The disks B_r and B_{br} have positive radii at this stage. The maps and their derivatives converge on a neighborhood of them; their images, including the lattice-cell error, lie between arbitrarily close smooth offsets of the limiting targets. For a selected pair, convergence of the full labelled tuple brackets the lattice probability of buffer avoidance and two target contacts between the corresponding limiting probabilities for an inner and an outer offset. Inner hits have a positive margin and survive small curve perturbations; limits of lattice contacts lie in every outer offset. The buffer indicator converges by the preceding minimum-distance argument.

To make these two bounds agree, fix a contributing tuple of the other curves with $S_{ij} > R_0$. Its selected pair has the two-SLE law in Ω_{ij}, and its crossing probability $p_{\mathrm{cr},\Omega_{ij}}$ is positive. The two-contact probability is the lost-crossing probability divided by this number. Thus the strip estimate, applied to the lost crossing, gives continuity of $H_{\Omega_{ij}}(K)$ under small target offsets; see [29, (6.3) and the proof of Lemma 7.4]. For a nonsmooth complementary domain, first map to the disk. The buffer separates the target from every other curve, so the normalized map is nearly affine on the target when r/R_0 is small. The images of its circular offsets then satisfy the controlled analytic-target bounds required in (6.3). Hence, for each such tuple,

$$H_{\Omega_{ij}}(K^{(+h)}) - H_{\Omega_{ij}}(K^{(-h)}) \longrightarrow 0 \qquad (h \downarrow 0).$$

Here $K^{(\pm h)}$ are the outer and inner normal offsets, respectively. The continuity estimate for a fixed tuple may contain $p_{\mathrm{cr},\Omega_{ij}}^{-1}$. The displayed difference itself lies between zero and one, so bounded convergence integrates it against the original marginal $\mu_{\alpha,ij}$. In the other-component cases the joint hitting probability is zero. The limiting inner and outer brackets therefore agree at the original target radius. This proves convergence of the joint selected-pair event before its limiting law is disintegrated, with the original pattern and marginal probabilities as its weights.

The limiting row consequently has the probability-weighted decomposition (5.5). The shell and buffer bounds use only the independent colors in the protected disk, so they give the same constant $C(r/R)^{119/60}$ for every such limit. For the fixed number of tips the partition space is finite; convergence of its coordinates implies convergence in variation norm. If the limiting upper bound were not uniform over the transcripts, one could select meshes and transcripts exceeding it by a fixed positive amount. The sequence just considered would preserve that excess in its limiting row, contradicting the shell bound. Original frontier labels enter through the norm-one completion and impose no continuity requirement on that completion.

The excluded transcripts have probability at most $Ce^{-cM_0} + C\delta/R$. On them use the elementary defect bound $2(1 + 2^y)$. The norm-one completion and the estimate just obtained

therefore give, uniformly in the original microscopic boundary data,

$$\limsup_{a\downarrow 0} \|D^{a,D}_{r,b}\|_{\mathrm{var}} \le C(r/R)^{119/60} + 2(1+2^y)\{Ce^{-cM_0} + C\delta/R\}. \tag{5.9}$$

Send M_0 to infinity and δ to zero at fixed r, R, before any factor r^{-y} is allowed to diverge. Since R is comparable with d, the full-frontier defect is

$$\limsup_{a\downarrow 0} \left\| (\nu^{a,D}_{\varnothing} - \nu^{a,D}_{B_r}) - b^{-y}(\nu^{a,D}_{\varnothing} - \nu^{a,D}_{B_{br}}) \right\|_{\mathrm{var}} \le C(r/d)^{119/60}. \tag{5.10}$$

The same bound holds after any admissible common exterior identification, because that operation is a norm-one kernel.

Dividing (5.10) by r^y compares R_r and R_{br}. For any fixed $0 < r \le \epsilon$, telescope a finite chain of dyadic scales and use one final factor $b \in [1/2, 1]$. The mesh upper limit is taken after this finite telescoping. Its bound is at most

$$Cd^{-y}(\epsilon/d)^{\beta} \sum_{k\ge 0} 2^{-k\beta}. \tag{5.11}$$

This is uniform in r, and hence proves the Cauchy conclusion in (4.8). Finally compare with one reference radius $r_0 = cd$, for which $\|R^{a,D}_{r_0}\|_{\mathrm{var}} \le 2r_0^{-y}$. The same telescoping proves the bounded-row assertion. This completes the proof of Theorem 4.3.

5.3 Arbitrary finite joint insertions

Take finitely many scalar disks, stress ellipses, and density roots with disjoint fixed protecting neighborhoods. Let $\tau_{a,r}$ denote the holomorphic angular source of [29, (4.8) and Theorem 9.1], and use its complex conjugate for $\bar{T}$. Conjugation preserves its variation norm, its bounded-row estimate, and its $1/4$ Cauchy rate. At positive source radii, expand the product of factors $1 - H_{B_r}$ and the angular integrals. Every term is a density correlation in a domain with a fixed finite number of smooth holes. It has a mesh limit by [29, Theorem 10.1]; angular dominated convergence is valid because all radii are fixed at this stage.

The normalized exterior completion is uniformly bounded before the source rows are integrated. Given any realizable tuple of source records, the cluster-sign completion is an indicator that every final marked cluster has even parity. It can be nonzero only if each density root has an open arm through its own disjoint root disk. Factoring these independent probabilities before the density normalization gives a bound by a constant on every compact separated configuration set. This is pointwise in the density roots; the established density-coordinate testing may subsequently be applied. Finite-hole existence, covariance and the multilinear completion bound are supplied by [29, Theorem 10.1 and Sections 15–17]; the sign-parity identity is [1, (1.8)–(1.11)].

Now replace one source row at a time. Use Theorem 4.3 in a changed scalar slot, the angular Cauchy estimate in a changed stress slot, and bounded rows in every unchanged slot. If the scalar reference radii are ϵ_j and the stress reference radii are r_k, the finite multilinear telescoping identity gives

$$|\langle F_{\boldsymbol{\rho},\boldsymbol{s}} - F_{\boldsymbol{\epsilon},\boldsymbol{r}}, \psi\rangle| \le C_\psi \left(\sum_j \epsilon_j^{11/15} + \sum_k r_k^{1/4} \right), \qquad \rho_j \le \epsilon_j, \quad s_k \le r_k. \tag{5.12}$$

Fixed separation lengths are absorbed in C_ψ. Compare two cutoff tuples through their coordinatewise minimum. This proves a unique joint limit with all radii tending to zero at

arbitrary relative rates, and the same bound estimates its cutoff error. The constants may depend on the fixed insertion count. The symmetry of the finite-radius products passes to the joint limit. Multilinear telescoping of complete rows uses [29, Theorems 9.1 and 17.1, Sections 9 and 17] for angular slots and Theorem 4.3 for scalar slots. Conjugating any subset of the angular rows leaves this existence argument unchanged.

5.4 Conformal covariance and pointwise two-root correlations

Let f be conformal and regular on the separated source neighborhoods. The image of a radius-r disk differs from its affine image by normal displacement $O(r^2)$. For every fixed $1 < p < 5/4$, the strip estimate (4.5) and the relaxed four-arm bound give the scalar-row error

$$Cr^{-y}\alpha_4(Cr,d)\frac{r^2}{r} \le C_p r^{p-1/4} = o(1). \tag{5.13}$$

The affine radius is $|f'(z)|r$, so the scalar multiplier is $|f'(z)|^y$. The corresponding normalized angular-row error is $O(r^{p-1})$, and changing the angular variable gives the exact affine multipliers $f'(w)^2$ and $\overline{f'(w)}^2$ for T and $\bar{T}$. Finite-hole density covariance and bounded multilinear completion pass these comparisons through every fixed finite word. Thus the weights are

$$(h,\bar{h})_\Phi = (5/96,5/96), \quad (h,\bar{h})_{E^\circ} = (5/8,5/8), \quad (h,\bar{h})_T = (2,0), \quad (h,\bar{h})_{\bar{T}} = (0,2). \tag{5.14}$$

In particular all the plane words have their asserted Möbius covariance. The same local transport proves covariance in the controlled finite-hole domains whenever the conformal map is admissible for the finite-hole theorem. Finite-hole covariance is [29, Theorem 10.1], with the angular affine multiplier calculated in its Section 17.

We also need continuous representatives. To move a scalar center by h with $|h| \ll d$, first use an intermediate radius $\epsilon \gg |h|$. The row Cauchy estimate at the two centers and then the strip estimate for translating the fixed-radius disk give

$$Cd^{-y}\left\{(\epsilon/d)^{11/15} + (|h|/d)(\epsilon/d)^{p-y-1}\right\}. \tag{5.15}$$

For $p = 6/5$, choose $\epsilon/d = (|h|/d)^{60/107}$. Both terms are $O((|h|/d)^{44/107})$. Stress centers have the sufficient modulus $O(|h|^{5/41})$ obtained from their $1/4$ Cauchy rate and the same strip comparison. Multilinear telescoping transfers these moduli to every fixed finite joint word after the required density tests, and also pointwise for fixed external density roots. The corresponding stress-center estimate is [29, Section 9.4, (9.13)–(9.14)].

Suppose now that there are exactly two density roots $u \neq v$. At every fixed separated configuration the finite-hole theorem and the pointwise root-completion bound give the finite-radius mesh limit. Applying (5.12) before testing the two roots gives a pointwise limit, uniformly on separated compact sets of root and source positions. This convergence is uniform in the source cutoffs after taking the pointwise mesh limit. Continuity in the source centers follows from (5.15) and its stress counterpart at fixed u, v.

To obtain continuity in the roots as well, use $A_{u,v}(\zeta) = (\zeta - u)/(v - u)$. It sends them to the fixed pair $0, 1$. The exact affine source multipliers and the two density factors express the original correlation as a smooth nonzero prefactor times the correlation at these fixed roots and at the continuously moving source centers $A_{u,v}(z_j)$. On a neighborhood of any separated configuration these transformed centers remain separated. Their just-proved continuity therefore proves joint continuity in all original coordinates. This argument applies to any fixed finite numbers of scalar, holomorphic stress, and antiholomorphic stress insertions.

Equality of such a continuous representative with a distributionally identified continuous formula holds everywhere, by testing their difference. This proves the two-root assertion of Theorem 4.4, including the two-scalar correlations used in Section 15.

5.5 The Ward hierarchy with both stress chiralities

We give the extension explicitly, since the principal theorem of Paper I is stated for holomorphic stress words. For a separated word $X = \prod_j X_j(\xi_j)$ with weights from (5.14), the asserted identities are

$$\langle T(w)X\rangle = \sum_j \left\{ \frac{\partial_{\xi_j}}{w-\xi_j} + \frac{h_j}{(w-\xi_j)^2} \right\} \langle X\rangle, \tag{5.16}$$

$$\langle \bar{T}(w)X\rangle = \sum_j \left\{ \frac{\partial_{\bar{\xi}_j}}{\bar{w}-\bar{\xi}_j} + \frac{\bar{h}_j}{(\bar{w}-\bar{\xi}_j)^2} \right\} \langle X\rangle. \tag{5.17}$$

The coordinate derivatives act on the full expression to their right and are distributional in the original scalar and density coordinates. The central charge is zero. The differential form is the standard zero-central-charge Ward recursion, with a conformal-restriction antecedent in [19, (4.11)]. The following argument proves its realization on the enlarged class, including mixed chirality.

Insert first a holomorphic stress at w with ellipse radius s. Its circularizing map and inverse are

$$f_t(\zeta) = \zeta + \frac{t}{\zeta - w}, \qquad t = es^2 e^{2i\phi}, \qquad g_t(\zeta) = \zeta + \frac{t}{w-\zeta} + O(t^2). \tag{5.18}$$

The derivatives of the remainder are uniform on the other source neighborhoods. In particular $g_t'(\zeta) = 1 + t/(w-\zeta)^2 + O(t^2)$, and the true image of another radius-r target differs from its affine image by normal width $O(|t|r^2)$. The single-slot image errors consequently satisfy

$$\|E_j(t)\|_{\mathrm{var}} \le C_p |t| a_j, \qquad a_j = \begin{cases} r_j^{p-1/4}, & \text{scalar slot,} \\ r_j^{p-1}, & \text{either stress chirality.} \end{cases} \tag{5.19}$$

The unchanged affine rows have a common bound $B \ge 1$ on a fixed separated compact set. For N other source slots, expanding the multilinear completion in all nonempty error subsets and dividing by the first angular normalization $|t| = es^2$ gives

$$C \sum_{\varnothing \ne I \subseteq \{1,\dots,N\}} |t|^{|I|-1} B^{N-|I|} \prod_{j\in I} a_j \le C_N \sum_{j=1}^{N} a_j = o(1). \tag{5.20}$$

Every exponent in a_j is positive. This proves vanishing as the source radii tend jointly to zero. The estimate also holds with the first ordinary circular hole present, whose probability row has norm one. Joukowski circularization and the stress-image estimate are from [29, Section 17]. Applying (4.5) with the scalar normalization $r^{-5/4}$ gives the scalar estimate in (5.19); the finite-product calculation controls the mixed words.

To remove the first circle, we transfer the coordinate changes to smooth test functions. For this proof only, test all moving coordinates and average each remaining source radius r_j over $r_j e^{\ell_j}$ with a smooth compactly supported kernel $\chi_j(\ell_j)$ of integral one. These averages have the independently constructed raw limit by (5.12). A coordinate transport together with its affine radius changes acts, after change of variables, on a smooth test Ξ_t. Radius

multiplication becomes translation of ℓ_j and acts on the smooth kernel χ_j. For one fixed sufficiently high test seminorm p_M,

$$\begin{aligned} p_M(\Xi_t - \Xi_0) &\le C|t|, \\ p_M(\Xi_t - \Xi_0 - t\Xi_+ - \bar{t}\Xi_-) &\le C|t|^2. \end{aligned} \tag{5.21}$$

Thus a distribution family of size A contributes only $O(A)$ to its normalized second angular coefficient after its constant term is subtracted. This follows directly by pairing the family with $\Xi_t - \Xi_0$ and then dividing by es^2. This applies the smooth-test duality of [29, Lemma 17.2 and Sections 17.3–17.4] to scalar radius variables and both angular signs.

Let $B_{s;\boldsymbol{r}}$ be the difference between the remaining word with the ordinary circle $B_s(w)$ closed and the same word in the plane. The ordinary-hole estimate (4.6), bounded other source rows, and root completion give

$$|\langle B_{s;\boldsymbol{r}}, \psi\rangle| \le C_{\psi,p} s^p.$$

This is uniform on the enlarged logarithmic-radius windows. The untransported circle term is independent of ϕ and has zero second harmonic. Apply (5.21) to its transported difference: its normalized angular contribution is $O(s^p)$ and tends to zero. Similarly the plane correlation of the remaining regulators differs from its raw limit by $O(\sum_{\text{scalar}} r_j^{11/15} + \sum_{\text{stress}} r_j^{1/4})$. Transporting that error by duality retains this same vanishing bound after angular normalization. Therefore only the transport of the existing radius-independent limit contributes.

The coefficient of t in this transport is the operator in (5.16). A scalar multiplier $|g_t'|^y$ contributes $y/2 = 5/8$, a density multiplier contributes $x/2 = 5/96$, and the two angular multipliers $g_t'^2$ and $\overline{g_t'}^2$ contribute holomorphic weights 2 and 0. The velocity of every unbarred coordinate is $1/(w - \xi_j)$. The $\bar{t}$ coefficient is killed by $e^{-2i\phi}$, and the tested second-order remainder contributes $O(s^2)$. Using the conjugate angular source selects $\bar{t}$ instead and proves (5.17).

Induct on the total number of stress insertions, keeping the arbitrary finite scalar–density word as the initial correlation. The two preceding error estimates and (5.20) prove the induction at each order. After testing the original scalar and density coordinates, the recursion is holomorphic in each T center and antiholomorphic in each $\bar{T}$ center: start with all stresses of one chirality and then add the others. A term differentiating the opposite chirality vanishes, and the remaining rational kernels preserve this property. Permutation symmetry of the raw lattice products then gives the same identity in every insertion order.

Finally remove the temporary logarithmic averages using the raw joint Cauchy bound. The equality holds as a distribution in all moving centers. The center moduli above identify its continuous representative at every fixed separated source configuration whenever the original density tests are kept. The pointwise two-root interpretation was proved separately and is compatible with this equality. This establishes the Ward part of Theorem 4.4.

5.6 The probability-weighted four-tip calibration

In a clean quad there are two open boundary arcs. Write e_{join} and e_{separate} for the two boundary partitions, and let p be the probability that the open arcs join. Closing the disk can only change join to separate. The finite lost-crossing identity therefore gives, after the fixed-radius mesh limit,

$$\nu_\varnothing - \nu_{B_r(z)} = pH_\Omega(r)(e_{\text{join}} - e_{\text{separate}}). \tag{5.22}$$

Together with (5.3), it identifies the scalar row as $c_* p\mathcal{G}_\Omega(z)$ times this signed vector. The lost-crossing identity is the two-interface surgery of [29, Lemma 6.1]. Its continuum version follows from the strip-controlled target offsets established there, and its positive limit is given by Zhan's theorem.

To determine the angular dependence, map z to 0 in $\mathbb{D}$ and label the four endpoints a_1, b_1, a_2, b_2 in cyclic order for the selected link pattern. Put $d_{uv} = |u - v|$ and

$$R = \frac{d_{a_1b_2}d_{a_2b_1}}{d_{a_1a_2}d_{b_1b_2}}, \qquad F(R) = {}_2F_1(1/3, 2/3; 4/3; R), \qquad c_C = \frac{\Gamma(2/3)}{\Gamma(1/3)\Gamma(4/3)}.$$

Cardy's formula for the selecting crossing and Zhan's conditional Green factor, in the normalization of (5.3), are

$$p = c_C R^{1/3} F(R), \qquad \mathcal{G}_{\mathbb{D}}(0) = \frac{1}{4}\frac{(d_{a_1b_1}d_{a_2b_2})^{1/3}(d_{a_1a_2}d_{b_1b_2})^{2/3}}{F(R)}. \tag{5.23}$$

Their product is

$$c_* p\mathcal{G}_{\mathbb{D}}(0) = c_E \prod_{j<k\le 4} |e^{i\theta_j} - e^{i\theta_k}|^{1/3}, \qquad c_E = \frac{c_* c_C}{4} > 0. \tag{5.24}$$

This proves the probability-weighted formula (4.13), with its join-minus-separate sign. In a general domain it has the scalar conformal factor $|f'(z)|^y$. Cardy's formula is quoted in [11, (1.2)]; its application to the selecting crossing is worked out in [29, Section 6.4]. The second identity in (5.23) is [12, Theorem 1.1] at $\kappa = 6$. Direct algebra cancels F and the six chord factors.

5.7 The positive plane calibration

The pointwise construction with two roots and Möbius covariance give the three-point form (4.11), initially with a finite constant $C_\circ \ge 0$. The exponent of $|u - v|$ is $y - 2x = 25/24$. Its nonnegativity follows at each mesh from the probability of a connection lost on closing the disk. To prove that the scalar couples nontrivially to the density pair, we construct a connection that the disk must interrupt.

The positive quad calculation first gives the lower four-arm bound needed for this construction. Choose one fixed nondegenerate quad containing $B_{2R}(0)$. Its lost-crossing event supplies four alternating sampled arms from $B_{2r}(0)$ to $\partial B_R(0)$: two portions of the original open crossing and two portions of the closed separator created by disk deletion. Outside the deleted disk the latter are closed in the original configuration. The annulus is wholly inside the quad, where the sampled sites have the ordinary product law. Hence, after removing the mesh,

$$\alpha_4(2r, R) \ge pH_\Omega(r) \ge c_R r^y \tag{5.25}$$

for sufficiently small r; harmless fixed inner-radius offsets are absorbed by separated-arm comparison. The last inequality is (5.3) in this one fixed quad. This lower bound follows directly from the Green estimate. The four sampled arms form the standard pivotal-disk witness. The fixed-factor and separated-arm comparisons are from [7, Section 2.1 and Appendix A]. Equation (5.25) gives the required lower bound; the upper shape estimates continue to use $p < 5/4$.

It is enough to test $z = 0, u = -2, v = 2$. Choose a small fixed R and disjoint fixed root disks around u, v. Require four alternating arms across the annulus from $2r$ to R, with separated landing arcs. At the inner boundary use fixed-ratio corridors to join the two open

arms through B_r and bring the two closed arms to that disk. At the outer boundary join the open arms to the two root disks. Join the two closed arms by a closed corridor outside B_R which, after completion through the closed source disk, surrounds u and excludes v. The fixed corridors can be chosen disjoint except at their same-color junctions. Before deletion they give an open u–v connection; after deletion the closed circuit prevents every such connection, including any path attempting a distant detour.

Separated-arm extension and RSW give a constant cost for these fixed-aspect corridors. The two root arms use disjoint root disks, and their probabilities are comparable to the two density normalizing factors π_a. Therefore, at sufficiently fine mesh,

$$\mathbb{P}_a\{u^a \leftrightarrow v^a,\ u^a \not\leftrightarrow v^a \text{ after closing } B_r\} \geq c\pi_a^2\alpha_4^a(2r, R). \tag{5.26}$$

The open and closed parts are glued through disjoint corridors. Divide by $\pi_a^2 r^y$, remove the mesh at fixed r, and then let r tend to zero using (5.25). The limiting scalar–two-density correlation is strictly positive, so $C_\circ > 0$. This completes the calibration part of Theorem 4.4. The RSW and separated-arm gluing inputs are standard [7]. Comparison of fixed-radius root-arm probabilities with π_a uses [1, (2.1)].

The constant c_E calibrates a boundary-partition response, whereas $C_\circ$ uses the normalized plane density pair. Every scalar regulator has mean zero, as does each angular regulator. Products of any nonempty finite family supported in disjoint source neighborhoods therefore have zero vacuum expectation by product independence. Their limiting vacuum correlations vanish as well. The positive calibrations above identify its nonzero correlations with boundary partitions and density pairs.

6 Leading scalar–density fusion

At a distance, a small group of marked clusters can lose the details of its internal connections. An open circuit screens those details while preserving the total parity of the marks. We use this mechanism to prove that $\rho^y E^\circ(z)\Phi(z + \rho u)$ approaches a multiple of one density row, uniformly under bounded exterior completion. The three-point function (4.11) then identifies that multiple.

The open-cutset coupling follows the methods of [1, Lemma 2.1] and [10, Lemmas 2.1–2.3 and Section 2.5]. We extend it below to odd parity and signed rows.

6.1 Odd survival is an increasing event

Work first at a fixed mesh a, with $a \ll s < d/10$. An incoming realizable record c on the cut surrounding $B_s(z)$ specifies all occupied ports, their connections through the inner region, and a parity for each open block. Its connections are realized entirely inside the cut; the annular occupations retain their product law. Assume that its total parity is odd. The number and geometry of its even blocks are unrestricted. For the scalar–density packet there is just one odd block, but the finite argument permits any odd total parity.

Fill the collar to the cut at radius d with its original product law. Let S_c be the event that every component that fails to reach the outer cut has even parity. Write

$$K_{s,d}^a(c, \cdot) = \mathbb{P}_a(\text{complete outgoing marked record} \in \cdot, \mathsf{S}_c), \qquad q_c = K_{s,d}^a(c, \mathbf{1}) = \mathbb{P}_a(\mathsf{S}_c). \tag{6.1}$$

Thus $K_{s,d}^a$ is substochastic: a trapped odd component kills the row; a trapped even component is erased. The outgoing record retains every frontier occupation and every equivalence class,

including the even classes. Denote an ordinary radial open-arm probability by $\alpha_1^a(s,d)$, allowing fixed changes of the two radii in inequalities with a constant C. After the inner and annular partitions are joined, the killing and parity rule follows from the cluster-sign identity [1, (1.8)–(1.11)].

Lemma 6.1 (Odd survival and its mass)**.** *The event S_c is increasing in the sampled occupations. Its surviving output has odd total parity, and*

$$q_c \le C\alpha_1^a(s,d). \tag{6.2}$$

Proof. Opening sites joins existing open components or adds unmarked vertices. An old component touching the outer cut still touches it. A new component that does not touch that cut is a union of old components that did not touch it, together with unmarked vertices. On S_c each such old component was even, so the new component is even. This proves monotonicity. The event therefore allows odd blocks to merge.

Erasing trapped even components leaves the odd total parity unchanged. At least one odd component therefore reaches the outer cut. Its path contains an ordinary open arm across the sampled annulus, proving (6.2). □

6.2 A sampled open cutset screens the full partition

Lemma 6.2 (Odd-parity screening)**.** *Let Γ be a connected set of sampled open sites separating the inner cut from the outer cut, with $\Gamma \subset B_{d/3}(z)$. Fix any history on and inside Γ that declares Γ open and has positive probability conditional on S_c. The remaining exterior law is product percolation conditioned on $\Gamma \leftrightarrow \partial B_d(z)$. The outgoing record can be computed by assigning one odd mark to Γ and using only this exterior configuration. It is independent of the interior input and history.*

Proof. On the event that Γ is open, every inner component reaching the exterior joins the same connected open set Γ. Let H_c be the event, determined on its inner side, that all components failing to reach Γ are even. On the event that Γ is open,

$$\mathsf{S}_c = H_c \cap \{\Gamma \leftrightarrow \partial B_d(z)\}. \tag{6.3}$$

Indeed, on H_c the total parity joining Γ is odd; consequently that component must reach the outer cut. Conversely these two conditions leave no trapped odd component. The two factors in (6.3) involve disjoint unqueried interior and exterior variables. Product independence cancels the interior factor from every exterior conditional probability, including after a partial interior history has been fixed.

Any connection between exterior sites that uses the interior can be rerouted through Γ, since Γ is connected. Thus the exterior and its one odd mark determine every outgoing equivalence class. This proves the record assertion as well as the conditional-law assertion. □

Figure 1 illustrates the replacement of the inner history by its surviving parity, while every exterior connection is kept.

The factorization extends the usual open-circuit screening identity to odd total parity; compare [1, (2.10)–(2.11)].

Proposition 6.3 (Uniform conditional coupling)**.** *For any two realizable odd inputs c, c' with $q_c, q_{c'} > 0$,*

$$\left\| q_c^{-1} K_{s,d}^a(c,\cdot) - q_{c'}^{-1} K_{s,d}^a(c',\cdot) \right\|_{\mathrm{var}} \le C\mathbb{P}_a\big(B_{2s}(z) \overset{\text{closed}}{\longleftrightarrow} \partial B_{d/4}(z)\big). \tag{6.4}$$

The constant is independent of $q_c, q_{c'}$ and of the even input connections.

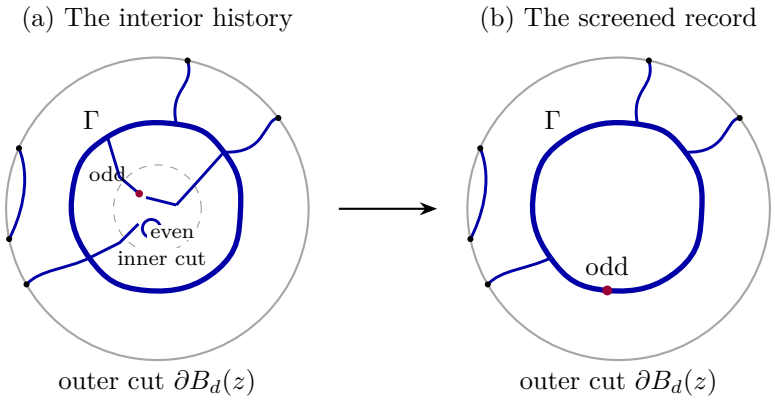


Figure 1: A sampled connected open cutset screens the complete marked record. The cutset Γ is shown here as a circuit. On the survival event, all marked components trapped on its inner side are even, and the total parity reaching Γ is odd. Every exterior connection that enters the interior can be rerouted along Γ. Keeping the same exterior configuration and placing one odd mark on Γ therefore preserves all outgoing connections, including the unmarked component at the left of each panel.

Proof. Use fresh independent uniform variables when querying sites. A base sample declares a queried site open when its uniform variable is at most $1/2$. Two further samples use the same variable, with thresholds equal to the correct single-site probabilities under $\mathbb{P}_a(\cdot \mid \mathsf{S}_c)$ and $\mathbb{P}_a(\cdot \mid \mathsf{S}_{c'})$, respectively, given each sample's own previously exposed colors. By Lemma 6.1, the survival event remains increasing in the unexposed product variables after any history of positive conditional probability. The Harris–FKG inequality therefore makes each conditional threshold at least $1/2$.

The query order may depend on all previously used uniforms. Backward induction on the number of unqueried sites shows that this adaptive order preserves each marginal law. At a fixed past history the next chosen site is deterministic, and its new uniform is independent of that history. Its specified threshold gives the target conditional probability at that site. By the induction hypothesis the rest of the algorithm, with whatever subsequent adaptive choices it makes, samples the target law conditional on the enlarged color history. Summing over the next color recovers the target law conditional on the current colors. The same argument applies to the base product law. The thresholds always use the sample's own revealed colors, while the past uniforms determine the query order.

Choose this order by exploring, in the base sample, the closed cluster attached to an artificial closed seed $B_{2s}(z)$. The seed belongs to the auxiliary exploration; both percolation samples retain their inner records. Reveal neighboring sites until the cluster is surrounded or reaches radius $d/4$. In the latter case declare failure. Otherwise fill the bounded holes of the discovered cluster. Its outer boundary is a connected open cutset Γ around the seed; all queried sites lie on or inside it. On the triangular lattice the outer vertex boundary of a connected set with connected complement is connected. With fixed lattice buffers, Γ lies in $B_{d/3}(z)$. Failure implies a base closed arm from $B_{2s}(z)$ to $\partial B_{d/4}(z)$. The connected-boundary fact is [10, Lemma 2.3]. The inner-to-outer exploration is the corresponding version of the circuit coupling in [1, Lemma 2.1]; fixed cell adjustments change only the constants.

Every base-open site is open in both conditional samples. Hence, on success, the same Γ is open in both. Continue by querying the exterior of Γ in the same deterministic order in the two samples. Lemma 6.2 makes their single-site conditional probabilities equal, first with no exterior colors fixed and then inductively after each common exterior color. The

shared uniforms give identical exterior configurations. Their complete outgoing marked records therefore coincide. Query any remaining interior sites last, using each sample's own conditional probabilities as before. Both full marginal laws are preserved by the sequential construction.

The base sample has its unconditioned product marginal, so the failure probability is the unconditioned closed-arm probability in (6.4). The full variation distance is at most twice a coupling's failure probability. This proves the asserted bound uniformly in the two survival probabilities. □

6.3 Survival probabilities and signed projection

Let F_d^a be the positive row of a single density root at z, including its canonical normalization $g_a = c_\Phi \pi_a^{-1}$. Kill the row unless the root reaches the cut at radius d. Set

$$m_d^a = F_d^a(\mathbf{1}) = g_a \mathbb{P}_a(z^a \leftrightarrow \partial B_d(z)), \qquad \sigma_d^a = F_d^a / m_d^a. \tag{6.5}$$

The one-arm ratio gives $m_d^a \longrightarrow c_\Phi d^{-x} > 0$. Disintegrating the density experiment at the inner cut expresses σ_d^a as a mixture of the normalized laws $q_c^{-1} K_{s,d}^a(c, \cdot)$ for one-odd-block inputs. Its mixture weights are the inner-input probabilities multiplied by the survival masses q_c and normalized by their sum. Proposition 6.3 and convexity therefore allow σ_d^a to replace one of the laws in (6.4). The root normalization and one-arm ratio are from [1, (2.1)].

For a signed input row ξ, multiply that conditional estimate by $|\xi(c)| q_c$ and sum. Inputs with $q_c = 0$ contribute zero. Using (6.2) and color symmetry gives

$$\left\| \xi K_{s,d}^a - (\xi K_{s,d}^a \mathbf{1}) \sigma_d^a \right\|_{\mathrm{var}} \le C \alpha_1^a(s,d) \alpha_1^a(2s, d/4) \|\xi\|_{\mathrm{var}}, \tag{6.6}$$

$$\|\xi K_{s,d}^a\|_{\mathrm{var}} \le C \alpha_1^a(s,d) \|\xi\|_{\mathrm{var}}. \tag{6.7}$$

Both estimates retain the survival masses and hold before the local field limits. The second follows directly from the necessary arm event.

The first arm factor has the bound with exponent x and a constant after the fixed-scale mesh limit. If $p_a(t) = \mathbb{P}_a(z^a \leftrightarrow \partial B_t(z))$, quasi-multiplicativity gives

$$\alpha_1^a(s,d) \le C \frac{p_a(d)}{p_a(s)}, \qquad \limsup_{a \downarrow 0} \alpha_1^a(s,d) \le C (s/d)^x. \tag{6.8}$$

The one-arm ratio and quasi-multiplicativity thus give the exponent x with a constant. For the second factor it suffices to use $C_\gamma (s/d)^\gamma$ for any fixed $0 < \gamma < x$. The one-arm ratios are from [1, (2.1)], quasi-multiplicativity from [7, Sections 2.1 and 5.1], and $x = 5/48$ from [4]. The weaker exponent γ suffices for the present theorem.

Consequently a family with local variation bound $C s^{-x}$ satisfies

$$\limsup_{\mathrm{reg}} \|\xi_s^a K_{s,d}^a - b_s^a F_d^a\|_{\mathrm{var}} \le C_\gamma d^{-x} (s/d)^\gamma, \qquad b_s^a = \frac{\xi_s^a K_{s,d}^a \mathbf{1}}{m_d^a}. \tag{6.9}$$

Here $\limsup_{\mathrm{reg}}$ means the mesh upper limit first and then the required local source-regulator upper limits, with s, d fixed. The coefficients b_s^a are bounded in the same order of limits by (6.7) and (6.5). We retain the coefficients at finite mesh in the comparisons below.

6.4 The local scalar–density response

Translate z to 0, put the density at ρu with $|u| = 1$, and use disjoint local disks of radius $\rho/8$ around these two points. Take the scalar source radius $\epsilon < \rho/100$, and surround the two

local disks by the cut $s = 3\rho$. Let $\xi^a_{\rho,\epsilon}$ be the signed row on that cut for

$$\rho^y E^\circ_{a,\epsilon}(0)\Phi_a(\rho u). \tag{6.10}$$

The exact forcing identity (4.3) writes its scalar factor as a difference of two genuine percolation experiments. Every record in this signed expansion is therefore realizable. The scalar introduces no density mark. Whenever the packet survives it has one odd block, together with all the even blocks created by the two fillings.

The scalar row at its own local cut has norm at most $C\rho^{-y}$ by Theorem 4.3. The normalized density row has mass at most $C\rho^{-x}$, by extracting its independent root arm before normalization. The remaining unmarked filling in $B_{3\rho}$ is a substochastic gluing kernel. Hence

$$\limsup_{\epsilon\downarrow 0}\limsup_{a\downarrow 0}\|\xi^a_{\rho,\epsilon}\|_{\mathrm{var}} \le C\rho^y\rho^{-y}\rho^{-x} = C\rho^{-x}. \tag{6.11}$$

This estimate is uniform in u. With $\rho < cd$ small enough that $3\rho < d/10$, (6.9) applies to $R^a_{\rho,\epsilon,d} = \xi^a_{\rho,\epsilon}K^a_{3\rho,d}$. It makes this whole row close to a bounded multiple of F^a_d. The multiple must now be calibrated at this same outgoing cut. The mesh limit is taken before ϵ is removed, at fixed positive collision distance ρ.

6.5 Calibration at the fixed outgoing cut

Place one additional density at $v = 2d$, in a local disk disjoint from $B_d(0)$. Its exterior completion, multiplied by d^x, defines a test φ^a_d on every outgoing odd record. Join the record to the remote-root experiment and impose the final even-parity rule. For a nonzero result the remote root must have an arm out of its own disk, of radius comparable with d. Consequently

$$\limsup_{a\downarrow 0}\|\varphi^a_d\|_\infty \le C, \qquad F^a_d(\varphi^a_d) \longrightarrow d^x\langle\Phi(0)\Phi(2d)\rangle = 2^{-2x}d^{-x} > 0. \tag{6.12}$$

Also $\|F^a_d\|_{\mathrm{var}} = m^a_d \asymp d^{-x}$ for sufficiently small mesh at this fixed d. The two-density and scalar–two-density correlations have the pointwise representatives established in Theorem 4.4, so this bounded completion can be evaluated at the fixed remote root. Independent remote root-arm extraction, (4.1) and the pointwise three-point conclusion of Theorem 4.4 give this detector. Its cut is the completion cut d, held fixed throughout the extraction.

The following finite-dimensional inequality compares the projected row with its calibrated coefficient. For any signed row R, positive row F, bounded test φ with $F(\varphi) > 0$, and scalars b, c,

$$\|R - cF\|_{\mathrm{var}} \le \left(1 + \frac{\|F\|_{\mathrm{var}}\|\varphi\|_\infty}{F(\varphi)}\right)\|R - bF\|_{\mathrm{var}} + \frac{\|F\|_{\mathrm{var}}}{F(\varphi)}|(R - cF)(\varphi)|. \tag{6.13}$$

Indeed, test $R - bF$ by φ to bound $|b - c|F(\varphi)$, then apply the triangle inequality to $R - cF = (R - bF) + (b - c)F$. The prefactors in (6.13) are bounded when $F = F^a_d$ and $\varphi = \varphi^a_d$, by (6.12) and (6.5).

The proved three-point formula (4.11) gives the exact continuum identity

$$\frac{\rho^y\langle E^\circ(0)\Phi(\rho u)\Phi(v)\rangle}{\langle\Phi(0)\Phi(v)\rangle} = C_\circ\left|1 - \frac{\rho u}{v}\right|^{y-2x}, \qquad y - 2x = \frac{25}{24}. \tag{6.14}$$

For $v = 2d$ and $\rho < cd$, its right side differs from $C_\circ$ by $O(\rho/d)$ uniformly in u. It follows, with precisely the mesh-first and then scalar-regulator limits specified above, that

$$\limsup_{\epsilon\downarrow 0}\limsup_{a\downarrow 0}|(R^a_{\rho,\epsilon,d} - C_\circ F^a_d)(\varphi^a_d)| \le Cd^{-x}\rho/d. \tag{6.15}$$

Substitution in (4.11) and the bounded first derivative of $|1-w|^{25/24}$ on $|w| \le 1/4$ give the estimate. The coefficient $C_\circ$ is fixed by the disk-source normalization in Theorem 4.4.

Apply (6.13) at finite mesh, with $R = R^a_{\rho,\epsilon,d}$, $F = F^a_d$, $c = C_\circ$, and b the mass coefficient in (6.9). Use (6.11), (6.9), and (6.15), and then take the stated regulator limits. Since $0 < \gamma < x < 1$, the error ρ/d is absorbed into $(\rho/d)^\gamma$. This proves

$$\|\rho^y E^\circ(z)\Phi(z+\rho u) - C_\circ \Phi(z)\|_{d,*} \le C_\gamma d^{-x}(\rho/d)^\gamma, \qquad |u| = 1, \tag{6.16}$$

which is (4.12) and completes the proof of Theorem 4.5. The norm projection has been proved independently of the detector, which identifies its coefficient. Consequently the conclusion holds for every bounded completion of the complete record.

Every mesh-dependent test of norm at most one is included in (6.16). Separated finite spectator words are included after their local root normalizations and source-row bounds are extracted as in Theorem 4.4. Constants may depend on that fixed word and its separation geometry. Section 12 uses the null identity to extract the subleading coefficient.

7 Identification of the six-tip signed response

With three open boundary arcs, closing a small disk can separate the arcs in several ways. The five possible partitions record these changes simultaneously.

We work in a simply connected domain with six cyclically ordered alternating boundary tips. The three open arcs are denoted by $A = (12)$, $B = (34)$ and $C = (56)$. The response $R_D(z)$ retains their complete open-cluster partition, with coordinates indexed by

$$s_0 = A|B|C, \qquad s_1 = A|BC, \qquad s_3 = AC|B, \qquad s_5 = AB|C, \qquad s_* = ABC. \tag{7.1}$$

Thus $R_D(z)$ is a signed row on five states and has total mass zero. The source is the disk-deletion scalar E°, with dimension $y = 5/4$. All mesh limits in this section precede the removal of source regulators. An exterior completion may retain arbitrarily many additional labels; it acts on this row only after the five-state response has been computed. The disk prescription and common-cut interpretation are those of Sections 4 and 5. Finite planar partition algebra gives the five-state description.

7.1 Finite-tip covariance and stopped exploration

An exploration reveals the outside of the experiment while leaving its small central disk untouched. The response in the remaining domain is therefore a conditional expectation of the original response. We first justify this statement through the mesh and source limits; it will then give the differential equations.

We use marked Carathéodory convergence in the following precise sense. For a simply connected source domain U containing z, normalize $f_U : U \to \mathbb{D}$ by $f_U(z) = 0$ and $f'_U(z) > 0$. The inverse maps converge locally uniformly in $\mathbb{D}$, and the images of the finitely many labelled boundary prime ends converge in their cyclic order. A compact class below has a common interior disk $B_d(z)$, a common upper bound on the diameter, and a positive lower bound on the circular separations of its marked images. The source is translated to a fixed reference point when comparing these maps. These are the disk-coordinate conventions of [29, Section 7.2 and Lemma 8.3]. Harmonic measure of a boundary arc from an interior point is its Brownian exit probability; under the disk map normalized at that point, it is the angular length of the image arc divided by 2π [29, Section 8.3].

This compactness includes the normalized maps, not just the Euclidean locations of the tips. The inverse maps take values in a fixed bounded disk, so they form a normal family. Their derivatives at zero are bounded below by the radius of the common interior disk; thus every convergent subsequence has a nonconstant univalent limit. The marked images lie on the compact unit circle, and their separation bound keeps their limiting prime ends distinct. This proves sequential compactness in the stated topology. Every lattice domain used below is the simply connected source component of an exploration, with the two banks of each slit retained separately. Its unexplored colors have the unconditioned product law and its boundary word is alternating. It therefore belongs to the model family verified in [29, Lemma 7.3]. Together with the map and mark convergence, these facts are precisely the checks in [29, Proposition 8.5, proof, Steps 1–3] for applying Theorem 7.2 there to remaining domains.

For positive holes, the compact classes also fix their number and use common upper bounds on boundary lengths, positive analytic-chart and tubular radii, chart derivatives bounded above and away from zero, and positive lower bounds on their sizes and mutual separations. Their boundaries converge in C^2 normal coordinates inside a common compact interior set. These are the fixed-scale boundary bounds of [29, Section 12]; they allow analytic Jordan holes, including conformal images of the small convex source targets.

Lemma 7.1 (Covariance for finite-tip partition responses)**.** *In a simply connected domain with any fixed finite alternating boundary word, the bounded tests of the open boundary partition have conformally invariant limits after any fixed finite family of separated analytic Jordan holes has been forced closed at positive size. These limits are continuous under marked Carathéodory convergence with the target convergence and bounds stated above. On every compact class just described, the mesh convergence is uniform and the scalar source limit is uniform. The resulting row satisfies*

$$R_U(z) = |f'(z)|^{5/4} R_{f(U)}(f(z)), \tag{7.2}$$

with all boundary labels transported by f, and

$$\|R_U(z)\|_{\mathrm{var}} \le C \operatorname{dist}(z, \partial U)^{-5/4}. \tag{7.3}$$

The constant in the last bound is independent of the separations of the boundary tips.

Proof. Boundary partitions and interior events. We first prove a joint convergence statement for the ordinary model, with no closed interior targets. Its boundary partition can be recovered from finitely many ordinary crossing events. For two open boundary arcs A_i, A_j, let E^a_{ij} require an open path between them whose other cells are free interior cells; the path may not use any other fixed boundary cell. Regard all the other fixed boundary arcs as closed when testing this event. Thus E^a_{ij} is a four-mark crossing in the same underlying sample of free colors. The original open-arc partition is the connected-component partition of the finite graph with edges $\{i, j\}$ for which E^a_{ij} occurs. Indeed, an open path in the original model splits at its visits to fixed open arcs into paths of this kind; conversely, paths for a chain of graph edges concatenate through the fixed open arcs.

We claim that these finitely many edge indicators converge jointly with any finite family of closed-circuit indicators in fixed smooth annuli compactly contained in the domain. This assertion also holds along every marked Carathéodory convergent sequence of domains. Only ordinary four-mark crossing convergence and positive-scale interior events are needed. The former follows from Cardy's formula and [29, Theorem 7.2 and Lemma 7.3]; the latter use the quad-crossing configuration of [6, Section 1.3]. Its fixed quad and annular event limits

are summarized in [29, Section 11.1], with the precise joint-event input in [7, Lemma 2.9 and Remarks 2.11–2.12]. We give the approximation linking these two inputs.

Consider one edge event along a sequence $U_n^{a_n}$, with $a_n \downarrow 0$. Write $f_n : U_n^{a_n} \to \mathbb{D}$ and $f : U \to \mathbb{D}$ for the normalized maps. In the limiting disk coordinate, its two designated arcs are (α_1, α_2) and (α_3, α_4), with the angles in cyclic order. For small $\epsilon > 0$, put a shallow cap over each entire designated arc: in polar coordinates its angular interval extends by ϵ beyond both endpoints and its radial interval is $1 - \epsilon \le r < 1$. The caps are disjoint; their inward boundaries are piecewise analytic crosscuts. Denote by V_ϵ the disk with these two caps removed. Its two crosscuts are the designated sides of a four-mark quad. The word *quad* has the meaning of [6, Section 1.3]. Its crossing probability p_ϵ^+ satisfies

$$p_\epsilon^+ \longrightarrow p \qquad (\epsilon \downarrow 0),$$

where p is Cardy's probability for the original four disk marks: the boundaries and the four corners of V_ϵ approach those of the original marked disk.

Transport the caps by f_n^{-1} and cut them off on the lattice. Write $H_{1,n}, H_{2,n}$ for the two filled sets of removed cells; the filling convention and its convergence are specified below. Let E_n^+ be the crossing between their two crosscuts in the component containing the reference point. For this auxiliary test, the boundary faces on the two crosscuts are open and every other fixed boundary face is closed. Every cell still free in this four-tip domain keeps its color from the original sample. Thus the original crossing and E_n^+ are defined on one probability space.

We verify the cell approximation and the four new marked coordinates. The largest diameter in disk coordinates of a lattice cell whose interior lies in the domain tends to zero, uniformly for the bounded domains with a protected reference disk used here. For cells at distance at least $\sqrt{a_n}$ from the boundary, Cauchy's estimate for the bounded analytic function f_n gives image diameter $O(\sqrt{a_n})$. For a cell closer to the boundary, choose $p_n \in \partial U_n^{a_n}$ within $2\sqrt{a_n}$ of it and a fixed R_0 smaller than a quarter of the protected disk radius. The reference point lies outside $B(p_n, R_0)$. With $L_n(t)$ the total length of the images of the arcs $U_n^{a_n} \cap \partial B(p_n, t)$, the conformal area formula and Cauchy–Schwarz give

$$\int_{C\sqrt{a_n}}^{R_0} L_n(t)^2 \, \frac{dt}{t} \le 2\pi \int_{U_n^{a_n}} |f_n'(w)|^2 \, dA(w) = 2\pi^2.$$

There is therefore a regular circle with total image length $O(|\log a_n|^{-1/2})$. Its intersections with the simply connected lattice domain are crosscuts: a whole circle would enclose the exterior point p_n. In the prime-end disk, with slit banks counted separately, their complementary components form a tree. The cell interior is connected and disjoint from the circle, so it lies in one such component; the reference point lies in another. An edge of the unique tree path between them is a crosscut separating the whole cell from the reference point. A disk crosscut of length $\ell < 1$ cuts off, on the side away from 0, a component of diameter at most 2ℓ. This proves the claimed vanishing cell size. This is also the length–area argument of [29, Appendix C, Lemma C.1, proof, part (d)].

For each $H_{k,n}$, take the cells meeting its transported cap, follow their frontier facing the reference point, and fill the pockets on the cap side of that frontier. In disk coordinates the filled set lies between arbitrarily small inward and outward perturbations of the corresponding fixed cap, by the cell-size estimate. Indeed, the complement of an outward perturbation is connected to the reference point, so the pockets being filled lie inside that perturbation as well. The two neighborhoods stay disjoint and contain the entire corresponding designated boundary arcs, with an angular buffer. Their frontiers are the two crosscuts of the reference component. A component cut off on the other side of either frontier is incident only to

that cap; hence every path in the complement joining the two frontiers lies in the reference component. One-cell choices of the crosscuts or incoming marked edges change only the width of the vanishing neighborhoods. Keep the two new boundary sides in their cyclic order, with the boundary-face convention of [29, Lemma 8.1].

These same inner and outer crosscut bounds give kernel convergence to $f^{-1}(V_\epsilon)$. They also give marked convergence. In disk coordinates, choose an anchor on the unchanged unit-circle side adjacent to a corner, at distance ρ from that corner. A neighborhood of this anchor is untouched by the cap cuts for all sufficiently fine meshes. Let g_n be the normalized map of the cap-cut domain in disk coordinates onto $\mathbb{D}$. Its inverse maps $\mathbb{D}$ into $\mathbb{D}$ and fixes 0, so Schwarz's lemma gives $|g_n(\zeta)| \geq |\zeta|$ in that domain. Across the unchanged unit-circle arc the reflected map is $1/\overline{g_n(1/\bar{\zeta})}$, bounded by $|\zeta|$ on the outside. Together with $|g_n| \leq 1$ on the inside, this supplies a normal family across the arc. Kernel convergence therefore extends to the anchor. The connected ordered boundary interval from the anchor to the new marked corner stays in a disk of radius $C\rho$ about the limiting corner, by the cap bounds and the vanishing image-cell size. Its harmonic measure from the reference point is $O(1/|\log \rho|)$, by comparison with the logarithmic annular harmonic function. Its image is therefore a circle arc of vanishing angular length. First taking the mesh limit and then $\rho \downarrow 0$ identifies each of the four marked corner coordinates. This argument uses the connected arc on its specified side. It takes place entirely in disk coordinates, without using Euclidean landing points of the original prime ends. Cardy's marked-domain limit applies, and gives $\mathbb{P}(E_n^+) \to p_\epsilon^+$.

There is a fixed interior quad with the same Cardy probability as the original domain; see Figure 2. Take

$$Q_\epsilon = f^{-1}\big((1-\epsilon/2)\mathbb{D}\big), \qquad \text{with marks } f^{-1}\big((1-\epsilon/2)e^{i\alpha_k}\big), \quad 1 \leq k \leq 4.$$

Its boundary is analytic and its closure lies in U. Its two designated sides lie strictly inside the two limiting caps. Local uniform convergence of f_n implies that, for all large n, this fixed quad lies in $U_n^{a_n}$ and its designated sides lie inside $H_{1,n}$ and $H_{2,n}$, respectively. Let $F_\epsilon^{a_n}$ be its usual quad-crossing event: the crossing path uses sampled open cells throughout, including at its two endpoints. The positive buffers put the endpoint cells inside the respective removed sets, regardless of the one-cell convention used to approximate the analytic sides. Scaling the concentric disk to $\mathbb{D}$ preserves the four angles, so $\mathbb{P}(F_\epsilon^{a_n}) \to p$.

Both event inclusions follow by the same pathwise restriction. On either $E_{ij}^{a_n}$ or $F_\epsilon^{a_n}$, orient a crossing $\gamma = (c_0, \dots, c_\ell)$ from the first designated side to the second. Its first cell belongs to $H_{1,n}$ and its last to $H_{2,n}$. Let j_2 be its first index in $H_{2,n}$ and j_1 its last index in $H_{1,n}$ before j_2. Then

$$(c_{j_1+1}, \dots, c_{j_2-1})$$

is a path outside both removed sets, adjacent to the first crosscut at one end and to the second at the other. It lies in the reference component by the preceding geometric construction. Each of its cells was sampled open and keeps that color if it remains free in the auxiliary domain. Cells on either new crosscut are open by the auxiliary boundary condition. The path uses no old fixed boundary cell outside the two caps: this is part of the definition of $E_{ij}^{a_n}$, while the quad defining $F_\epsilon^{a_n}$ is compactly contained in the original domain. Thus closing the other boundary faces removes none of the cells of this subpath. The separation of the two caps makes the subpath nonempty for all large n. Attaching its endpoint cells to the two open boundary sides proves, for every color configuration,

$$E_{ij}^{a_n} \subseteq E_n^+, \qquad F_\epsilon^{a_n} \subseteq E_n^+.$$

Consequently,

$$\begin{aligned} \mathbb{P}(E_{ij}^{a_n} \triangle F_\epsilon^{a_n}) &\le 2\mathbb{P}(E_n^+) - \mathbb{P}(E_{ij}^{a_n}) - \mathbb{P}(F_\epsilon^{a_n}), \\ \limsup_{n\to\infty} \mathbb{P}(E_{ij}^{a_n} \triangle F_\epsilon^{a_n}) &\le 2(p_\epsilon^+ - p) \longrightarrow 0. \end{aligned} \tag{7.4}$$

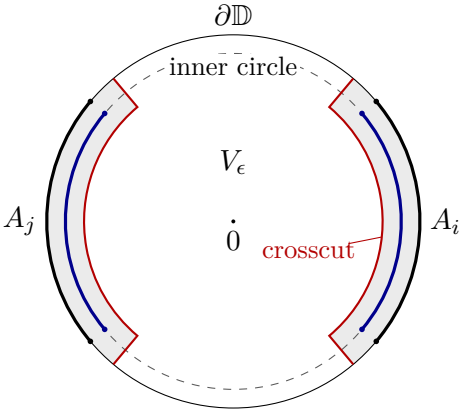


Figure 2: The two caps and the common upper crossing event in disk coordinates. The designated sides of the inner circle lie strictly inside the shaded caps. A crossing between the original arcs, or between the inner designated sides, contains a segment joining the two cap crosscuts through V_ϵ. This gives the common upper event E^+. Radial scaling preserves the four marked angles, so the inner quad has the original Cardy probability p.

The finitely many fixed interior quad events $F_\epsilon^{a_n}$ converge jointly with the fixed annular circuit events. They are all events of the same unmodified interior color sample, which can be taken from full-plane percolation. The quad-crossing convergence and the annular indicator convergence in [29, Section 11.1], [6, Corollary 5.2], and [7, Lemma 2.9 and Remark 2.12] apply in that common sample. Apply (7.4) to every graph edge and use a union bound. First take the mesh limit at fixed ϵ, then let $\epsilon \downarrow 0$. The finite joint law is Cauchy and its limit is unique. This proves the claimed joint convergence of the boundary partition and the interior circuit events, including along moving marked domains. Conformal covariance follows as well: the interior quad and circuit laws are conformally invariant, and the errors in (7.4) depend only on the disk angles and caps.

Closed targets from closed circuits. Let $K_1, \dots, K_h$ be the fixed analytic targets. Their normal offsets and the common chart bounds are those of [29, Section 12]. Choose disjoint analytic surrounding cuts at positive distance from them and from the outer boundary. For small $\delta > 0$, require a closed circuit in each annulus

$$\operatorname{int}(K_j^{+2\delta/3}) \setminus K_j^{+\delta/3}, \qquad 1 \le j \le h,$$

and denote the intersection by C_δ^a. At fixed δ, the circuit probability has a positive limit by RSW. The joint convergence just proved gives a limit for the ordinary boundary-partition law conditioned on C_δ^a.

The circuit exploration of [29, Lemma 13.1] applies without change with the alternating outer boundary kept fixed. Starting on the inner side of each collar, it selects an inner-facing closed circuit and reveals no cell strictly outside it. Conditional on the successful transcripts, all cells outside the selected circuits retain their independent fair colors and the original outer boundary word. Filling the selected circuits and their interiors closed leaves the open boundary partition unchanged. Each filled set J_j^a lies between K_j^a and $(K_j^{+\delta})^a$.

For every fixed selected circuit collection, sample fresh fair colors outside the filled sets and compare with the model having the deterministic holes K_j. On each surrounding cut,

[29, Lemma 12.1] bounds the probability of a difference between the complete frontier records by $C\delta$, uniformly over every intermediate cell set J_j^a. If all records agree, the same exterior sample gives the same boundary partition. Summing over the finitely many cuts and then averaging over the selected circuits gives a comparison of the two partition laws. Write π for the ordinary open boundary partition and $\mu^a_{U;K_1,\dots,K_h}$ for its row after the holes are forced closed. Then

$$\limsup_{a\downarrow 0} \left\| \mu^a_{U;K_1,\dots,K_h} - \mathrm{Law}^a_U(\pi \mid C^a_\delta) \right\|_{\mathrm{var}} \le C\delta. \tag{7.5}$$

The estimate is uniform over the exterior boundary completion because that completion is a contraction. In particular, the constant has no factor $\mathbb{P}(C^a_\delta)^{-1}$: the comparison was made for each circuit collection before averaging.

At fixed δ the conditional law has a limit; then (7.5) makes the family of such limits Cauchy as $\delta \downarrow 0$ and identifies the unique mesh limit of $\mu^a_{U;K_1,\dots,K_h}$. The same construction along every marked convergent sequence proves sequential convergence for the lattice rows. For moving targets, take the collars around their limiting analytic boundaries. For all large indices the moving targets and the selected filled circuits lie between common inward and outward offsets of width $O(\delta)$; Lemma 12.1 gives the same uniform comparison. This uses their common positive chart, tubular-radius, separation and size bounds. Conformal images of these collars lie between shrinking normal collars of the image targets, so the joint conformal covariance of the unforced events also proves conformal invariance of the forced-hole rows.

The uniformity follows from two continuity statements. First, every deterministic sequence of lattice domains and analytic targets converging in the stated marked topology has rows converging to the row of the limiting geometry; this is the sequential conclusion just proved. Second, the continuum rows are continuous in that geometry. To prove the second assertion, approximate the nth continuum domain and its targets by a mesh smaller than $1/n$, with geometry error and row error smaller than $1/n$. The first assertion applied to this diagonal sequence gives the second. If convergence of the lattice rows were not uniform on a compact geometric class, a sequence with variation error bounded below would have a convergent subsequence. Both its lattice rows and its continuum rows converge to the same limiting row by these two assertions, a contradiction. The partition space is finite, so coordinate convergence is convergence in variation norm. Composing with any exterior completion preserves all these error bounds.

Removing the source disk. Place a round completion cut inside $B_d(z)$. The scalar Cauchy estimate of Theorem 4.3, followed by the contraction of exterior completion, gives

$$\sup_U \|R_{U,r}(z) - R_U(z)\|_{\mathrm{var}} \le C_d r^{11/15}.$$

Here $R_{U,r}$ is the fixed-radius mesh limit, and the supremum is over the compact class. Exterior completion preserves the same bound. For a marked sequence $U_n \to U$, the fixed-radius responses are continuous by the positive-hole assertion. Consequently

$$\|R_{U_n}(z) - R_U(z)\|_{\mathrm{var}} \le 2C_d r^{11/15} + \|R_{U_n,r}(z) - R_{U,r}(z)\|_{\mathrm{var}}.$$

First let $n \to \infty$ at fixed r, and then let $r \downarrow 0$. This proves continuity of the scalar row and shows why the common Cauchy estimate makes the source limit uniform. The norm of the row on the round cut is $Cd^{-5/4}$. Completion has norm at most one, so choosing d to be a fixed fraction of $\mathrm{dist}(z, \partial U)$ proves (7.3), with a constant independent of the tip gaps.

The conformal factor. For a conformal map regular near z, the image of $B_r(z)$ differs from $B_{|f'(z)|r}(f(z))$ by normal displacement $O(r^2)$. On a fixed separated completion cut, the strip estimate gives

$$Cr^{-5/4}\alpha_4(Cr, d)r = o(1). \tag{7.6}$$

Indeed, the bound $\alpha_4(Cr, d) \le C_{p,d} r^p$ is sufficient for any $1/4 < p < 5/4$. On compact classes the constants in the Taylor and strip estimates are uniform, by local uniform convergence of the maps and their derivatives. The radius normalization supplies $|f'(z)|^{5/4}$, and the uniform Cauchy estimate removes the regulators. This proves (7.2). □

An ordinary exploration can be stopped as it approaches a protected source by using a slightly displaced target boundary. The displacement can be chosen before sampling the curve.

Lemma 7.2 (Regular offsets for first contact)**.** *Fix finitely many separated analytic targets in a compact interior region and a finite tuple of ordinary exploration curves. For Lebesgue-almost every sufficiently small vector of normal offsets, the first-contact time, contacted target, and stopped prefix of each curve are almost surely continuous under uniform convergence of parametrized curve representatives. The same assertion holds along a marked convergent sequence of domains and targets after transport to disk coordinates. The offsets may be chosen deterministically for the law of the limiting ordinary tuple.*

Proof. For one target, let ρ be signed distance from its boundary, negative inside. For small s, its normal offset is $K^{(s)} = \{\rho \le s\}$. Truncate ρ to constants outside a fixed normal neighborhood. After mapping the domain to the disk, use this transported defining function, so that its sublevel sets are the images of the same targets. Parametrize one curve continuously on $[0, 1]$ and define

$$\tau_s = \inf\big(\{t \in [0,1] : \rho(\gamma(t)) \le s\} \cup \{2\}\big), \qquad \tau_s^< = \inf\big(\{t \in [0,1] : \rho(\gamma(t)) < s\} \cup \{2\}\big).$$

The value 2 records avoidance. These are respectively the first weak and strict entrance times. Continuity and compactness give

$$\lim_{\epsilon \downarrow 0} \tau_{s+\epsilon} = \tau_s, \qquad \lim_{\epsilon \downarrow 0} \tau_{s-\epsilon} = \tau_s^<.$$

For the first equality, a limit of entrance points into the larger targets belongs to $K^{(s)}$; if the curve avoids this target, its minimum value of ρ is strictly larger than s. For the second, every strict entrance point belongs to a sufficiently small inward offset, and an entrance into an inward offset is a strict entrance into $K^{(s)}$.

If $s < t$, an entrance into $\{\rho \le s\}$ is a strict entrance into $\{\rho < t\}$, so $\tau_t^< \le \tau_s$. The nonempty intervals $(\tau_s, \tau_s^<)$ are therefore disjoint for distinct levels. Each contains a rational number, so there are at most countably many exceptional levels with $\tau_s < \tau_s^<$. In particular, the minimum of $\rho \circ \gamma$ is exceptional: weak contact occurs there and strict contact never occurs. These entrance times are jointly measurable in the path and the level. For $0 \le t \le 1$, $\{\tau_s \le t\}$ is the event $\{\min_{0 \le u \le t} \rho(\gamma(u)) \le s\}$, and this minimum is a continuous path functional. Strict entrance is tested by a countable union over rational curve times. Fubini's theorem therefore gives a full Lebesgue-measure set of deterministic s for which $\tau_s = \tau_s^<$ almost surely. Intersect these full-measure sets over the finitely many curve–target pairs. This gives arbitrarily small inward and outward regular offset vectors without conditioning on a realized curve.

Choose representatives with $\gamma_n \to \gamma$ uniformly. If the domains or targets vary, their transported truncated defining functions converge uniformly as well: the nonconstant parts lie in a common compact interior set, where the normalized maps and their inverses converge uniformly. Choose $\epsilon_n \downarrow 0$ with

$$\epsilon_n \ge \|\rho_n \circ \gamma_n - \rho \circ \gamma\|_\infty,$$

enlarged to absorb the cell-contact error in the normal coordinate when a lattice query defines contact. The sublevel-set inclusions give

$$\tau_{s+\epsilon_n}(\gamma) \le \tau_s(\gamma_n;\rho_n) \le \tau_{s-\epsilon_n}(\gamma). \tag{7.7}$$

At a regular offset, both bounds converge to τ_s. If contact occurs, uniform continuity of γ gives convergence of its location and its stopped prefix. If contact does not occur, the regularity of s excludes equality with the path minimum; hence there is a positive gap and avoidance is eventually unchanged. Disjoint targets cannot first be reached at the same time by one continuous curve. The contacted target is therefore stable, too. The contacted target and stopped-prefix conclusions are invariant under increasing reparametrization and therefore hold in the curve metric used in [29, Theorem 7.2]; entrance-time convergence uses the chosen converging representatives. The conclusions also hold after taking the minimum with a continuous local stopping rule. For a moving sequence, select the offsets for its limiting ordinary law and keep them fixed along that sequence. □

We now make the exploration limit, including its residual response, explicit. Map the source to 0 in $\mathbb{D}$ and explore from tip i. The radial Loewner maps g_t are normalized by $g_t(0) = 0$ and $g_t'(0) = e^t$; this equality defines the radial time. Write $e^{i\theta_j(t)}$ for the images of the surviving marked prime ends, with $e^{i\theta_i(t)}$ the driving point. A compact stopping rule below is a bounded continuous modification of the exit from a local neighborhood of the starting tip, as defined in [30, Section 2.1.5 and Appendix B] and used in [29, Theorem 7.2, hypothesis (K4)]. Such a neighborhood contains a neighborhood of that tip, avoids the other marks and a fixed source disk, and has simply connected complement in $\mathbb{D}$. We restrict to stopped intervals on which the normalized marked images remain in a compact separated configuration. This is the localization used in the driving convergence theorem, so the joint limit below concerns precisely its admissible stopping rules. First contact with a regular offset of a protected target may be included using Lemma 7.2, while the same marked separation and time bounds are imposed.

Lemma 7.3 (Joint stopped exploration and response limit)**.** *Fix a compact stopping rule and finitely many times in its bounded time interval. The lattice exploration, its normalized remaining domains, and the conditional disk-deletion responses at these times converge jointly as the mesh tends to zero at fixed disk radius. The exploration limit is radial SLE_6 up to that rule, with*

$$d\theta_i = \sqrt{6}\, dB_t, \qquad d\theta_j = \cot\frac{\theta_j - \theta_i}{2}\, dt \quad (j \ne i). \tag{7.8}$$

The source radius may then tend to zero, uniformly over these stopped domains. In that second limit the conditional response becomes

$$e^{yt} R_{\mathbb{D}}(0;\theta(t)), \qquad y = 5/4,$$

on the original boundary-partition coordinates. This stopped process is a bounded martingale. The joint convergence also holds with any bounded continuous function of the exploration up to an earlier time.

Proof. The exploration law and the remaining domain. The local driving convergence in [29, Theorem 7.2, hypothesis (K4), and Lemma 7.3] is for the unconditioned alternating-boundary law. Its local multiple-SLE partition function is 1, and its half-plane driver has drift zero. Schramm–Wilson's coordinate-change theorem [14, Theorem 3] changes the additional force coefficient to $\kappa - 6$ on passing between chordal and radial coordinates. At $\kappa = 6$ this coefficient

vanishes. The radial driver is therefore $\sqrt{6}B_t$, and the radial Loewner equation at each other boundary mark gives the second equation in (7.8).

On the stopped interval, convergence of the driving functions is uniform in time. The Loewner equations then give local uniform convergence of the normalized maps and their derivatives on the fixed protected source disk; the images of the other marks converge before their first collision. The curve topology is the disk-coordinate uniform topology modulo increasing reparametrizations from [29, Theorem 7.2]. These statements identify the joint limit of the path, maps, and marked remaining domains. If a local boundary return swallows a component without the source and without another active mark, its colors and connections are simply retained in the exterior completion. Up to the stated stopping rule the component containing the source still has the same six labelled active tips.

The conditional response kernel. At mesh a and fixed source radius r, write $\mathcal{F}_t^a$ for the revealed colors and let π be the partition of the original open arcs. Closing $B_r(0)$ changes no revealed color, since this disk is protected. Thus the exact conditional row is

$$M_t^{a,r} = r^{-5/4}\mathbb{E}\Big[e_{\pi(\omega)} - e_{\pi(\omega^{B_r})} \mid \mathcal{F}_t^a\Big].$$

It is the disk-response kernel in the remaining domain, followed by the deterministic completion that restores the original arc labels. The remaining colors have their product law conditional on the entire transcript. In particular, this kernel is evaluated without conditioning on a future connection or on a final link pattern.

The stopped marked domains lie in the compact classes of Lemma 7.1: they contain the protected disk, remain bounded, and their normalized marks remain separated. For fixed r, that lemma provides both uniform mesh convergence of the response kernel and continuity of its continuum value as a function of the marked remaining domain. Joint convergence of the path, maps, and marks therefore implies joint convergence of the conditional response and the path. Indeed, subtract first the continuum kernel evaluated at the lattice remaining domain; the uniform mesh error tends to zero. The continuum kernel at these domains then converges by continuity and the joint domain limit. This applies simultaneously at any finite set of stopped times, and with any bounded continuous function of the earlier exploration. Before a marked collision, each surviving open arc has its original label, and a swallowed component contains no other active mark. Its completion is therefore the same cyclic label-identification map throughout this local exploration. This fixed linear map has norm at most one and preserves the joint convergence.

The scalar limit and the martingale identity. The completion contraction and the Cauchy estimate give, uniformly on the stopped interval, a source-radius error bounded by $C_d r^{11/15}$ after the mesh limit. They also bound the limiting conditional rows by $C_d d^{-5/4}$, independently of r small enough. The image of the source circle under g_t may be replaced by a round circle using (7.6), uniformly in t. Formula (7.2) then identifies the limiting row as $e^{yt}R_{\mathbb{D}}(0;\theta(t))$.

For $s < t$ and a bounded continuous function H of the exploration up to time s, the finite-mesh conditional expectation gives

$$\mathbb{E}[H(M_t^{a,r} - M_s^{a,r})] = 0.$$

First take the mesh limit at fixed r, using the joint kernel convergence. Then take $r \downarrow 0$, using the uniform bound and the uniform Cauchy error. The same identity holds for the displayed limiting process. Bounded continuous path functions generate the stopped path sigma-field, so a monotone-class argument extends the identity to every bounded past-measurable H. This proves the martingale assertion. The identical argument applies to four tips. □

7.2 The finite surgery quotient

Let e_s be the unit row at state s and define six cap vectors by

$$\begin{aligned} v_1 &= e_{s_1} - e_{s_0}, \quad v_2 = e_{s_*} - e_{s_5}, \quad v_3 = e_{s_3} - e_{s_0}, \\ v_4 &= e_{s_*} - e_{s_1}, \quad v_5 = e_{s_5} - e_{s_0}, \quad v_6 = e_{s_*} - e_{s_3}. \end{aligned} \tag{7.9}$$

Let e_i be the standard basis of $\mathbb{R}^6$. Write $Ve_i = v_i$ and let M be the symmetric circulant matrix

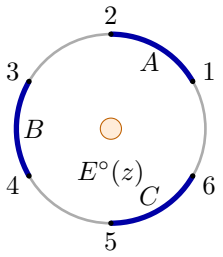
$$(Mw)_i = w_{i-1} + w_i + w_{i+1}, \qquad i \pmod 6. \tag{7.10}$$

Since M is real symmetric, define M^+ to be its inverse on $(\ker M)^\perp$ and zero on $\ker M$; this is its Moore–Penrose pseudoinverse. After complexifying the maps, their kernels satisfy, with $\omega = e^{2\pi i/3}$,

$$\ker M = \ker V = \operatorname{span}_{\mathbb{C}}\{(\omega^i)_{i=1}^6, (\omega^{-i})_{i=1}^6\}. \tag{7.11}$$

Indeed, $\operatorname{rank} V = 4$ and $v_1 + v_4 = v_2 + v_5 = v_3 + v_6 = e_{s_*} - e_{s_0}$. Consequently the quotient VW is determined by MW even when W itself has a two-dimensional ambiguity. Figure 3 shows these partitions and the six cap vectors.

(a) Six tips and three open arcs



(b) The five boundary partitions

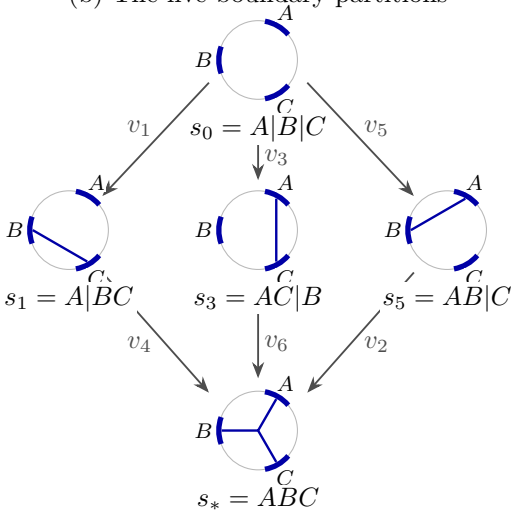


Figure 3: The six-tip partition and cap vectors. Thick boundary arcs are open. Interior blue segments indicate which of the three arcs belong to the same open component; the drawings represent partitions, rather than particular cluster geometries. An arrow points from the negative to the positive state in the corresponding vector v_i of (7.9). Closing the source follows the reverse transition, consistently with the unforced-minus-closed response. The three paths from s_0 to s_* give $v_1 + v_4 = v_3 + v_6 = v_5 + v_2$.

7.3 Screening integrals and their differential identities

For $x_1 < \cdots < x_6$ in the upper half-plane boundary, write $b = \bar{z}$. Euler's beta function is denoted by B [25, 5.12.1]. Set

$$F_0(\mathbf{x}; z, b) = (-i(z-b))^{3/4} \prod_{j<k} (x_k - x_j)^{1/3} \prod_j [(z - x_j)(b - x_j)]^{-1/2}, \tag{7.12}$$

$$K_i(\mathbf{x}; z) = \frac{F_0(\mathbf{x}; z, \bar{z})}{B(1/3, 1/3)} \int_{x_i}^{x_{i+1}} |z-u|^2 \prod_{j=1}^6 |x_j - u|^{-2/3}\, du, \qquad 1 \le i \le 5. \tag{7.13}$$

The branch of F_0 is positive when $b = \bar{z}$ and the boundary tips are real and ordered. For K_6 use the sum of the integrals over (x_6, ∞) and $(-\infty, x_1)$. The integrand is $O(u^{-2})$ at infinity. With the source at the center of the disk, these functions become

$$K_i(\theta) = \frac{\Delta(\theta)^{1/3}}{B(1/3,1/3)} \int_{I_i} \prod_{j=1}^{6} d(t,\theta_j)^{-2/3}\, dt, \qquad d(s,t) = |e^{is} - e^{it}|, \quad \Delta = \prod_{j<k} d(\theta_j,\theta_k), \tag{7.14}$$

where $I_i = (\theta_i, \theta_{i+1})$ and $\theta_7 = \theta_1 + 2\pi$. The measure in (7.14) is the ordinary angle measure dt. For example, at $z = i$ the substitution $x = -\cot(\theta/2)$ gives

$$K_{\mathbb{H}}(i; \mathbf{x}) = 2^{-5/4} K_{\mathbb{D}}(0; \theta), \tag{7.15}$$

in agreement with the derivative modulus $1/2$ of $(\zeta - i)/(\zeta + i)$ at i. The half-plane integral K_i in (7.13) is precisely $L\mathcal{K}_{i+1}$ of [15, (53), (55)] at $\kappa = 6$, with cyclic indices and all normalization factors included. Their prefactor L becomes F_0, and (7.14) is the conformal transport of this product to the disk.

Lemma 7.4 (Algebraic differential identities)**.** *Define*

$$g(u) = F_0(z-u)(b-u)\prod_j (x_j - u)^{-2/3},$$

and treat z, b as independent variables for differentiation. The operator $\mathcal{N}_z$ below is the differential realization of (4.16); Proposition 8.3 derives this realization from the boundary Ward identity. Here $\mathcal{N}_b$ is obtained by interchanging z and b, before setting $b = \bar{z}$. Then

$$\mathcal{B}_i g = -\partial_u\left(\frac{2g}{u - x_i}\right), \tag{7.16}$$

$$\mathcal{N}_z g = -\partial_u\left(\frac{g}{z - u}\right), \tag{7.17}$$

where

$$\mathcal{B}_i = 3\partial_{x_i}^2 + \sum_{j\neq i} \frac{2}{x_j - x_i}\partial_{x_j} + \frac{2}{z - x_i}\partial_z - \frac{5/4}{(z-x_i)^2} + \frac{2}{b - x_i}\partial_b - \frac{5/4}{(b-x_i)^2}, \tag{7.18}$$

$$\mathcal{N}_z = \sum_j \frac{1}{z - x_j}\partial_{x_j} + \frac{5/8}{(z-b)^2} + \frac{1}{z-b}\partial_b - \frac{2}{3}\partial_z^2. \tag{7.19}$$

In particular,

$$\mathcal{B}_i K_j = 0, \qquad \mathcal{N}_z K_j = \mathcal{N}_b K_j = 0 \quad (1 \le i, j \le 6). \tag{7.20}$$

Proof. Put $\ell = \log g$. The derivatives needed for (7.16)–(7.17) are

$$\begin{aligned}
\ell_z &= \frac{3}{4(z-b)} - \frac{1}{2}\sum_j \frac{1}{z - x_j} + \frac{1}{z-u},\\
\ell_b &= -\frac{3}{4(z-b)} - \frac{1}{2}\sum_j \frac{1}{b - x_j} + \frac{1}{b-u},\\
\ell_{x_i} &= \frac{1}{3}\sum_{j\neq i} \frac{1}{x_i - x_j} + \frac{1}{2(z-x_i)} + \frac{1}{2(b-x_i)} - \frac{2}{3(x_i - u)},\\
\ell_u &= -\frac{1}{z-u} - \frac{1}{b-u} + \frac{2}{3}\sum_j \frac{1}{x_j - u}.
\end{aligned}$$

Substitute $g_{vv}/g = \ell_{vv} + \ell_v^2$ in the two operators. Pairing the terms with denominators $x_i - x_j$ cancels their two-index sums. The remaining expressions are respectively $-2\ell_u/(u-x_i) + 2/(u-x_i)^2$ and $-\ell_u/(z-u) - 1/(z-u)^2$, which prove the identities.

Integrate on a boundary Pochhammer cycle around the two endpoints of the selected interval. Both endpoint exponents are $-2/3$, so the monodromy reduction factor is nonzero. Since $-2/3 > -1$, shrinking the cycle gives a constant nonzero multiple of the real interval integral. The total monodromy of the cycle is one; the exact derivatives in (7.16)–(7.17) therefore integrate to zero. On compact parameter sets one may keep a common cycle away from all singularities, which also justifies differentiation. The same argument on the real projective line handles the interval through infinity. Interchanging z and b gives the conjugate identity. □

The boundary BPZ system is the Coulomb-gas system of [15]; the calculation above also gives the required bulk identities.

There is also an elementary range relation. On the upper half-plane in the screening variable, choose $\arg(x_j - u) \in (-\pi, 0)$ and consider

$$g_+(u) = (z-u)(\bar{z}-u)\prod_j (x_j - u)^{-2/3}.$$

Its boundary value on interval I_i is ω^i times the positive integrand in (7.13); both tails through infinity have phase one. It has no interior pole, and is $O(u^{-2})$ at infinity. Closing the contour above the real line and then conjugating yields

$$\sum_i \omega^i K_i = \sum_i \omega^{-i} K_i = 0, \qquad K_1 + K_4 = K_2 + K_5 = K_3 + K_6. \tag{7.21}$$

In particular $K \in \operatorname{ran} M$. Define

$$R_{\mathrm{an}} = V M^+ K, \tag{7.22}$$

where M^+ is the Moore–Penrose inverse. Its first circulant row is

$$(1/18,\ 11/36,\ -7/36,\ 1/18,\ -7/36,\ 11/36).$$

If $S_o = K_1 + K_3 + K_5$ and $S_e = K_2 + K_4 + K_6$, then

$$\begin{aligned} R_{\mathrm{an}}(s_0) &= (S_o - 2S_e)/3, & R_{\mathrm{an}}(s_*) &= (2S_o - S_e)/3, \\ R_{\mathrm{an}}(s_1) &= (K_2 + K_6 - K_3 - K_5)/2, \\ R_{\mathrm{an}}(s_3) &= (K_2 + K_4 - K_1 - K_5)/2, \\ R_{\mathrm{an}}(s_5) &= (K_4 + K_6 - K_1 - K_3)/2. \end{aligned} \tag{7.23}$$

Remark 7.5 (The percolation value of the loop parameter). The loop parameter of [15, (9)] is $n = -2\cos(4\pi/\kappa)$, hence $n = 1$ at $\kappa = 6$. Their adjacent-triple relation (56), with its five cyclic translates, is $MW = K$ in our indexing. Their solved formula (57) divides by $(n^2-4)(n^2-1)$, which vanishes at $n = 1$. We do not use (57). The relation $K \in \operatorname{ran} M$ in (7.21) gives a solution, and any two solutions $W, W' \in \mathbb{R}^6$ satisfy

$$W - W' \in \ker M = \ker V, \qquad VW = VW'.$$

Thus the signed partition row is uniquely determined even though its six coefficients have a two-dimensional ambiguity. Choosing $W = M^+K$ gives (7.22).

7.4 A uniform estimate and the collision boundary data

When two neighboring tips meet, the short boundary arc between them disappears. The remaining experiment has four tips. For the uniqueness argument we need this reduction uniformly as the other tips move in a separated configuration, including the probability that the small arc continues to influence the interior.

Lemma 7.6 (Uniform angular estimate)**.** *There is a numerical constant C such that*

$$\sum_{i=1}^{6} K_i(\theta) \le C \tag{7.24}$$

uniformly over all strictly ordered circular configurations.

Proof. The sum is a single integral over the full circle. At an integration point t, choose the two nearest marks i, j, and order the remaining distances as $r_3 \le r_4 \le r_5 \le r_6$. The triangle inequality bounds each distance to a later mark by twice that mark's distance from t. Retaining the distance between i, j gives

$$\Delta^{1/3} \le C\, d(\theta_i, \theta_j)^{1/3} \prod_{m=3}^{6} r_m^{(m-1)/3}.$$

After multiplication by the screening factors, the integrand is at most

$$C\, d(\theta_i, \theta_j)^{1/3} d(t, \theta_i)^{-2/3} d(t, \theta_j)^{-2/3} r_3^0 r_4^{1/3} r_5^{2/3} r_6.$$

The last four factors are bounded, since every chord distance is at most 2. If $\ell = d(a, b)$, integrate $d(t, a)^{-2/3} d(t, b)^{-2/3}$ first in neighborhoods of size comparable to ℓ around the two marks. Rescaling these neighborhoods gives $C\ell^{-1/3}$. On a remaining dyadic shell of radius $2^k\ell$, both factors are bounded by $C(2^k\ell)^{-2/3}$ and the shell has length at most $C2^k\ell$. Summing gives

$$\int_0^{2\pi} d(t, a)^{-2/3} d(t, b)^{-2/3}\, dt \le C\ell^{-1/3}.$$

The factor $d(\theta_i, \theta_j)^{1/3}$ cancels this power. Partition the integration circle according to its nearest pair and sum over the fifteen possible pairs to obtain (7.24). □

Lemma 7.7 (Simple-pair cascade)**.** *Suppose that only the adjacent tips $i, i+1$ coalesce. The common limiting tip and the four remaining tips are assumed to range in a compact set of distinct circular points. Then*

$$K \longrightarrow M e_i G_4, \qquad R_{\mathrm{an}} \longrightarrow v_i G_4, \qquad R_{\mathbb{D}} \longrightarrow c_E v_i G_4, \tag{7.25}$$

locally uniformly on that simple collision face. Here G_4 is the product of the six chord distances between the four remaining tips, each raised to the power $1/3$, and c_E is the calibration constant in (5.24).

Proof. The screening integrals. Write $\delta = \theta_{i+1} - \theta_i$ in a local angular chart, and let ξ be their limiting point. On the short interval, put $t = \theta_i + \delta v$. The factor from the distance between the colliding tips is $\delta^{1/3}(1 + o(1))$. The two singular factors and the integration element contribute $\delta^{-4/3}\delta[v(1-v)]^{-2/3}dv$. The two distances from the colliding tips to any surviving tip contribute its chord distance from ξ to the power $2/3$ in $\Delta^{1/3}$; the corresponding screening factor contributes its inverse. These factors cancel. The remaining factor is precisely G_4.

On the interval immediately before the pair, put $t = \theta_i - \delta v$; the interval immediately after the pair is treated by $t = \theta_{i+1} + \delta v$. The limiting integrands on these two half-lines are $[v(1+v)]^{-2/3}$. Their integrals agree with the integral over the short interval:

$$\int_0^1 [v(1-v)]^{-2/3}\,dv = \int_0^\infty [v(1+v)]^{-2/3}\,dv = B(1/3, 1/3).$$

The second equality follows from $v = u/(1-u)$.

For uniformity, choose a fixed small angular neighborhood of ξ disjoint from the four surviving tips, uniformly over the specified compact face. Inside it the nonsingular factors converge uniformly. After rescaling, the integrable functions just displayed dominate the two endpoint singularities and the half-line tail. Outside it the three neighboring integrals retain the factor $\delta^{1/3}$ and have bounded remaining integrals. The other three intervals also have bounded integrals after their integrable endpoint singularities are included, and therefore tend to zero with this same factor. It follows that exactly the coordinates $i-1, i, i+1$ tend to G_4, uniformly on the compact face. This proves $K \to Me_iG_4$. The equality $VM^+M = V$ then gives the analytic-row limit. The argument takes place on the circle and also covers the pair $6, 1$.

A boundary exploration with a quantitative exceptional event. Fix a compact subset of the simple face, and for each nearby configuration let ξ be the midpoint of its short boundary arc. Choose $R > 0$ so small that a boundary neighborhood $B(\xi, R)$ is disjoint from the four surviving tips and from $B_{1/2}(0)$. Initially take $a \ll \delta \ll R$. Explore the interface starting at tip i until it terminates at $i+1$ inside this neighborhood or first reaches its outer edge. All revealed cells then lie in $B(\xi, R + O(a))$. In the first case call the exploration successful; its hull closes a cap on the short boundary arc. In the second case call it exceptional.

An exceptional exploration has a bank of the boundary color on the short arc connecting that arc to distance comparable with R. The opposite color has a uniformly positive probability of making a blocking crosscut in each fixed-ratio boundary semiannulus between scales $C\delta$ and cR. The two outer boundary segments in those semiannuli have this opposite color. RSW and color independence on separated layers therefore give constants $C, \gamma > 0$ for which

$$\mathbb{P}_a\{\text{exceptional exploration}\} \le C\left(\frac{\delta + a}{R}\right)^\gamma. \tag{7.26}$$

The constants are uniform on the compact face. This is also the boundary-arm estimate used in [5]; only its positive power is needed here. The event is measured under the original color law.

Averaging the conditional response. Keep the source radius $r < 1/4$ fixed while taking the mesh limit. The cap exploration is identical before and after closing $B_r(0)$. Conditional on its transcript, all cells in the protected disk remain independent fair cells, and the record in its complement acts by a partition-completion map of norm at most one. The scalar row on a fixed cut inside $B_{1/2}(0)$ has norm bounded by a constant and has source-radius error at most $Cr^{11/15}$. Both bounds are uniform over every possible cap transcript, including exceptional ones. They follow by applying Theorem 4.3 before exterior completion.

It follows that the scalar limit may be taken inside the averaged conditional response. Its total source-radius error is at most $Cr^{11/15}$, because the transcript masses sum to one. The part on exceptional transcripts has variation norm at most

$$C\left(\frac{\delta}{R}\right)^\gamma \tag{7.27}$$

after the mesh limit. The factor in (7.27) is the original probability of an exceptional transcript, multiplied by the uniform bound on its conditional scalar row.

On a successful transcript the source component has four active tips. The explored cap specifies its completion into the original five partition coordinates. If the disappearing arc is open ($i = 1, 3, 5$), that arc is separated from the other two open arcs; its label remains as an isolated class. If the disappearing arc is closed ($i = 2, 4, 6$), the open bank of the cap joins the two neighboring open labels. Applying these six completion maps to the four-tip join-minus-separate row gives, respectively, the six vectors v_i in (7.9).

Let U be the source component on a successful transcript and $f_U : U \to \mathbb{D}$ its map normalized at zero. The four-tip calibration (5.24) and Lemma 7.1 identify the completed scalar response as

$$c_E v_i |f_U'(0)|^{5/4} \prod_{j<k\,;\,j,k\notin\{i,i+1\}} |f_U(e^{i\theta_j}) - f_U(e^{i\theta_k})|^{1/3}.$$

It is integrated with the original probability of the transcript.

Convergence of the remaining quad. Every successful hull lies inside $B(\xi, R)$, so its source component U contains $\mathbb{D} \setminus \overline{B(\xi, R)}$ and is contained in $\mathbb{D}$. Consider any sequence $R_n \downarrow 0$, of successful hulls, and of configurations on the chosen compact face. Pass to a limit of the boundary configurations. Every compact subset of $\mathbb{D}$ belongs to all sufficiently large U_n, so their kernel limit is $\mathbb{D}$. Their maps $f_n : U_n \to \mathbb{D}$, normalized by $f_n(0) = 0$ and $f_n'(0) > 0$, converge to the identity, together with their derivatives, on compact interior sets.

The four surviving tips stay a positive distance from the collapsing pair. Around each limiting surviving tip, a fixed neighborhood meets U_n in the unit disk for all large n. Schwarz reflection extends f_n through that circular boundary arc. These extensions are locally bounded uniformly in n: inside the disk $|f_n| \le 1$, while outside it

$$f_n(\zeta) = \frac{1}{\overline{f_n(1/\bar{\zeta})}}, \qquad |f_n(\zeta)| \le |\zeta|.$$

For the inequality, the inverse map sends $\mathbb{D}$ into $\mathbb{D}$ and fixes zero, so Schwarz's lemma gives $|f_n(u)| \ge |u|$ on U_n. Normal-family compactness and the known interior limit now force the reflected extensions to converge to the identity on these fixed neighborhoods. In particular, the images of the moving surviving tips converge to their original positions.

The derivative at zero and the six pairwise distances between the four surviving image tips therefore converge to those of the disk. The product in the preceding display is a continuous function of these quantities, with all four tips distinct. Its difference from $c_E v_i G_4$ tends to zero along every sequence just considered. If its supremum over successful transcripts did not tend to zero, choosing a sequence with a fixed positive discrepancy would contradict this conclusion. Hence that supremum is bounded by a modulus $\omega(R) \to 0$, uniformly on the compact simple face.

Combining successful and exceptional transcripts, and including the missing exceptional mass of the comparison row, gives

$$\|R_{\mathbb{D}} - c_E v_i G_4\|_{\mathrm{var}} \le C \left(\frac{\delta}{R}\right)^{\gamma} + \omega(R). \tag{7.28}$$

The mesh and source limits have been taken in this inequality. First send $\delta \downarrow 0$ at fixed R, and then send $R \downarrow 0$. Every bound is uniform on the compact simple face, which proves the required locally uniform cascade. □

Remark 7.8. Simple collision faces provide the boundary values used below. At a simultaneous triple collision, neighboring screening integrals may retain the ratios of the shrinking gaps. Lemma 7.10 shows that the stopped diffusion reaches a simple face almost surely.

7.5 The differential equation for the response

The stopped exploration gives a martingale for the percolation response. Testing that identity first produces the differential equation in distributions. Ellipticity then supplies the smoothness needed for its classical interpretation.

Define $\partial_i = \partial/\partial\theta_i$ and

$$L_i = 3\partial_i^2 + \sum_{j\neq i} \cot\frac{\theta_j - \theta_i}{2}\partial_j, \tag{7.29}$$

$$G = \sum_{i=1}^{6} L_i = 3\sum_i \partial_i^2 + \sum_j \sum_{i\neq j} \cot\frac{\theta_j - \theta_i}{2}\partial_j. \tag{7.30}$$

The boundary identities of Lemma 7.4, transformed to the disk with its source at zero, give

$$(L_i + y)R_{\mathrm{an}} = 0, \qquad (G + 6y)R_{\mathrm{an}} = 0. \tag{7.31}$$

Lemma 7.9 (Angular equation for the response)**.** *The row is smooth in the interior of the ordered angular chamber and satisfies*

$$(L_i + y)R_{\mathbb{D}} = 0, \qquad (G + 6y)R_{\mathbb{D}} = 0. \tag{7.32}$$

Proof. Lemma 7.1 gives continuity of the row on every compact interior set, as a uniform limit of continuous fixed-radius responses. Lemma 7.3 identifies, jointly with the exploration, its conditional residual value as $e^{yt}R_{\mathbb{D}}(0;\theta(t))$. In particular, for each i this is a bounded martingale under the diffusion with generator L_i until a compact stopping rule is reached. These rules may be restarted by the domain Markov property. On a compact angular set the coefficients of the displayed stochastic equation are smooth, so uniqueness of its local solutions identifies the successive restarts with the same angular diffusion. Boundedness of the row allows increasing localizations to be removed up to exit from that compact angular set. Thus the stopped martingale identity applies to its ordinary compact-set exit time as well.

Fix one coordinate F of the row and a test function $\varphi \in C_c^\infty$ supported in the interior chamber. Choose open sets with compact closure in that chamber so that $\operatorname{supp}\varphi$ lies a positive distance inside the smaller set U. Extend the drift coefficients of L_i smoothly outside the larger set, with bounded derivatives, while keeping its constant diffusion matrix. Write $P_t^i f(\theta) = \mathbb{E}_\theta[f(X_t)]$ for the transition operator of this extended equation, and extend F boundedly outside U. Up to the exit time τ_U, the extended equation agrees with the local angular equation.

The distance from $\operatorname{supp}\varphi$ to ∂U is positive. Its drift is bounded, so for sufficiently small t an exit before t requires a fixed positive Brownian displacement. The Brownian maximal inequality gives

$$\sup_{\theta\in\operatorname{supp}\varphi} \mathbb{P}_\theta(\tau_U \le t) \le Ce^{-c/t}.$$

The stopped martingale identity, followed by the bound on F, therefore implies

$$e^{yt}P_t^i F - F = O(e^{-c/t}) \tag{7.33}$$

uniformly on $\operatorname{supp}\varphi$.

Let $(P_t^i)^*$ be the adjoint on densities with respect to angular Lebesgue measure, and let L_i^* be the formal differential adjoint. For these smooth extended coefficients,

$$e^{yt}(P_t^i)^*\varphi = \varphi + t(L_i^* + y)\varphi + o_{L^1}(t). \tag{7.34}$$

One may verify this directly from the stochastic flow. The noise is additive, and the derivatives of the drift are bounded, so the flow is a smooth change of the initial point. Changing variables by its inverse expresses $(P_t^i)^*\varphi$ as the expected transported test function multiplied by the inverse Jacobian. Taylor expansion uses Brownian mean zero and covariance t; the first drift term and the first Jacobian term together give the adjoint of the first-order part of L_i. The second noise term gives $3\partial_i^2\varphi$. The remaining terms are $o(t)$ in L^1, since the test has compact support and the flow derivatives have bounded moments on a short time interval. This proves (7.34).

Multiply (7.33) by φ, integrate, and use (7.34). After division by t and letting $t \downarrow 0$, boundedness of F gives

$$\langle F, (L_i^* + y)\varphi\rangle = 0.$$

Thus $(L_i + y)F = 0$ distributionally for every i. Their sum is $(G + 6y)F = 0$. On every interior compact set, G has smooth coefficients and principal part $3\sum_i \partial_i^2$, so interior elliptic regularity gives a smooth representative [24, Theorem 15.2]. The continuity established identifies it with F at every interior point. Each individual L_i identity consequently holds classically as well. □

7.6 Killed uniqueness on the circular chamber

The boundary values determine the bounded solution because the diffusion reaches a collision sufficiently quickly. The rate of this exit is stronger than the exponential factor in the martingale. We compute both rates and prove the simple-face exit asserted in Remark 7.8.

For n ordered circular angles, the angular chamber is $\theta_1 < \cdots < \theta_n < \theta_1 + 2\pi$, with configurations identified after simultaneous addition of 2π. Thus the common rotation variable is periodic and the chamber has finite volume. Use the same chord-distance product Δ with n marks, and set

$$u = \log \Delta, \qquad d\mu = \Delta^{2/3}\, d\theta, \qquad h = \Delta^{1/3}.$$

The n-tip version of G satisfies

$$G = 3\mu^{-1} \operatorname{div}(\mu\nabla), \tag{7.35}$$

$$\Delta_\theta u = -\frac{1}{2}\sum_{i<j} \csc^2 \frac{\theta_j - \theta_i}{2},$$

$$|\nabla u|^2 = \frac{1}{2}\sum_{i<j} \csc^2 \frac{\theta_j - \theta_i}{2} - \frac{n(n^2-1)}{12}. \tag{7.36}$$

Indeed, $\partial_i u = \frac{1}{2}\sum_{j\neq i} \cot((\theta_i - \theta_j)/2)$. In the squared gradient the diagonal terms use $\cot^2 = \csc^2 - 1$. The three products associated with each unordered triple have sum -1, by the cotangent addition formula. Their sum gives the constant in (7.36). Since $\nabla \log \mu = (2/3)\nabla u$, direct substitution gives

$$Gh = -\lambda_n h, \qquad \lambda_n = \frac{n(n^2-1)}{12}. \tag{7.37}$$

Lemma 7.10 (Survival and exit face)**.** *Let τ be the first collision time of the six-tip diffusion with generator G. For every interior starting configuration,*

$$\mathbb{P}_\theta\{\tau > t\} \le C_\theta e^{-35t/2}, \qquad t \ge 1. \tag{7.38}$$

At time τ, exactly one adjacent pair collides almost surely.

Proof. The killed process. The stochastic equation in the chamber is

$$d\theta_j = \sqrt{6}\, dB_j + \sum_{k\neq j} \cot\frac{\theta_j - \theta_k}{2}\, dt,$$

with independent Brownian motions. On every compact interior set its coefficients are smooth, so it has a unique solution up to exit from that set. Exhaust the chamber by smooth subdomains compactly contained in it and stop at their exit times. Their increasing limit is the diffusion killed at its first collision. The circular repelling-particle construction in [17, Section 4] supplies its continuous boundary paths; equivalently, the successive stopped solutions define the same process up to that first exit.

Write $P_t f(\theta) = \mathbb{E}_\theta[f(\theta(t)); t < \tau]$ for its killed transition operator. This definition fixes the boundary realization directly from the stopped process.

The survival exponent. The positive function h in (7.37) gives the exact identity

$$3\int |\nabla f|^2\, d\mu - \lambda_6 \int |f|^2\, d\mu = 3\int h^2 |\nabla(f/h)|^2\, d\mu \tag{7.39}$$

for compactly supported smooth f: expand the right-hand side and integrate the cross term by parts, using $Gh = -\lambda_6 h$. For the required pointwise probability bound, use the associated positive transform

$$P_t^h f = e^{\lambda_6 t} h^{-1} P_t(hf).$$

Its interior generator is, by the product rule,

$$G^h f = h^{-1} G(hf) + \lambda_6 f = 3\sum_j \partial_j^2 f + 2\sum_j \sum_{k\neq j} \cot\frac{\theta_j - \theta_k}{2}\partial_j f.$$

Here the transition results in [16, Section 5] apply with an explicit change of variables. That paper uses half-angles $x_j = \theta_j/2$ and equation (43), whose Brownian coefficient is one. Set its time to $s = 3t/2$. Our original diffusion then has parameter $\alpha = 1/3$, and G^h has parameter $2\alpha = 2/3$. In [16, Proposition 5.6], $b_\alpha = (3\alpha - 1)/2 = 0$ at $\alpha = 1/3$. Its martingale is $e^{\lambda_6 t} h(\theta(t))/h(\theta(0))$ up to killing. Proposition 5.6 of [16] therefore identifies P_t^h as a conservative Markov transition operator. Its transformed process never collides, by [16, Proposition 5.4], since $2/3 \geq 1/2$.

Proposition 5.7 of [16] bounds the time-one transition density of that transformed process by a constant times its invariant density. Proposition 5.5 and the semigroup property give the same upper bound at every later time. In our variables, for $t \geq 1$ and angular Lebesgue measure this says

$$p_t^h(\theta, \theta') \leq C\Delta(\theta')^{4/3}.$$

The fixed factor between chord distances and the sine differences used in [16], and the Jacobian of the half-angle change, are absorbed into C. Since $h^{-1} = \Delta^{-1/3}$, we obtain

$$\mathbb{E}_\theta^h[h(\theta(t))^{-1}] \leq C\int \Delta(\theta')\, d\theta' < \infty.$$

The integral is finite because the circular chamber has finite volume and all chord distances are at most 2. Finally the transform identity gives

$$\mathbb{P}_\theta\{\tau > t\} = e^{-\lambda_6 t} h(\theta)\mathbb{E}_\theta^h[h(\theta(t))^{-1}] \leq Ch(\theta)e^{-\lambda_6 t}.$$

As $\lambda_6 = 35/2$, this proves (7.38).

Excluding several particles at one collision point. Localize near a proposed collision of m consecutive particles, with their angular distances from all other particles bounded below. Choose a circular chart in which this group has diameter less than π, let $\bar\theta$ be its mean, and put $Q = \frac{1}{6}\sum_{j=1}^{m}(\theta_j - \bar\theta)^2$. Its martingale part has quadratic variation $4Q\,dt$. For each pair inside the group, the singular drifts $2/(\theta_j - \theta_k)$ give a total contribution $2/3$ to the drift of Q. The centered Brownian variances contribute $m-1$. Using $\cot(s/2) = 2/s + O(s)$ therefore gives

$$dQ = 2\sqrt{Q}\,dB + [(m-1)(1+m/3) + O(Q)]\,dt. \tag{7.40}$$

The external drift is a smooth function of a particle's position in this chart. Its constant part disappears after centering, and its remaining contribution is bounded by CQ. The same bound holds for the nonsingular part of the internal cotangents.

For $m \geq 3$, the constant drift in (7.40) is at least 4. Up to the localization exit, comparison bounds Q below by the solution of $dZ = 2\sqrt{Z}\,dB + (4 - CZ)dt$ starting at the same positive value. After multiplication by e^{Ct} and the time change $(e^{Ct}-1)/C$, this is a squared Bessel process of dimension 4. It cannot hit zero. The Bessel comparison and its collision interpretation are the mechanism in [17, Theorems 1–3].

Excluding simultaneous collisions at different points. If two separated pairs were to collide at the first exit, form Q as the sum of their two centered squared radii, each divided by 6. The Brownian parts for the two pairs are orthogonal. Their sum therefore again has quadratic variation $4Q\,dt$. Each pair contributes $5/3$ to the drift, while the interaction between the separated pairs contributes $O(Q)$. The constant drift is now $10/3 > 2$, so the same comparison excludes zero. Three separated pairs are excluded by selecting any two of them. A cluster of three or more particles is covered by the preceding paragraph.

There are finitely many possible groups of particle labels. Choose local charts and positive separation bounds from countable families and start the comparisons at rational times before a proposed first collision. Every multiple-collision configuration belongs to one of these localizations. Their exclusion leaves precisely one simple adjacent pair. Its squared-radius dimension is $5/3$; the survival estimate also shows that the first collision time is finite almost surely. □

Proposition 7.11 (Bounded six-tip uniqueness)**.** *Two bounded smooth interior solutions of $(G + 15/2)F = 0$ with equal limits on every simple-pair face, locally uniformly along that face, agree throughout the chamber.*

Proof. Let U be their difference and let τ_ε be the first time that an adjacent circular gap becomes at most ε. For a fixed t, Itô's formula and the differential equation give

$$U(\theta) = \mathbb{E}_\theta\left[e^{(15/2)(t\wedge\tau_\varepsilon)}U(\theta(t\wedge\tau_\varepsilon))\right].$$

The integrand is bounded by $e^{15t/2}\|U\|_\infty$. As $\varepsilon \downarrow 0$, the stopping times increase to the first collision time. Lemma 7.10 says that the collision point lies on a simple face almost surely. At such a point all the other gaps are positive, so the sample path eventually lies in a compact subset of that face together with its adjacent interior. The locally uniform boundary hypothesis gives $U(\theta(\tau_\varepsilon)) \to 0$ on $\{\tau \leq t\}$. Dominated convergence consequently yields

$$U(\theta) = \mathbb{E}_\theta[e^{15t/2}U(\theta(t)); \tau > t].$$

The survival bound now gives $|U(\theta)| \leq C_\theta\|U\|_\infty e^{-10t}$. Letting $t \to \infty$ proves uniqueness. □

We apply Proposition 7.11 coordinatewise. The row is bounded by Lemma 7.1, and the analytic row is bounded by Lemma 7.6. Equation (7.31) and Lemma 7.9 give their differential equations; their locally uniform simple-face values agree by Lemma 7.7. Thus

$$R_D(z) = c_E\, V M^+ K_D(z). \tag{7.41}$$

Conformal covariance transports the disk equality to the original domain. Applying a common bounded exterior completion preserves it on every original boundary label. The analytic identity (7.20) now gives, coordinatewise,

$$\mathcal{N}_z R_D = \mathcal{N}_{\bar z} R_D = 0. \tag{7.42}$$

Section 8 identifies these differential operators with the stress descendants of the constructed scalar.

Remark 7.12. For four tips, $\lambda_4 = 5 = 4y$, and G_4 is a nonzero homogeneous solution. Its amplitude is the constant c_E fixed by the disk calibration (5.24).

8 The Ward identity in a marked domain

A rotating ellipse measures a directional change in the connections around the scalar source. The boundary tips also move when the ellipse is straightened. Keeping these motions in the calculation produces the boundary terms in the Ward identity.

We first construct the two local sources with the boundary partition still retained. The construction uses the complete-record estimates of Paper I; the boundary Ward identity is then obtained from the corresponding percolation experiment.

8.1 Joint sources in a marked domain

For a finite-tip domain D, let π_D be the partition of its labelled open boundary arcs in a percolation configuration. As in Section 7, e_{π_D} is the unit row at that partition. At positive scalar radius r and stress radius s, define the row

$$F_{D;r,s}(w,z) = \lim_{a\downarrow 0} \mathbb{E}_D^a\left[\tau_{a,s,e}(w) E^\circ_{a,r}(z) e_{\pi_D}\right],$$

where $E^\circ_{a,r}$ is the scalar regulator in (4.2) and $\tau_{a,s,e}$ is the angular regulator of Section 4.3. The expectation is coordinatewise in the finite boundary-partition space. A bounded function of this partition is attached after the row has been formed.

Lemma 8.1 (Joint source limits with boundary labels)**.** *Suppose the scalar and stress centers have disjoint source cuts of scale $d > 0$ contained in D. Then $F_{D;r,s}(w,z)$ has a limit $\langle T(w)E^\circ(z)\rangle_D$ as $r, s \downarrow 0$, independently of their relative rates. For sufficiently small r, s,*

$$\|\langle T(w)E^\circ(z)\rangle_D\|_{\mathrm{var}} \le C d^{-13/4}, \tag{8.1}$$

$$\|F_{D;r,s}(w,z) - \langle T(w)E^\circ(z)\rangle_D\|_{\mathrm{var}} \le C d^{-13/4}\left\{(r/d)^{11/15} + (s/d)^{1/4}\right\}. \tag{8.2}$$

The constants are independent of the number and separation of the boundary tips and of fixed exterior identifications of their labels. Fixed positive-radius limits, followed by these source limits, are continuous on compact classes of marked Carathéodory convergent domains whose source cuts remain in a common interior region. The same assertions hold with $\bar T$.

Proof. Fixed positive radii. The forcing identity (4.3) writes each coordinate of the regulated expectation as a linear combination, followed by an angular integral, of boundary-partition probabilities with two specified closed holes. The coefficients depend only on the fixed radii $r, s > 0$. Thus the required mesh limit concerns bounded connection events at positive scales.

Let $F^a_{D;r,s}$ denote the expectation before the mesh limit. Write $K_\phi = K_{s,e,\phi}(w)$, and use the boundary-partition rows of Lemma 7.1. At every mesh the forcing identity gives

$$F^a_{D;r,s}(w,z) = \frac{1}{2\pi e s^2 r^y} \int_0^{2\pi} e^{-2i\phi} \left(\mu^a_{D;K_\phi} - \mu^a_{D;K_\phi, B_r(z)} \right) d\phi. \tag{8.3}$$

Each term is a probability row on the same labelled boundary partitions, with one or two analytic holes. The finite-hole assertion of Lemma 7.1 therefore supplies its mesh limit, its conformal invariance, and its continuity along marked domain sequences. Its proof includes joint boundary connections and interior circuit events, followed by the complete-record collar comparison of [29, Lemmas 12.1 and 13.1].

At fixed $r, s > 0$, the hole boundaries have common analytic chart and separation bounds as ϕ varies. The normalized maps and their derivatives converge on the protected interior, so their images also converge in C^2 normal coordinates. The integrand in (8.3) has variation norm at most two. Thus the angular expression has the mesh-independent bound $2r^{-5/4}/(es^2)$, and bounded convergence passes the orientation integral to the limit. The same argument applies when the source centers and orientation vary in compact separated sets, and to the analytic image holes used below. A one-cell boundary adjustment is absorbed by the fixed-scale collar estimate. This proves existence of $F_{D;r,s}$ in both smooth and slit domains before either source radius is removed.

Removal of the local source radii. Inside the two disjoint cuts, form the scalar row and the angular row before completing them through the rest of D. The latter completion has norm at most one: for each pair of local records it samples the remaining colors, joins the partitions, and returns one boundary partition. Its definition is independent of r, s. Thus Theorem 4.3 and [29, Theorem 9.1] give, respectively, row norms $Cd^{-5/4}$ and Cd^{-2}, and normalized Cauchy errors $(r/d)^{11/15}$ and $(s/d)^{1/4}$. For two regulator pairs, change one row at a time. Multilinearity and the completion contraction bound the difference by the changed-row error times the norm of the unchanged row. Comparison through the coordinatewise smaller pair proves a unique joint limit and (8.1)–(8.2). The argument is unchanged when the exterior completion retains further labels or imposes a deterministic wiring.

Continuity and uniformity in the domain. Fix positive r, s and a compact class of marked domains with the two source cuts in a common interior region. For a convergent sequence $D_n \to D$, identify the finite partition spaces by the cyclic labels of the open arcs. The fixed-hole argument above gives convergence of each partition probability, both for continuum domains D_n and for lattice domains at meshes $a_n \downarrow 0$ converging to D. This also permits the centers and ellipse orientations to vary in compact parameter sets: on the protected interior the disk maps and all their derivatives converge, so the transported targets converge smoothly and are bracketed by vanishing offsets. After (4.3), the row is a linear combination of partition probabilities with coefficients bounded by $r^{-5/4}/(es^2)$, uniformly in the mesh. The probabilities lie between zero and one. Bounded convergence therefore passes the orientation integral to the limit. There are finitely many partition coordinates, so

$$\|F_{D_n;r,s} - F_{D;r,s}\|_{\mathrm{var}} \longrightarrow 0.$$

The same conclusion holds for the lattice rows in place of the first term, with their meshes tending to zero.

These two sequential statements give compact uniformity of the fixed-radius mesh limit. Otherwise choose meshes and marked domains for which the lattice row and its continuum row

differ by a fixed positive amount. Compactness supplies a marked-convergent subsequence. The lattice rows converge to the kernel of its limiting domain by the second statement, and the continuum rows converge to that same kernel by the first, contradicting the discrepancy.

Write F_D for the joint source limit. The local Cauchy bound gives

$$\|F_{D_n} - F_D\|_{\mathrm{var}} \le \|F_{D_n;r,s} - F_{D;r,s}\|_{\mathrm{var}} + 2Cd^{-13/4}\{(r/d)^{11/15} + (s/d)^{1/4}\}.$$

First let $n \to \infty$ at fixed r, s, then let $r, s \downarrow 0$. This proves continuity of F_D. The same Cauchy bound is uniform over the domain class and over the allowed centers, so it also proves locally uniform removal of the source radii. Source derivatives are taken by duality after smooth testing, and fixed separated contour integrals pass to these limits by the uniform row bounds. The scalar-only assertion follows by omitting the angular slot. Conjugating that slot proves the assertions for $\bar{T}$. □

This lemma constructs the boundary-domain stress–scalar correlation from its regulators. In particular, it supplies uniform convergence on a fixed stress contour separated from the scalar source. The local shape comparison also gives, for a conformal map f,

$$\langle T(w)E^{\circ}(z)\rangle_D = f'(w)^2|f'(z)|^{5/4}\langle T(f(w))E^{\circ}(f(z))\rangle_{f(D)}, \tag{8.4}$$

with all boundary labels transported. To verify this, apply fixed-hole covariance first. A radius-r scalar disk differs from its affine image by normal displacement $O(r^2)$, and a radius-s ellipse has displacement $O(s^2)$. After normalization, the strip bound gives errors $O(r^{p-1/4})$ and $O(s^{p-1})$, for $1 < p < 5/4$. The other local row is bounded. The affine changes give $|f'(z)|^{5/4}$ and $f'(w)^2$; both errors vanish. This argument requires regularity of f near the source cuts, which holds for the Riemann maps of the stopped domains.

8.2 The angular source and an exact reflected map

We compute the new correlation in $\mathbb{H}$, with ordered real tips $\mathbf{x} = (x_1, \dots, x_k)$, where $k = 4$ or 6. For e in a fixed compact subinterval of $(0, 1)$, the stress prescription is

$$T(w) = \lim_{s\downarrow 0}\lim_{a\downarrow 0}\frac{1}{2\pi e s^2}\int_0^{2\pi} e^{-2i\phi}H^a_{K_{s,e,\phi}(w)}\,d\phi \tag{8.5}$$

inside the boundary-partition correlations constructed above. An angularly constant term has zero contribution. The normalization is [29, (4.8)].

Fix $w \in \mathbb{H}$, separated from the scalar source z, the boundary, and the tips, and put

$$t = es^2e^{2i\phi}, \qquad f_t(\zeta) = \zeta + \frac{t}{\zeta - w} + \frac{\bar{t}}{\zeta - \bar{w}}. \tag{8.6}$$

For small s, this map is injective on $\mathbb{H} \setminus \overline{B_s(w)}$. Indeed,

$$f_t(\zeta_1) - f_t(\zeta_2) = (\zeta_1 - \zeta_2)\left[1 - \frac{t}{(\zeta_1 - w)(\zeta_2 - w)} - \frac{\bar{t}}{(\zeta_1 - \bar{w})(\zeta_2 - \bar{w})}\right], \tag{8.7}$$

and the modulus of the perturbation of 1 is at most $e + es^2/(\operatorname{Im} w)^2 < 1$. On the real axis f_t is real, strictly increasing, and fixes infinity. It maps the punctured half-plane onto the half-plane minus the analytic body $\widehat{K}_{s,t}$ bounded by $f_t(\partial B_s(w))$.

Without the reflected term, the circle image is $K_{s,e,\phi}(w)$. The reflected term changes its boundary by normal distance at most $C|t| = O(s^2)$, in a controlled analytic target class. The local strip estimate gives

$$\frac{1}{es^2}\|\nu_{\widehat{K}_{s,t}} - \nu_{K_{s,e,\phi}}\|_{d,*} \le C\frac{\alpha_4(Cs,d)}{s} = O(s^{p-1}), \qquad 1 < p < \frac{5}{4}. \tag{8.8}$$

Attaching the separated scalar row multiplies this error by at most its fixed-cut norm. Thus $\widehat{K}_{s,t}$ has the same limiting angular response as the specified ellipse.

On compact subsets separated from $w, \bar{w}$, the inverse map $g_t = f_t^{-1}$ satisfies

$$\begin{aligned} g_t(\zeta) &= \zeta + \frac{t}{w-\zeta} + \frac{\bar{t}}{\bar{w}-\zeta} + O(|t|^2), \\ g_t'(\zeta) &= 1 + \frac{t}{(w-\zeta)^2} + \frac{\bar{t}}{(\bar{w}-\zeta)^2} + O(|t|^2). \end{aligned} \tag{8.9}$$

The remainders and every fixed number of their spatial derivatives are uniform on these compact sets.

8.3 Transport of the scalar response

Let $R_s(\mathbf{x}; z, \bar{z})$ denote the scalar boundary-partition row in $\mathbb{H} \setminus \overline{B_s(w)}$, with the circle forced closed, and write $R = R_0$ for the row in $\mathbb{H}$. The center w and radius s of this ordinary circle remain fixed while the other coordinates move. Both rows are obtained by removing the scalar regulator using its uniform Cauchy estimate.

Apply fixed-hole covariance to g_t. The nonaffine image of the scalar disk has normal displacement $O(|t|r^2)$ from its affine image. Before removing the scalar radius, its normalized error is bounded by

$$C|t|r^{-5/4}\alpha_4(Cr,d)r \le C_p|t|r^{p-1/4}, \qquad 1 < p < 5/4. \tag{8.10}$$

At each fixed $s > 0$, this tends to zero as $r \downarrow 0$, including after division by $es^2 = |t|$. Consequently the scalar row with $\widehat{K}_{s,t}$ closed is

$$|g_t'(z)|^{5/4} R_s(g_t(x_1), \dots, g_t(x_k); g_t(z), \overline{g_t(z)}).$$

Denote this transport of a row F by $\mathcal{A}_t F$. This notation includes the scalar multiplier and the motion of all the real and complex coordinates in the displayed expression.

The extra circle has a small unnormalized effect. Choose its own local cut, disjoint from the scalar cut. The hole-influence estimate [29, (4.6)] and the scalar-row bound give

$$\sup_{\mathbf{x},z} \|R_s(\mathbf{x}; z) - R(\mathbf{x}; z)\|_{\mathrm{var}} \le C\alpha_4(Cs,d) \le C_p s^p$$

on any fixed separated compact set. This estimate is uniform in the scalar regulator before its removal.

We need its angular coefficient, rather than its value divided by s^2. Take a smooth test $\psi(\mathbf{x}, z)$ supported in the ordered tip chamber and away from the source and boundary collisions. A change of variables in the real tip coordinates and the two real coordinates of z gives

$$\langle \mathcal{A}_t F, \psi \rangle = \langle F, \psi_t \rangle.$$

The transported test ψ_t includes the inverse Jacobian and the scalar multiplier. Formula (8.9) and Taylor's formula give, on one enlarged compact support,

$$\|\psi_t - \psi\|_{L^1} \le C_\psi |t|, \qquad \|\psi_t - \psi - t\psi_+ - \bar{t}\psi_-\|_{L^1} \le C_\psi |t|^2$$

for fixed smooth tests ψ_+, ψ_-. This is the test-transport calculation of [29, Lemma 17.2], with the real boundary-tip coordinates included. In particular,

$$|\langle (\mathcal{A}_t - I)(R_s - R), \psi\rangle| \le C_{\psi,p}|t|s^p. \tag{8.11}$$

The untransported row $R_s - R$ is independent of ϕ, so its second angular coefficient is zero. Dividing (8.11) by es^2 bounds its remaining coefficient by $C_{\psi,p}s^p$, which tends to zero.

The transport of R itself has a second-order tested remainder $O(|t|^2)$. Its normalized angular integral is $O(s^2)$. Together with (8.8), these estimates leave the first-order transport of R. The calculation takes $a \downarrow 0$, then $r \downarrow 0$, and then $s \downarrow 0$. The uniform Cauchy estimate in Lemma 8.1 gives the same limit at arbitrary relative source radii.

8.4 The doubled boundary Ward operator

The coefficient of t in the motion of the tips is $\sum_j (w - x_j)^{-1}\partial_{x_j}$. The tips have weight zero: their boundary-partition probabilities are conformally invariant. The motions of z and $\bar{z}$, together with the scalar multiplier, produce the remaining terms. The elementary Fourier identities

$$\frac{1}{2\pi es^2}\int_0^{2\pi} e^{-2i\phi} t\, d\phi = 1, \qquad \frac{1}{2\pi es^2}\int_0^{2\pi} e^{-2i\phi}\bar{t}\, d\phi = 0$$

fix the sign and coefficient of this variation.

Proposition 8.2 (Finite-tip Ward identity)**.** *For the four-tip or six-tip scalar response in $\mathbb{H}$, coordinatewise in its boundary partition,*

$$\begin{aligned}\langle T(w)E^\circ(z)\rangle_{\mathbf{x}} = \Big[&\sum_j \frac{1}{w - x_j}\partial_{x_j} + \frac{5/8}{(w-z)^2} + \frac{1}{w-z}\partial_z \\ &+ \frac{5/8}{(w-\bar{z})^2} + \frac{1}{w-\bar{z}}\partial_{\bar{z}}\Big] R(\mathbf{x}; z, \bar{z}).\end{aligned} \tag{8.12}$$

The identity holds weakly in the tip and scalar coordinates. On separated configurations it has the smooth representative obtained by differentiating the response identified in Section 7.

Proof. The preceding subsection reduces the angular insertion to the coefficient of t in $\mathcal{A}_t R$. By (8.9), the velocities of $x_j, z, \bar{z}$ in that coefficient are $1/(w - x_j), 1/(w - z), 1/(w - \bar{z})$, respectively. The coefficient from $|g_t'(z)|^{5/4}$ is

$$\frac{5/8}{(w-z)^2} + \frac{5/8}{(w-\bar{z})^2}.$$

Pairing with a smooth test gives precisely the distributional operator in (8.12). The two Fourier integrals above select this coefficient and discard the conjugate one. The bounds (8.8), (8.10), and (8.11) justify each limiting step for the regulators. The identified four-tip and six-tip rows are smooth away from collisions, so the displayed differential expression is their representative. In particular, it is holomorphic in w away from $z, \bar{z}$ and the real tips. □

Proposition 8.3 (Four-tip and six-tip null identity)**.** *In a simply connected source domain with at most six alternating active boundary tips, the scalar response obeys both level-two null identities, coordinatewise in the boundary partition.*

Proof. First work in $\mathbb{H}$. For a positively oriented contour Γ surrounding z and no other insertion, the contour operation is

$$\langle (L_{-2}E^{\circ})(z)Y\rangle = \frac{1}{2\pi i}\oint_{\Gamma}\frac{\langle T(w)E^{\circ}(z)Y\rangle}{w-z}\,dw. \tag{8.13}$$

Here Y may be any fixed bounded completion of the boundary partition. Lemma 8.1 passes the regulator limits through this fixed contour. Holomorphy from Proposition 8.2 makes the value independent of the contour within the source neighborhood.

The integral extracts the coefficient regular at $w=z$ from (8.12). Its terms with poles at $w=z$ give no regular coefficient, while the remaining terms give

$$\langle (L_{-2}E^{\circ})(z)\rangle_{\mathbf{x}} = \left[\sum_j \frac{1}{z-x_j}\partial_{x_j} + \frac{5/8}{(z-\bar z)^2} + \frac{1}{z-\bar z}\partial_{\bar z}\right] R. \tag{8.14}$$

Subtracting $(2/3)\partial_z^2 R$ yields $\mathcal{N}_z R$ from (7.19). For six tips, this is zero by (7.42). For four tips, the calibrated row of Remark 7.12 is the fixed join-minus-separate vector times the factor

$$G_{4,\mathbb{H}}(\mathbf{x};z) = (2\operatorname{Im} z)^{3/4}\frac{\prod_{j<k\le 4}(x_k-x_j)^{1/3}}{\prod_{j=1}^4 |z-x_j|}. \tag{8.15}$$

The logarithmic derivatives of this factor are

$$\begin{aligned}
\partial_z \log G_{4,\mathbb{H}} &= \frac{3}{4(z-\bar z)} - \frac{1}{2}\sum_{j=1}^4 \frac{1}{z-x_j},\\
\partial_{\bar z} \log G_{4,\mathbb{H}} &= -\frac{3}{4(z-\bar z)} - \frac{1}{2}\sum_{j=1}^4 \frac{1}{\bar z-x_j},\\
\partial_{x_j} \log G_{4,\mathbb{H}} &= \frac{1}{3}\sum_{\ell\neq j}\frac{1}{x_j-x_\ell} + \frac{1}{2}\left(\frac{1}{z-x_j}+\frac{1}{\bar z-x_j}\right).
\end{aligned}$$

Use

$$\begin{aligned}
\sum_j \frac{1}{z-x_j}\sum_{\ell\neq j}\frac{1}{x_j-x_\ell} &= \sum_{j<\ell}\frac{1}{(z-x_j)(z-x_\ell)},\\
\frac{1}{(z-x_j)(\bar z-x_j)} &= \frac{1}{z-\bar z}\left(\frac{1}{\bar z-x_j}-\frac{1}{z-x_j}\right).
\end{aligned}$$

Substitution in (8.14), followed by $\partial_z^2 G/G = (\partial_z \log G)^2 + \partial_z^2 \log G$, gives $(2/3)\partial_z^2 G_{4,\mathbb{H}}$. This proves the four-tip identity. With zero or two tips, the boundary-partition space has one state: there is at most one open boundary arc. Its law is a unit mass for every source hole, so its scalar response and both descendants vanish.

The null combination transforms covariantly, as the following calculation shows. Choose a conformal map $f: D\to\mathbb{H}$ independently of the moving source point on its test patch. All fields on the right of the next two formulas are evaluated at $f(z)$, with the other labels transported. The tensor law (8.4) and the regular coefficient of the TE° expansion give

$$\begin{aligned}
(L_{-2}E^{\circ})_D(z) = |f'(z)|^{5/4}&\left[f'(z)^2 L_{-2}E^{\circ} + \frac{3}{2}f''(z)\partial E^{\circ}\right]\\
&+ |f'(z)|^{5/4}\left[\frac{5}{12}\frac{f'''(z)}{f'(z)} - \frac{5}{32}\left(\frac{f''(z)}{f'(z)}\right)^2\right]E^{\circ}.
\end{aligned}$$

Indeed, the regular coefficients of $f'(w)^2/(f(w)-f(z))$ and $f'(w)^2/(f(w)-f(z))^2$ are respectively $3f''(z)/2$ and $2f'''(z)/(3f'(z))-(f''(z)/f'(z))^2/4$. Direct differentiation of scalar covariance gives

$$\partial_z^2\Big[|f'(z)|^{5/4}E^\circ(f(z))\Big] = |f'(z)|^{5/4}\left[f'(z)^2\partial^2E^\circ+\frac{9}{4}f''(z)\partial E^\circ\right] + |f'(z)|^{5/4}\left[\frac{5}{8}\frac{f'''(z)}{f'(z)}-\frac{15}{64}\left(\frac{f''(z)}{f'(z)}\right)^2\right]E^\circ.$$

Subtracting two thirds of the second expression from the first leaves

$$|f'(z)|^{5/4}f'(z)^2\left(L_{-2}-\frac{2}{3}\partial^2\right)E^\circ(f(z)).$$

The extra terms cancel because $h_E=5/8$ and the stress tensor has zero central charge. Hence the zero identity transports to D. Complex conjugation proves the antiholomorphic identity. □

9 Localization of the null identity

A distant observation can distinguish local source experiments only through the connections that leave the source neighborhood. We expose those connections while keeping a disk untouched. Up to six remaining tips, the preceding section gives an exact null identity. Eight or more tips require an eight-arm event, whose decay is stronger than the cost of the two derivatives.

The disk and the exploration rule will stay fixed while the source point moves inside a smaller patch. This makes the transcript law independent of that point and allows source derivatives to pass through the conditional expectation. We use the null operation (4.16). Its contour is (8.13); source derivatives have the distributional meaning of Section 4.3.

Theorem 9.1 (Common-spectator null identity)**.** *For every fixed finite separated spectator word Y in the field and completion class of Section 4,*

$$\langle\mathcal{N}_zE^\circ(z)Y\rangle=0,\qquad \langle\mathcal{N}_{\bar z}E^\circ(z)Y\rangle=0 \tag{9.1}$$

as source-coordinate distributions away from the spectator supports.

Proof. A fixed local experiment on each source patch. Let ψ be a smooth source test whose compact support stays a distance $d>0$ from the spectator cuts. Take $R>0$ sufficiently small compared with d, and choose a smooth partition of unity $\{\chi_j\}$ on $\operatorname{supp}\psi$, subordinate to disks $B_R(c_j)$, with bounded overlap and

$$|\nabla^m\chi_j|\le C_mR^{-m},\qquad m=0,1,2.$$

For each patch choose an outer source cut of radius comparable with d, containing $B_{8R}(c_j)$ and disjoint from all spectator cuts. Apply the exploration of [29, Section 8.1] inside this outer cut, protecting $B_{4R}(c_j)$. The stress contour is the fixed circle $\Gamma_j=\partial B_{2R}(c_j)$, and the scalar point lies in $B_R(c_j)$. Small enough regulators about every such scalar point and every point of Γ_j lie inside the protecting disk.

The common-transcript statement in Lemma 4.2 therefore applies simultaneously to all these interventions. At finite mesh, conditional on a transcript τ, the remaining cells are independent fair cells. The source component $U_a(\tau)$ is simply connected, contains $B_{4R-Ca}(c_j)$,

and has an even number $k_a(\tau)$ of active alternating tips. Joining its arc partition to the stored outside connections gives a completion map $C_a(\tau)$ of norm at most one. These assertions, including the retained-edge convention and the short access paths at the tips, are [29, Lemma 8.1 and Theorem 8.4(i)]. In particular both the law Π_a of the transcript and $C_a(\tau)$ are independent of z and of all the local regulator radii.

The spectator word gives a bounded exterior functional on the record at the outer cut. To see the bound before integration, first retain the rows in its own disjoint source cuts. Their scalar and angular row norms are bounded by Theorem 4.3 and [29, Theorem 9.1]; the normalized density-root bounds are Lemma 4.1. The final parity and connectivity completion is a contraction. Thus the exterior functional has norm at most a constant C_Y, uniform in its remaining source regulators. The cut scales here are fixed independently of R. It is enough to prove estimates for the local row after integrating against Π_a; exterior completion then multiplies them by C_Y.

The regularized conditional identity. For a scalar radius r, an angular radius s, and a smooth test φ supported in $B_R(c_j)$, the regulated and tested row for $\mathcal{N}_z E^\circ$ is

$$\begin{aligned}\mathcal{N}^a_{r,s}[U_a;\varphi] = \frac{1}{2\pi i}\oint_{\Gamma_j}\int \frac{\varphi(z)}{w-z}\mathbb{E}^a_{U_a}[\tau_{a,s,e}(w)E^\circ_{a,r}(z)e_{\pi_{U_a}}]\,d^2z\,dw \\ -\frac{2}{3}\int(\partial_z^2\varphi)(z)\mathbb{E}^a_{U_a}[E^\circ_{a,r}(z)e_{\pi_{U_a}}]\,d^2z. \qquad (9.2)\end{aligned}$$

The second line is integration by parts in the source coordinate. The finite-mesh completion identity is exact for each expectation in this formula. Since the transcript and its completion map do not depend on z, it remains exact after testing, differentiation by duality, and integration over the fixed contour: the local tested row is

$$\int \mathcal{N}^a_{r,s}[U_a(\tau);\varphi]C_a(\tau)\,\Pi_a(d\tau).$$

This equality is established before any limit or division according to the number of tips.

Uniform passage to the finite-tip null identity. Call a transcript good when $k_a \le 6$. For $0 < \delta < R$, restrict first to good transcripts whose distinct retained-edge marks are at Euclidean distance at least δ. Write sep_a for the minimum of these distances, with value $+\infty$ when fewer than two marks remain. At fixed R, δ, every deterministic sequence of these domains has a marked Carathéodory convergent subsequence, with a fixed number and cyclic order of tips and distinct limiting prime ends. The limiting domain contains $B_{4R}(c_j)$. This is [29, Lemma 8.3 and Theorem 8.4(iii)].

Keep $r, s > 0$ fixed and consider a deterministic sequence of these domains at meshes $a_n \downarrow 0$. Choose the marked-convergent subsequence just described, with limit U, and identify its partition coordinates by their cyclic labels. For each z in the support of φ and $w \in \Gamma_j$, Lemma 8.1 gives convergence of the regulated stress–scalar row to its row in U; the scalar-only statement gives the other term of (9.2). The centers and every target remain in the common protected interior. At fixed radii the elementary bounds $2r^{-5/4}/(es^2)$ and $2r^{-5/4}$ dominate the two regulated rows. Moreover $|w - z| \ge R$ on the contour and test support. Bounded convergence therefore passes both the source integral and the contour integral to the limit. Since the partition space is finite, this is convergence of the tested row in variation norm.

In the limiting domain, compare that fixed-radius tested row with its source limit. The contour kernel has uniformly bounded absolute integral, so the scalar and joint Cauchy estimates give a difference at most

$$C\left\{R^{-13/4}\|\varphi\|_{L^1} + R^{-5/4}\|\partial_z^2\varphi\|_{L^1}\right\}\left\{(r/R)^{11/15} + (s/R)^{1/4}\right\}.$$

The source limit is zero by Proposition 8.3, including the cases $k = 0, 2$; its conformal transport to U follows from the cancellation proved there. The constant in the last bound uses only the protected interior, so it is independent of U.

It follows that

$$\limsup_{a\downarrow 0} \sup_{\substack{\tau:\ k_a(\tau)\le 6\\ \mathrm{sep}_a(\tau)\ge\delta}} \|\mathcal{N}^a_{r,s}[U_a(\tau);\varphi]\|_{\mathrm{var}} \le C_{R,\varphi}\left\{(r/R)^{11/15} + (s/R)^{1/4}\right\}. \tag{9.3}$$

Indeed, if the left side exceeded this bound by a fixed amount, choose meshes and transcript values attaining that excess up to a smaller fixed error. Their marked-convergent subsequence has tested rows converging in variation norm to the fixed-radius row in U. The preceding estimate for that row contradicts the excess. This argument proves uniformity of the conditional row before its exterior completion. The maps $C_a(\tau)$ may vary arbitrarily: $\|mC_a(\tau)\|_{\mathrm{var}} \le \|m\|_{\mathrm{var}}$ transfers the same estimate without any assumption on their convergence.

It remains in this step to remove the separation restriction. The local scalar and joint row bounds, using cuts of scale R inside the protected disk, give

$$\|\langle E^\circ(z)\rangle_U\|_{\mathrm{var}} \le CR^{-5/4}, \qquad \|\langle T(w)E^\circ(z)\rangle_U\|_{\mathrm{var}} \le CR^{-13/4}, \quad z \in B_R(c_j),\ w \in \Gamma_j. \tag{9.4}$$

Their upper-limit versions hold uniformly before the source radii are removed. A finite cover by disjoint scalar and stress cuts supplies the same constants for all z, w in these sets. No tip separation enters these bounds. Since $\sup_z \oint_{\Gamma_j} |dw/(w-z)| \le C$, they imply

$$\limsup_{r,s\downarrow 0} \limsup_{a\downarrow 0} \sup_{U_a} \|\mathcal{N}^a_{r,s}[U_a;\varphi]\|_{\mathrm{var}} \le C\left\{R^{-13/4}\|\varphi\|_{L^1} + R^{-5/4}\|\partial_z^2\varphi\|_{L^1}\right\}$$

uniformly over all residual domains. The separation estimate [29, Theorem 8.4(ii)] gives $\limsup_{a\downarrow 0} \Pi_a(\mathrm{sep}_a < \delta) \le C\delta/R$. Multiply the last two bounds. For fixed R, their product tends to zero as $\delta \downarrow 0$. Equation (9.3), followed by this separation exhaustion, proves that all good transcripts have zero total contribution. The order is the mesh limit, removal of r, s, and then $\delta \downarrow 0$, with R fixed throughout.

Eight arms on the remaining transcripts. A bad transcript has $k_a \ge 8$. For this probability estimate only, fill the unexplored component with its unconditioned colors. Every surviving prefix is part of an original boundary-to-boundary interface chord entering $B_{4R+Ca}(c_j)$, and each original chord has at most two endpoint prefixes. At least four original chords therefore enter that disk.

Retain the first incoming and last outgoing portions of each of four such chords across the annulus between radii $8R$ and a fixed fraction of d. Orient a full chord with its open bank on the left. After both retained portions are oriented from the inner circle to the outer one, their left banks have opposite colors. The banks chosen from successive portions lie in distinct regions between the disjoint interfaces. They therefore give eight disjoint sampled arms, including both colors; one-cell displacements are absorbed by fixed changes of the annular radii. This is the bank extraction of [29, Section 7.3], with four chords in place of three. The polychromatic eight-arm exponent [5, Theorem 4, (9), and Remark 6] gives

$$\limsup_{a\downarrow 0} \Pi_a(k_a \ge 8) \le C_\zeta (R/d)^{21/4-\zeta}, \qquad \zeta > 0. \tag{9.5}$$

These probabilities are taken in the original product law, with the original transcript probabilities. The bound is uniform over boundary colors at the outer cut, since the annulus used here lies strictly inside that cut and all its cells are sampled independently.

Summation over the source patches. Use (9.4) on a bad transcript, multiply by (9.5), and take $\varphi = \psi\chi_j$. The contour contribution is bounded by

$$C_Y C_\zeta (R/d)^{21/4-\zeta} R^{-13/4} \|\psi\chi_j\|_{L^1}.$$

For the derivative contribution, integration by parts in (9.2) gives the bound

$$C_Y C_\zeta (R/d)^{21/4-\zeta} R^{-5/4} \|\partial_z^2(\psi\chi_j)\|_{L^1}.$$

The use of the transcript probability is legitimate in the presence of signed spectators: their bounded functional was attached after the local conditional row, and its norm is at most C_Y.

The bounded overlap and the derivative bounds for the partition of unity give

$$\sum_j \|\partial_z^2(\psi\chi_j)\|_{L^1} \le C\left(\|\nabla^2\psi\|_{L^1} + R^{-1}\|\nabla\psi\|_{L^1} + R^{-2}\|\psi\|_{L^1}\right), \tag{9.6}$$

and $\sum_j \|\psi\chi_j\|_{L^1} \le C\|\psi\|_{L^1}$. Thus no additional power arises from the number of patches. After taking the fixed-R limits and the compact exhaustion specified, only the bad-transcript contribution remains, and

$$|\langle \mathcal{N}_z E^\circ, Y; \psi\rangle| \le C_{\psi,Y,\zeta} R^{21/4-13/4-\zeta} = C_{\psi,Y,\zeta} R^{2-\zeta}. \tag{9.7}$$

Choose $0 < \zeta < 2$ and let $R \downarrow 0$. This proves the holomorphic identity in (9.1). Complex conjugation proves the antiholomorphic identity with the same estimates. □

10 The disk response and the energy field

A nearby pair of density marks can first join at any of many annular scales. Each scale changes the same local connection choice seen by a small obstacle. The logarithm in the microscopic energy normalization counts these contributions. We compare the energy source of Camia and Feng [27, (1.8)–(1.9)], defined in (4.24), with the disk row (4.4), keeping the entire outgoing record. A four-arm coupling compares the annular responses with the same disk row; the assumed three-point limit (4.26) fixes its coefficient.

10.1 Local response and pivotality

Closing a region measures the dependence of connections on its colors. For a single site this has a direct differential interpretation. Let ω_v be the open indicator at a site v, and let $\mathbb{E}_{\mathbf{p}}$ denote expectation for independent percolation with site-open probabilities $\mathbf{p} = (p_w)_w$. At criticality the one-site forcing source is $2\omega_v - 1$. For an integrable observable Y whose rule is independent of $\mathbf{p}$,

$$\mathbb{E}[(2\omega_v - 1)Y] = \frac{1}{2}\{\mathbb{E}[Y \mid \omega_v = 1] - \mathbb{E}[Y \mid \omega_v = 0]\} = \frac{1}{2}\,\frac{\partial}{\partial p_v}\mathbb{E}_{\mathbf{p}} Y\Big|_{\mathbf{p}\equiv 1/2}. \tag{10.1}$$

Indeed, conditioning on ω_v makes the expectation affine in p_v, and differentiating gives the displayed difference. For a connection event, the derivative is the probability that v is pivotal, meaning that changing only its color changes the event. The shrinking-disk response is the corresponding geometric local experiment. Integrating a field of dimension $y = 5/4$ against area gives the scaling exponent $2 - y = 3/4$, consistent with the pivotal-measure scaling and its role in near-critical percolation [7, 9].

For the comparison, fix an outgoing cut $D = B_d(z)$ and lattice centers $z^a \to z$, with $0 < a < 1$. We use the marked pair row σ_a^D and normalized energy row L_a^D from (4.25). All row differences are formed on the common finite-mesh record space of Section 4.2. Lemma 4.1 gives the contraction under exterior completion, and Theorem 4.3 gives the disk-row bounds (4.8).

The sharp four-arm estimate needed here is

$$\alpha_4^a(s,t) \asymp (s/t)^{5/4}, \qquad Ca \le s < t/C. \tag{10.2}$$

It follows from [8, Theorems 1.2–1.3 and (1.6)] by scaling the lattice and applying quasi-multiplicativity. We also use the bound $C(s/t)^2$ for the probability of any of the finitely many polychromatic six-arm patterns. The exponent 2 is below the six-arm exponent 35/12 [5, Theorem 4]. Fixed-factor changes of the annular radii are absorbed into the constants. Arm separation and RSW extensions are used as in [7, Section 2.1 and Appendix A.1].

10.2 The microscopic pair and its annular contributions

The two marks either join before reaching the cut, or they leave it as two odd components. Only the latter case can remember their separate signs outside the source region.

For example, with two further marks u, v outside D, the sign average includes configurations in which $z^a - a$ and u belong to one open cluster and $z^a + a$ and v to another, together with the interchanged pairing. These contributions survive centering because u and v are then in different clusters. For the disk regulator, the sign average is

$$\mathbb{E}[E^\circ_{a,r}(z) S_a(u) S_a(v) \mid \text{colors}] = E^\circ_{a,r}(z) \mathbf{1}_{\{u \leftrightarrow v\}}.$$

The marked row keeps all these possibilities until the surrounding cut. The estimate below shows that the additional outgoing odd components disappear under the energy normalization.

Choose dyadic radii $r_m = 2^m(4a)$ up to a last radius in $[d/8, d/4]$. Let A_1 be the event that $z^a - a$ and $z^a + a$ are connected inside $B_{r_1}(z^a)$. For $m \ge 2$, let A_m be their connection inside $B_{r_m}(z^a)$ but not inside $B_{r_{m-1}}(z^a)$. Put $p_m = \mathbb{P}(A_m)$ and

$$\rho_m^{a,D} = \mathbb{E}[(\mathbf{1}_{A_m} - p_m)\delta_{\mathcal{R}_D}], \tag{10.3}$$

where $\mathcal{R}_D$ is the unmarked outgoing record and δ_s denotes unit mass at a record s.

Lemma 10.1 (Localization and uniform shell bound)**.** *There is a remainder W_a^D such that*

$$\sigma_a^D - p_\infty \nu_0^{a,D} = \sum_m \rho_m^{a,D} + W_a^D, \qquad \|W_a^D\|_{\mathrm{var}} \le C(a/d)^y. \tag{10.4}$$

Every shell satisfies

$$\|\rho_m^{a,D}\|_{\mathrm{var}} \le C a^y d^{-y}. \tag{10.5}$$

The bounds hold uniformly under bounded exterior completion and under fixed frontier occupations at the outgoing cut.

Proof. First cut at the last dyadic radius, which is comparable with d and lies strictly inside D. If the marks join there, their two parity labels cancel and the row is the unmarked row weighted by $\sum_m \mathbf{1}_{A_m}$. If they remain in different components and one component dies before this cut, parity kills the contribution. The remaining positive marked row has two distinct open components reaching the cut. The two open paths and a closed separator on each side

give four alternating arms from a fixed multiple of a to a fixed fraction of d. Its total mass is at most $C\alpha_4^a(a,d)$.

The centering difference $p_\infty - \sum_m p_m$ requires the same two distinct internal components to reach this cut. It has the same bound. Completing the inner cut to D contracts both errors, proving (10.4) by (10.2).

For a shell of radius $r = r_m$, let $X = \mathbf{1}_{A_m} - p_m$. Close a slightly larger disk, say B_{2r}, while keeping every outside color fixed. Since X is centered and supported in B_r,

$$\rho_m^{a,D} = \mathbb{E}\big[X(\delta_{\mathcal{R}_D} - \delta_{\mathcal{R}_D^{\text{closed } B_{2r}}})\big].$$

If the all-open and all-closed fillings of B_{2r} give the same frontier partition, every filling gives that partition. Otherwise there are four alternating arms from scale $2r$ to a fixed fraction of d. This exterior event is independent of X. The difference of two delta records has norm at most two, and $\mathbb{E}|X| = 2p_m(1-p_m) \le 2p_m$. Moreover A_m requires four arms from scale a to $r/2$, so $p_m \le C\alpha_4^a(a,r)$. Quasi-multiplicativity, with fixed annular gaps, gives

$$\|\rho_m^{a,D}\|_{\text{var}} \le Cp_m\alpha_4^a(r,d) \le C\alpha_4^a(a,d) \le Ca^y d^{-y}.$$

For the last few shells, use an interior cut at a fixed fraction of d and completion, or the direct bound $2p_m$; the radii are then comparable with d. The first fixed number of lattice shells is handled by $p_m \le 1$ and the same exterior four-arm bound. □

There are $O(1+\log(d/a))$ shells. Lemma 10.1 therefore implies

$$\|\mathsf{L}_a^D\|_{\text{var}} \le Cd^{-y}\frac{1+\log(d/a)}{|\log a|}. \tag{10.6}$$

In particular, the normalized marked remainder in (10.4) has norm $O(d^{-y}/|\log a|)$.

10.3 Comparison in a quad

Four alternating boundary faces leave one unresolved question: whether the two open faces are joined. Centering makes every local source act on this same binary choice.

Let Q be a simply connected lattice domain with four alternating boundary faces, in the convention of [7, Section 3], containing $B_b(z^a)$. Let U_Q be the indicator of the connection of its two open faces. For $s < b/100$, define $A_Q(s)$ to be the event, measurable from the colors outside B_s, that the all-open filling of B_s gives $U_Q = 1$ and the all-closed filling gives $U_Q = 0$. Planar duality identifies $A_Q(s)$ with the four alternating face connections to the target. Define the lost-crossing probability

$$q_Q^a(s) = \mathbb{E}U_Q - \mathbb{E}U_Q^{\text{closed } B_s} = \mathbb{P}(A_Q(s), U_Q = 1). \tag{10.7}$$

Fix a nondegenerate reference quad Q_0 at unit scale, centered at zero and containing $B_1(0)$; translate the microscopic source with its lattice orientation. We take $0 < b \le 1$. All comparisons below use the same mesh and target shape in Q and Q_0.

Lemma 10.2 (Buffered source comparison)**.** *There are constants $C, \kappa > 0$ such that the following holds for $Ca < r < b/C$. If A depends only on the colors in B_r, $p = \mathbb{P}(A)$, and*

$$b_{a,r} = \mathbb{P}(A \mid A_{Q_0}(2r), U_{Q_0} = 1) - p,$$

then $|b_{a,r}| \le Cp$ and

$$\Big|\mathbb{E}[(\mathbf{1}_A - p)U_Q] - b_{a,r}q_Q^a(2r)\Big| \le Cp(r/b)^\kappa q_Q^a(2r). \tag{10.8}$$

The constants are independent of the separation of the four outer tips.

Proof. Closing B_{2r} leaves an observable measurable outside the support of A. Centering and (10.7) give the exact identity

$$\mathbb{E}[(\mathbf{1}_A - p)U_Q] = q_Q^a(2r)\big[\mathbb{P}(A \mid A_Q(2r), U_Q = 1) - p\big]. \tag{10.9}$$

We compare the conditional probabilities with an error proportional to p.

Consider four stopped faces g surrounding B_{64r}. Let $A_g(2r)$ be their four-arm extension event to B_{2r}, and let U_g be the crossing indicator of the remaining quad. Under their ordinary interior product law, strong separation conditional on the four arms reaching B_{2r} gives a fixed positive probability of well-separated arms at an intermediate radius. RSW in a fixed number of annuli and inside the target then completes either crossing state with a fixed positive probability. Consequently, uniformly in these faces g, including arbitrarily crowded faces,

$$\mathbb{P}(U_g = 1 \mid A_g(2r), g) \geq c > 0. \tag{10.10}$$

This is the strong-separation setting of [7, Lemma 3.3]; choose the intermediate radii strictly between $2r$ and $64r$. The four-arm event $A_g(2r)$ is measurable outside B_{2r}, whereas A is supported in B_r. Before conditioning on U_g, independence therefore gives $\mathbb{P}(A \mid A_g(2r), g) = p$. By (10.10),

$$\mathbb{P}(A \mid A_g(2r), U_g = 1, g) \leq c^{-1}p. \tag{10.11}$$

Apply the four-face coupling of [7, Proposition 3.1] to the laws conditioned on $A_Q(64r), U_Q = 1$ and their reference-quad counterparts. Stop the faces around B_{64r}, keeping the crossing state. The failure probability is $O((r/b)^\kappa)$. To impose extension from $64r$ to $2r$, reweight each stopped-face law by

$$w(g) = \mathbb{P}(A_g(2r) \mid g, U_g = 1),$$

The average of w is bounded below uniformly. Indeed, strong separation conditional on reaching $64r$ gives a fixed positive probability of separated landing faces at a fixed larger radius. RSW crossings through the intervening fixed-ratio annuli then arrange both extension to $2r$ and $U = 1$ with positive probability. Dividing by the probability of $U = 1$ under the original four-arm conditioning preserves this lower bound.

Matched faces have identical w and identical inner laws. Since $0 \leq w \leq 1$, the two normalizing constants differ by at most the original unmatched mass. Both are bounded below, so the common part of the reweighted measures has mass $1 - O((r/b)^\kappa)$.

Decide success or failure before sampling the remaining inner filling. On success use the same inner configuration. On failure (10.11) bounds the probability of A in either marginal by Cp. Thus the difference of the two conditional probabilities is at most $Cp(r/b)^\kappa$. This proves (10.8) and $|b_{a,r}| \leq Cp$. The proof of the coupling uses stopping faces, their colors and the crossing state; these determine the remaining quad law, as in [8, Remark 3.7 and Section 5.2]. The usual square cuts can be replaced by round cuts with fixed comparable buffers, using the same separation and RSW estimates. □

Lemma 10.3 (A ratio comparison at a fixed radius)**.** *For $Ca < s < \rho/C$ and $C\rho < b$, uniformly in the quad Q,*

$$\frac{q_Q^a(s)}{q_{Q_0}^a(s)} = \frac{q_Q^a(\rho)}{q_{Q_0}^a(\rho)}\big[1 + O((\rho/b)^\kappa)\big]. \tag{10.12}$$

If the numerator vanishes, the corresponding comparison is read in its undivided form.

Proof. Nested targets give

$$q_Q^a(s) = q_Q^a(\rho)\mathbb{P}(A_Q(s) \mid A_Q(\rho), U_Q = 1).$$

Couple the stopped faces around $B_{64\rho}$ under the displayed conditioning and its reference-quad counterpart. Use the same extension reweighting as in Lemma 10.2. Success preserves the four face labels, their colors, and the crossing state. Inner continuation to s is then the same event in both configurations.

On failure, continuation to s requires an ordinary four-arm event from s to $\rho/2$. That event is supported inside $B_{\rho/2}$ and is independent of the extension event $A_Q(\rho)$ outside B_ρ before conditioning on U. The analogue of (10.10) therefore bounds its conditional probability by $C\alpha_4^a(s,\rho)$. The difference of the two continuation probabilities is at most $C\alpha_4^a(s,\rho)(\rho/b)^\kappa$. In the fixed reference quad, arm separation and RSW give the lower bound $c\alpha_4^a(s,\rho)$ for the continuation probability. Division by this lower bound proves (10.12).

The comparison is uniform when s depends on a and ρ is fixed. It is the buffered four-arm form of the relative arm comparison in [8, Proposition 3.9]. □

10.4 The complete outgoing record

The outer boundary may carry many different connections. Revealing the configuration toward a protected inner disk leaves a single local connection choice whenever four tips reach that disk. The cases with more tips require extra long arms and have a smaller contribution.

Proposition 10.4 (Uniform projection of a shell)**.** *Fix $\rho \ll b \ll d$, with $b \le 1$. For every shell with $Ca < r_m < \rho/C$ there is a number $c_{a,m,\rho}$, independent of the exterior record, with $|c_{a,m,\rho}| \le C$, such that*

$$\|a^{-y}\rho_m^{a,D} - c_{a,m,\rho}R_\rho^{a,D}\|_{\mathrm{var}} \le Cd^{-y}\big[(\rho/b)^\kappa + (b/d)^{3/4}\big]. \tag{10.13}$$

The bound holds for all sufficiently fine meshes, with fixed-factor changes of the protective radii. In particular it holds in mesh upper limits uniformly over frontier occupations.

Proof. Protect $B_b(z^a)$ and use the exploration of Lemma 4.2 and Section 9, completing every component separated from this disk. The transcript queries only outside colors. Its law is the same for $X_m = \mathbf{1}_{A_m} - p_m$ and for either disk intervention. The remaining target component contains the protected disk, has independent fair colors, and has an even number N of active alternating tips. All original labels and exterior identifications are restored by the same completion map of norm at most one. In particular X_m remains centered under every conditional interior law.

For $N = 0$ or 2 there is at most one open boundary face. Its frontier labels are connected through its revealed boundary path. The outgoing partition is independent of the inner filling, so both centered rows vanish. For $N = 4$ the remaining component is an ordinary quad Q, and its completed record is

$$\delta_{s_0} + U_Q(\delta_{s_1} - \delta_{s_0}), \qquad \|\delta_{s_1} - \delta_{s_0}\|_{\mathrm{var}} \le 2.$$

If the outside wiring identifies s_0 with s_1, both responses vanish on this transcript. The exploration leaves the final connection choice unconditioned.

Apply Lemmas 10.2 and 10.3, with $s = 2r_m$. They compare the shell row with the radius-ρ disk row using the same scalar coefficient for every quad:

$$c_{a,m,\rho} = a^{-y}\rho^y \frac{\mathbb{E}_{Q_0}[(\mathbf{1}_{A_m} - p_m)U_{Q_0}]}{q_{Q_0}^a(\rho)}. \tag{10.14}$$

The uniform shell bound in the unit reference quad and $q^a_{Q_0}(\rho) \geq c\rho^y$ imply $|c_{a,m,\rho}| \leq C$. The latter lower bound follows from separation, RSW, and the sharp four-arm bound (10.2).

Keep the original transcript probabilities when summing the errors, and sum only over transcripts with $s_1 \neq s_0$. For these transcripts, loss of the residual crossing on deleting B_s changes the original outgoing record. If Π denotes the transcript law, then

$$\int_{\{N=4,\ s_1 \neq s_0\}} q^a_Q(s)\, d\Pi \leq \mathbb{P}(\mathcal{R}_D \neq \mathcal{R}_D^{\text{closed } B_s}) \leq C\alpha_4^a(s,d).$$

The last event requires four arms from s to a fixed fraction of d. Transcripts with $s_1 = s_0$ contribute zero before taking norms. Using $\|\delta_{s_1} - \delta_{s_0}\|_{\text{var}} \leq 2$, the error from the four-tip transcripts is at most

$$Cp_m\alpha_4^a(r_m,d)(\rho/b)^\kappa \leq Ca^y d^{-y}(\rho/b)^\kappa.$$

If $N \geq 6$, at least three original boundary chords enter the protecting disk. The bank extraction in Section 9 gives six polychromatic arms in an annulus between scale b and a fixed fraction of d. Thus its transcript probability is at most $C(b/d)^2$, by the six-arm bound stated above. In an inner cut of scale b, the shell bound is $Ca^y b^{-y}$, uniformly in the residual domain and its boundary colors. Completion contracts it. The contribution from these transcripts is at most

$$Ca^y b^{-y}(b/d)^2 \leq Ca^y d^{-y}(b/d)^{2-y} = Ca^y d^{-y}(b/d)^{3/4}.$$

The normalized disk row has the corresponding conditional bound Cb^{-y}, from the four-arm influence estimate. Since $|c_{a,m,\rho}| \leq C$, its contribution from these transcripts has the same bound after normalization.

All bounds hold at the common mesh and are preserved by exterior completion. The constants are uniform in the number and separation of the original frontier labels. Combining the two estimates proves (10.13). □

10.5 Logarithmic averaging and normalization

Each annular response has now been reduced to the same disk experiment. The remaining scalar coefficient is determined by the correlation with two distant density marks.

Proof of Theorem 4.9. Fix $\rho \ll b \ll d$, with $b \leq 1$. In (10.4), omit the fixed number of first lattice shells and all shells with $r_m \geq \rho/C$. Their number is $O(1 + \log(d/\rho))$, independently of a. By (10.5), their contribution after division by $a^y|\log a|$ tends to zero. The marked remainder in (10.4) has the same vanishing normalized bound.

Sum Proposition 10.4 over the remaining shells. Their number divided by $|\log a|$ is bounded. Thus the real numbers

$$c_{a,\rho} = \frac{1}{|\log a|} \sum_{m:\, Ca < r_m < \rho/C} c_{a,m,\rho}$$

are bounded, and

$$\limsup_{a \downarrow 0} \|\mathsf{L}_a^D - c_{a,\rho} R_\rho^{a,D}\|_{\text{var}} \leq Cd^{-y}\big[(\rho/b)^\kappa + (b/d)^{3/4}\big]. \tag{10.15}$$

Set $b = \sqrt{\rho d}$. For sufficiently small ρ, this choice satisfies the separation conditions, and the right-hand side tends to zero as $\rho \downarrow 0$.

Choose fixed separated density points u, v outside D, and let F_a be their normalized exterior completion on the outgoing record. Its norm is uniformly bounded after the independent

root-arm factors are extracted, by Lemma 4.1 and Theorem 4.4. At fixed ρ, the pairing $R_\rho^{a,D}(F_a)$ has a mesh limit by the fixed-hole density construction. Equation (4.8) shows that this limit approaches the strictly positive correlation $\langle E^\circ(z)\Phi(u)\Phi(v)\rangle$ in (4.11) as $\rho \downarrow 0$. The energy pairing $\mathsf{L}_a^D(F_a)$ converges to the assumed value (4.26).

At the common mesh,

$$\begin{aligned}&\left|c_{a,\rho} - \frac{c_\Phi^2 C_2}{C_\circ}\right| |R_\rho^{a,D}(F_a)| \\ &\quad \le \left|(\mathsf{L}_a^D - c_{a,\rho} R_\rho^{a,D})(F_a)\right| + \left|\mathsf{L}_a^D(F_a) - \frac{c_\Phi^2 C_2}{C_\circ} R_\rho^{a,D}(F_a)\right|.\end{aligned}$$

The first term tends to zero in the mesh upper limit followed by $\rho \downarrow 0$, by (10.15) and the bound on F_a. The two three-point formulas show the same for the second term. The limiting denominator is positive. Hence

$$\lim_{\rho\downarrow 0} \limsup_{a\downarrow 0} \left|c_{a,\rho} - \frac{c_\Phi^2 C_2}{C_\circ}\right| = 0. \tag{10.16}$$

Combining (10.16) with (10.15) and the uniform disk-row bound (4.8) proves (4.27).

For finitely many disjoint source cuts, the local rows form a tensor product before their common exterior completion. Expand the difference of two such products by replacing one factor at a time. The variation norm of each term is bounded by the norm of its differing factor times the norms of the other factors. These are uniformly bounded by (10.6), (4.8), and the density and stress bounds of Lemma 4.1 and Section 4.3. Completion contracts the product. Applying (4.27) in each slot proves the joint statement for every fixed finite separated word. The local estimates are uniform on compact separated configuration sets, so integration against smooth source tests gives the same identification in the source-distribution convention of Section 4.3. □

10.6 Signed connection events

Two source regions can form successive bottlenecks, or they can lie on alternative routes between the same marks. Centering records these two possibilities with opposite signs. Lemma 10.1 reduces the microscopic sign pairs to centered internal-connection indicators in the complete-record norm, including their joint action on separated spectators. The following identity describes the exterior completion of two such local sources.

Proposition 10.5 (Two-region centering)**.** *Consider independent site percolation at a fixed mesh, two disjoint sets of sites D_1, D_2, and two marked sites outside them. Let C be the event that the marked sites are connected, let C_i be the event that a connection exists avoiding D_i, and let C_{12} be the event that a connection exists avoiding $D_1 \cup D_2$. For $i = 1, 2$, let X_i be a bounded function of the colors in D_i with $\mathbb{E}X_i = 0$. Then*

$$\mathbb{E}[X_1 X_2 \mathbf{1}_C] = \mathbb{E}\Big[X_1 X_2 \left(\mathbf{1}_{C\setminus(C_1\cup C_2)} - \mathbf{1}_{(C_1\cap C_2)\setminus C_{12}}\right)\Big]. \tag{10.17}$$

Proof. The inclusions $C_{12} \subseteq C_1 \cap C_2 \subseteq C$ give

$$\mathbf{1}_C - \mathbf{1}_{C_1} - \mathbf{1}_{C_2} + \mathbf{1}_{C_{12}} = \mathbf{1}_{C\setminus(C_1\cup C_2)} - \mathbf{1}_{(C_1\cap C_2)\setminus C_{12}}.$$

The product $X_2\mathbf{1}_{C_1}$ depends only on colors outside D_1. Independence and $\mathbb{E}X_1 = 0$ therefore give $\mathbb{E}[X_1 X_2 \mathbf{1}_{C_1}] = 0$. Interchanging the indices gives $\mathbb{E}[X_1 X_2 \mathbf{1}_{C_2}] = 0$. The same argument applies to C_{12}. Multiply the indicator identity by $X_1 X_2$ and take expectations. □

Proposition 10.5 applies to the centered annular connection indicators in [27, Section 3.1, Step 3] whenever their supporting disks are disjoint. If the second and third events are read as a connection avoiding one disk and no connection avoiding the other, the four events listed immediately before (3.32) are

$$C_{12}, \qquad C_1 \setminus C_2, \qquad C_2 \setminus C_1, \qquad C \setminus (C_1 \cup C_2).$$

Their union is $C \setminus ((C_1 \cap C_2) \setminus C_{12})$. The additional event $(C_1 \cap C_2) \setminus C_{12}$ completes the partition of C. On this event one route avoids the first disk, another avoids the second, and every route meets their union. Its contribution is the second term of (10.17). In particular,

$$\mathbb{E}[X_1 X_2 \mathbf{1}_{C_1 \setminus C_2}] = \mathbb{E}[X_1 X_2 \mathbf{1}_{C_2 \setminus C_1}] = -\mathbb{E}[X_1 X_2 \mathbf{1}_{(C_1 \cap C_2) \setminus C_{12}}].$$

If instead the second and third events mean avoiding one disk but not their union, they are $C_1 \setminus C_{12}$ and $C_2 \setminus C_{12}$. Their centered expectations vanish, but the events overlap on $(C_1 \cap C_2) \setminus C_{12}$, whose contribution must be subtracted. Thus, under either reading of the notation, (3.32) of [27] omits the alternative-route term in (10.17). Lemma 3.2 evaluates the successive-bottleneck term; the full centered correlation also contains the alternative-route contribution.

The sign can also be read directly from the two local binary choices. Let (X_1, B_1) and (X_2, B_2) be independent, with $\mathbb{E}X_i = 0$ and $B_i \in \{0, 1\}$. For any completion function $F : \{0, 1\}^2 \to \mathbb{R}$, expansion in the basis $1, B_1, B_2, B_1 B_2$ gives

$$\begin{aligned} \mathbb{E}[X_1 X_2 F(B_1, B_2)] = \mathbb{E}[X_1 B_1]\mathbb{E}[X_2 B_2] \\ \times \{F(1,1) - F(1,0) - F(0,1) + F(0,0)\}. \end{aligned} \tag{10.18}$$

The constant and linear terms vanish by centering and independence. The final coefficient is 1 for the serial connection $F(B_1, B_2) = B_1 B_2$ and -1 for the parallel connection $F(B_1, B_2) = B_1 + B_2 - B_1 B_2$.

Consider, for example, two parallel routes, each controlled by one of two independent Bernoulli variables B_1, B_2 of parameter $1/2$. Put $X_i = B_i - 1/2$. The connection event is $C = \{B_1 = 1\} \cup \{B_2 = 1\}$, whereas $C_1 = \{B_2 = 1\}$, $C_2 = \{B_1 = 1\}$ and $C_{12} = \varnothing$. The successive-bottleneck event is empty and the alternative-route event is $\{B_1 = B_2 = 1\}$. Equation (10.18) gives

$$\mathbb{E}[X_1 X_2 \mathbf{1}_C] = -\frac{1}{16}, \qquad \mathbb{E}[X_1 X_2 \mathbf{1}_{(C_1 \cap C_2) \setminus C_{12}}] = \frac{1}{16}. \tag{10.19}$$

Figure 4 in Section 15 shows the corresponding percolation geometries. That section applies the signed identity to the two-obstacle observable.

10.7 Null identities and density fusion

The identification connects the geometric disk experiment to the energy insertion obtained from a nearby pair of density marks. Assuming the one-energy/two-density asymptotic [27, (1.9)], Theorem 4.9 gives $\phi = E^\circ$ in the normalization (4.29), jointly with every fixed finite collection of separated density, scalar, and stress insertions.

Define the stress descendant of ϕ by replacing E° with ϕ in (4.15), and use the same replacement in (4.16) to define $\mathcal{N}_z\phi$ and $\mathcal{N}_{\bar{z}}\phi$. Choose the stress contour at positive distance from the scalar source and all spectators. The joint identification on this contour, the uniform stress bounds, and linearity of contour integration identify the descendants. Equality in source distributions also identifies their second derivatives. Theorem 4.7 therefore gives

$$\langle \mathcal{N}_z\phi(z) Y \rangle = 0, \qquad \langle \mathcal{N}_{\bar{z}}\phi(z) Y \rangle = 0 \qquad (Y \in \mathscr{C}_0),$$

with the same conclusion when any of the scalar spectators in Y are written as ϕ.

In particular,

$$\langle\phi(z)\phi(w)\Phi(u)\Phi(v)\rangle = \langle E^\circ(z)E^\circ(w)\Phi(u)\Phi(v)\rangle$$

for four distinct points. Theorem 4.8 thus gives the mixed four-point function of the energy field in this normalization. Section 11 derives that formula from the null identities, reducing them to the differential equation (11.3).

Comparison with Camia–Feng. Under the assumption of Theorem 4.9, the identified two-energy/two-density correlation changes sign by Theorem 4.8. This contradicts the positive formula [27, (3.37)] and the strict-positivity assertion in [27, (1.11)] for $\ell \geq 2$, already at $\ell = 2$, $k = 1$. The discrepancy originates in (3.32); it affects the use of Lemma 3.2 for the full centered correlation and the resulting positivity conclusions. The proofs of (1.9) and the one-energy case $\ell = 1$ are separate from this argument. The statements (1.10), (1.12), and (1.13) are consistent with the identification.

The logarithmic partner $\hat{\phi}$ defined in [27, (1.23)–(1.26)] has weights $(5/8, 5/8)$. Its construction uses the centered density-pair fusion. The field Ψ of Theorem 4.10 has weights $(77/96, 77/96)$ and is the coefficient of the relative power $3/2$ in the scalar–density fusion. Section 12 constructs this coefficient, and Section 13 gives its joint separated insertions.

11 The mixed four-point function

The null identity turns a geometric connection response into an ordinary differential equation. Its two local solutions describe two different rates of change as a scalar source approaches a density mark. We determine their coefficients from leading fusion and single-valuedness. The second solution will provide a nonzero correlation for the field extracted in Section 12.

11.1 The differential equation for the response

Write

$$F(z,\bar{z}) = \langle E^\circ(\infty)\Phi(1)E^\circ(z)\Phi(0)\rangle, \qquad h_\Phi = \frac{5}{96}, \quad h_E = \frac{5}{8}. \tag{11.1}$$

The insertion at infinity uses the spherical chart convention:

$$F(z,\bar{z}) = \lim_{|w|\to\infty} |w|^{5/2}\langle E^\circ(w)\Phi(1)E^\circ(z)\Phi(0)\rangle.$$

The continuation is taken in the chart $1/w$ while $z \notin \{0,1\}$ remains fixed. Primary covariance and the continuous two-root representatives of Theorem 4.4 make this definition well posed. The function is real and single-valued because it is obtained from real percolation observables.

Before fixing the two density coordinates, translation and dilation covariance give

$$\partial_0 F + \partial_1 F + \partial_z F = 0, \qquad \partial_1 F + z\partial_z F = -2h_\Phi F. \tag{11.2}$$

Thus $\partial_1 F = -zF' - 2h_\Phi F$ and $\partial_0 F = (z-1)F' + 2h_\Phi F$, where a prime denotes ∂_z. The null equation at z becomes

$$-\frac{2}{3}F'' + \frac{1-2z}{z(z-1)}F' + h_\Phi\left[\frac{1}{z^2} + \frac{1}{(z-1)^2} - \frac{2}{z(z-1)}\right]F = 0.$$

Consequently,

$$F'' + \frac{3}{2}\frac{1-2z}{z(1-z)}F' - \frac{5}{64z^2(1-z)^2}F = 0. \tag{11.3}$$

The conjugate equation holds as well.

11.2 From the weak equation to conformal blocks

Away from $0, 1$, the operator in (11.3) is elliptic as a complex operator on two real variables: its principal symbol is a nonzero constant times $(i\xi_1 + \xi_2)^2$, which does not vanish on a nonzero real covector. Interior elliptic regularity makes a distributional solution smooth on this punctured domain [24, Theorem 15.2].

Choose a simply connected patch and a holomorphic fundamental system f_0, f_1 of the ordinary differential equation. Its Wronskian is nonzero, so

$$Y(z) = \begin{pmatrix} f_0 & f_1 \\ f_0' & f_1' \end{pmatrix}, \qquad c = Y^{-1} \begin{pmatrix} F \\ \partial_z F \end{pmatrix}$$

is well defined. The holomorphic equation gives $\partial_z c = 0$. Let $\overline{\mathcal{L}}$ denote the differential operator in the conjugate of (11.3). Applying the antiholomorphic equation to F and then differentiating that equation once in z gives $Y\overline{\mathcal{L}}c = 0$. Thus each component of c solves the conjugate second-order equation. On the patch,

$$F = \sum_{j,k=0}^{1} H_{jk} f_j \overline{f_k} \tag{11.4}$$

for a constant matrix H. Reality of F makes this matrix Hermitian.

The substitution $f = [z(1-z)]^{-5/8} u$ gives

$$z(1-z)u'' + \left(\frac{1}{4} - \frac{z}{2}\right) u' + \frac{15}{16} u = 0. \tag{11.5}$$

Its two solutions normalized at zero are (4.23). Their local exponents are $-5/8$ and $1/8$. Because their difference $3/4$ is not integral, single-valuedness around zero eliminates the off-diagonal terms in (11.4). Hence

$$F = A_0 |f_0|^2 + A_1 |f_1|^2, \qquad A_0, A_1 \in \mathbb{R}. \tag{11.6}$$

The leading fusion of Theorem 4.5 and (4.11) give

$$A_0 = \lim_{z \to 0} |z|^{5/4} F(z, \bar{z}) = C_\circ^2. \tag{11.7}$$

This limit can first be read in the weak topology; the block representation identifies its scalar coefficient uniquely. The solutions are the standard hypergeometric solutions [25, 15.10.2]; leading mixed fusion fixes their normalization.

11.3 The connection matrix

On $0 < z < 1$, write $g_j(z) = f_j(1-z)$. The Gauss connection formula gives

$$\begin{pmatrix} f_0 \\ f_1 \end{pmatrix} = \begin{pmatrix} -\sqrt{2} & -\mathfrak{k} \\ 1/\mathfrak{k} & \sqrt{2} \end{pmatrix} \begin{pmatrix} g_0 \\ g_1 \end{pmatrix}, \qquad \mathfrak{k} = \frac{5}{12} \left[\frac{\Gamma(1/4)}{\Gamma(3/4)}\right]^2. \tag{11.8}$$

The four coefficients are

$$\begin{aligned} \frac{\Gamma(1/4)\Gamma(3/4)}{\Gamma(3/2)\Gamma(-1/2)} &= -\sqrt{2}, & \frac{\Gamma(1/4)\Gamma(-3/4)}{\Gamma(-5/4)\Gamma(3/4)} &= -\mathfrak{k}, \\ \frac{\Gamma(7/4)\Gamma(3/4)}{\Gamma(9/4)\Gamma(1/4)} &= 1/\mathfrak{k}, & \frac{\Gamma(7/4)\Gamma(-3/4)}{\Gamma(-1/2)\Gamma(3/2)} &= \sqrt{2}. \end{aligned} \tag{11.9}$$

The matrix squares to the identity. In the g basis the off-diagonal coefficient in (11.6) is $\sqrt{2}(A_0\mathfrak{k} + A_1/\mathfrak{k})$. Single-valuedness around one therefore implies

$$A_1 = -\mathfrak{k}^2 A_0 = -\mathfrak{k}^2 C_\circ^2. \tag{11.10}$$

Equations (11.6) and (11.10) prove (4.22). Monodromy invariance around zero and one also establishes branch independence on the entire punctured sphere. The connection algebra is standard [25, 15.10.21]. Equations (11.8)–(11.10) also specialize [23, (A.3)–(A.5)] at $\beta^2 = 2/3$, $P_2 = P_4 = 1/(4\beta)$ and $P_3 = 1/\beta - \beta/2$. The two-channel fusion and mixed four-point problem appear in [22, (4.28a), (4.40)–(4.41), and (4.52)]. Their derivation here fixes the disk-response normalization; the formal CFT coefficients are known.

12 The second odd fusion coefficient

Bring a scalar source close to a density mark and average over the direction of approach. The leading term is a density insertion. The null equations control the remaining angular modes and reveal the next scalar coefficient. We work with the class $\mathscr{C}_0$ and the source-distribution topology defined in Section 4.

Put $x = 5/48$, $y = 5/4$, and $p = 3/2$. For separated spectators Y, let

$$\begin{aligned} H(z,s) &= \langle E^\circ(z)\Phi(z+s)Y\rangle, \qquad P(z,s) = |s|^y H(z,s), \\ P_n(z,r) &= \frac{1}{2\pi}\int_0^{2\pi} e^{-in\theta} P(z, re^{i\theta})\, d\theta. \end{aligned} \tag{12.1}$$

All spectator variables that require testing are included among the distribution variables. Constants in distribution seminorms may depend on a fixed separated compact set and on the finite spectator word. Theorem 4.5 says, uniformly in the angle,

$$P = C + O_{\mathcal{D}'}(r^\gamma), \qquad C = C_\circ\langle\Phi(z)Y\rangle, \qquad 0 < \gamma < x. \tag{12.2}$$

Thus $P_0 - C = O_{\mathcal{D}'}(r^\gamma)$ and $P_n = O_{\mathcal{D}'}(r^\gamma)$ for $n \neq 0$.

12.1 Continuity of the collision family

Lemma 12.1 (Weak continuity in the collision displacement)**.** *Fix a compact set of the variables tested in the correlation and a compact set of nonzero displacements s such that all the resulting insertion configurations are separated. For every fixed smooth test in those variables, the family*

$$P(z,s) = |s|^{5/4}\langle E^\circ(z)\Phi(z+s)Y\rangle$$

is continuous in s after pairing with that test. The continuity is locally uniform on these compact displacement sets. In particular, its angular averages $P_n(r)$ are weakly continuous for every $r > 0$ for which the insertions remain separated.

Proof. First keep the scalar source apart from a fixed outgoing cut by a distance comparable with $d > 0$. For a displacement $\eta \in \mathbb{C}$, write $h = |\eta|$. The source centers z and $z + \eta$ can use the same cut when h is sufficiently small. Replace their scalar regulators by the same positive radius ϵ, with $h < c\epsilon < cd$. The scalar Cauchy estimate (4.8) and the translated-disk case of the strip estimate (4.5) give

$$\|E^\circ(z+\eta) - E^\circ(z)\|_{d,*} \le Cd^{-5/4}\left[(\epsilon/d)^{11/15} + (h/d)(\epsilon/d)^{-21/20}\right].$$

The second term follows by multiplying the ordinary hole difference by $\epsilon^{-5/4}$; a translation by h has normal displacement bounded by Ch. We used the four-arm upper bound with exponent $6/5$, so that $6/5 - 5/4 - 1 = -21/20$. The comparison is made on the same finite-mesh outgoing record, followed by the specified upper limits. Choosing $\epsilon/d = (h/d)^{60/107}$ yields

$$\|E^\circ(z+\eta) - E^\circ(z)\|_{d,*} \le Cd^{-5/4}(h/d)^{44/107}.$$

To apply this estimate to a collision displacement, make the change of variables $q = z + s$ in the source test, first at finite positive source regulators. The density is then at q, the scalar is at $q - s$, and a test $\psi(z, \boldsymbol{\xi})$ becomes $\psi(q - s, \boldsymbol{\xi})$. On replacing s by $s + t$, the density and the spectators stay fixed. Only the scalar center and the smooth test move. Use the preceding common-cut estimate for the former change and the ordinary smooth-test translation estimate for the latter. The bounded root and spectator completions of Lemma 4.1 and Theorem 4.4 supply constants uniform on the fixed separated compact sets. The comparison is made before removing the regulators and passes to their joint limits by (5.12). It is therefore an estimate for the original family at every positive displacement. It proves the asserted weak continuity; the factor $|s|^{5/4}$ is smooth away from zero. Uniformity for $s = re^{i\theta}$ on compact annuli and bounded angular integration give the last assertion. □

This continuity will identify the family at every positive radius with the representatives obtained from the radial equations.

12.2 A distributional Euler lemma

For a family $u(r)$ of distributions on a fixed open set, the notation $O_{\mathcal{D}'}(r^\beta)$ means a uniform bound by Cr^β times one finite smooth-test seminorm on each compact test set. Derivatives in $\log r$ are interpreted distributionally until the estimates below establish the necessary representatives. Write $T_r = r\partial_r$.

Lemma 12.2 (Euler equations with a derivative in the forcing)**.** *Let $a \neq b$ and $\beta \notin \{a, b\}$ be real numbers. Suppose f, g are weakly measurable families of distributions, $f, g = O_{\mathcal{D}'}(r^\beta)$, and*

$$(T_r - a)(T_r - b)u = T_r f + g \tag{12.3}$$

on $0 < r < r_0$. Then there are distributions A, B and a particular solution v such that

$$u = Ar^a + Br^b + v, \qquad v, T_r v = O_{\mathcal{D}'}(r^\beta). \tag{12.4}$$

If the right side of (12.3) is simply $O_{\mathcal{D}'}(r^\beta)$, the same conclusion holds.

The derivative in the forcing is handled by an explicit right inverse. In the application below the families are weakly continuous at every positive radius by Lemma 12.1.

Proof. For $c \neq \beta$, define a right inverse of $T_r - c$ on a family $F = O_{\mathcal{D}'}(r^\beta)$ by

$$I_c F(r) = \begin{cases} r^c \displaystyle\int_0^r t^{-c-1} F(t)\, dt, & \beta > c, \\ -r^c \displaystyle\int_r^{r_0} t^{-c-1} F(t)\, dt, & \beta < c. \end{cases}$$

The integrals are weak integrals against source tests. Elementary power integration gives $I_c F = O_{\mathcal{D}'}(r^\beta)$ and $T_r I_c F = cI_c F + F = O_{\mathcal{D}'}(r^\beta)$. Set

$$v = I_b f + I_b I_a (af + g).$$

Then $(T_r-a)(T_r-b)v = T_r f + g$ and $v, T_r v$ have the stated bounds. After the change of variable $t = \log r$, the homogeneous equation is an ordinary constant-coefficient distributional equation. Its solutions are $Ae^{at} + Be^{bt}$, with distribution-valued coefficients. This proves (12.4). The case without a derivative in the forcing is obtained by setting $f = 0$. □

12.3 The two null equations and their first angular modes

Let $\mathcal{W}_z^Y$ denote the constructed holomorphic Ward operator acting on the spectator word. Its coefficients are smooth on the separated compact sets used here and it does not depend on s. Define

$$\mathcal{A} = 4\partial_z^2 - 6\mathcal{W}_z^Y, \qquad \overline{\mathcal{A}} = 4\partial_{\bar z}^2 - 6\overline{\mathcal{W}}_z^Y.$$

In the variables (z, s), differentiation of the scalar coordinate with the density coordinate held fixed is $\partial_z - \partial_s$. Theorem 9.1 consequently gives

$$\left[-\frac{2}{3}(\partial_z - \partial_s)^2 + \frac{h_\Phi}{s^2} - \frac{1}{s}\partial_s + \mathcal{W}_z^Y\right] H = 0.$$

Substitute $H = (s\bar s)^{-5/8}P$ and put $D = s\partial_s$. Multiplication by $-6s^2$ yields

$$\left[4D^2 - 3D + s(5-8D)\partial_z + s^2\mathcal{A}\right] P = 0, \tag{12.5}$$

together with its conjugate. The constant term vanishes because $4(5/8)^2 - 2(5/8) - 6(5/96) = 0$.

On the nth angular mode, $D = (T_r + n)/2$. Thus

$$(T_r+n)(T_r+n-p)P_n = -r(9-4n-4T_r)\partial_z P_{n-1} - r^2\mathcal{A}P_{n-2}, \tag{12.6}$$

$$(T_r-n)(T_r-n-p)P_n = -r(9+4n-4T_r)\partial_{\bar z} P_{n+1} - r^2\overline{\mathcal{A}}P_{n+2}. \tag{12.7}$$

These equations initially hold as joint source and logarithmic-radius distributions.

Apply (12.7) with $n = 1$. Its left side is $(T_r - 1)(T_r - 5/2)P_1$. Its right side has the form $T_r f + g$, where

$$f = 4r\partial_{\bar z}P_2, \qquad g = -17r\partial_{\bar z}P_2 - r^2\overline{\mathcal{A}}P_3.$$

By (12.2), $f, g = O_{\mathcal{D}'}(r^{1+\gamma})$. Lemma 12.2, with $1 < 1+\gamma < 5/2$, gives

$$P_1 = a_1 r + O_{\mathcal{D}'}(r^{1+\gamma}), \qquad T_r P_1 = a_1 r + O_{\mathcal{D}'}(r^{1+\gamma}). \tag{12.8}$$

The possible $r^{5/2}$ homogeneous term is absorbed by the remainder. Substitute into the holomorphic equation (12.6). At order r, its left coefficient is a_1, whereas its right coefficient is $-5\partial_z C$. To compare these coefficients rigorously, write $r = \epsilon e^v$, test in a fixed compact v interval, and divide the equation by ϵ. Derivatives of the error are moved to this test; they still vanish as $O(\epsilon^\gamma)$. Thus $a_1 = -5\partial_z C$ follows from the distributional equation and the uniform leading remainder.

Use the holomorphic equation with $n = -1$ first, and then the antiholomorphic equation, to obtain the conjugate conclusion. Therefore

$$P_1 = -5r\partial_z C + O_{\mathcal{D}'}(r^{1+\gamma}), \qquad T_r P_1 = -5r\partial_z C + O_{\mathcal{D}'}(r^{1+\gamma}), \tag{12.9}$$

$$P_{-1} = -5r\partial_{\bar z} C + O_{\mathcal{D}'}(r^{1+\gamma}), \qquad T_r P_{-1} = -5r\partial_{\bar z} C + O_{\mathcal{D}'}(r^{1+\gamma}). \tag{12.10}$$

The two null equations together eliminate the lower angular homogeneous mode that either equation alone would leave undetermined.

12.4 Extraction of the scalar second coefficient

Set $n = 0$ in (12.6). Equations (12.10) and (12.2) show that

$$T_r(T_r - p)P_0 = 25r^2\partial_z\partial_{\bar z}C + O_{\mathcal{D}'}(r^{2+\gamma}). \tag{12.11}$$

Indeed $9 - 4T_r$ applied to the leading term $-5r\partial_{\bar z}C$ produces $-25r\partial_{\bar z}C$, and $r^2\mathcal{A}P_{-2} = O_{\mathcal{D}'}(r^{2+\gamma})$. The Euler operator multiplies r^2 by $2(2-p) = 1$. Lemma 12.2 thus gives distributions C_0, Ψ_Y with

$$P_0 = C_0 + r^{3/2}\Psi_Y + 25r^2\partial_z\partial_{\bar z}C + O_{\mathcal{D}'}(r^{2+\gamma}).$$

The leading estimate identifies $C_0 = C$. The Euler calculation first identifies the radial distribution, and therefore the family for almost every radius. The right-inverse formulas give weakly continuous representatives on compact positive-radius intervals; the inputs to these formulas are weakly continuous by Lemma 12.1. That lemma also gives weak continuity of the original family. The two representatives consequently agree at every positive radius. The same continuity extends the uniform remainder bounds from almost every radius to every radius. This proves the following statement through all positive radii tending to zero, including uniformity on each fixed multiplicative window.

Theorem 12.3 (A weak second odd fusion insertion)**.** *There is a linear correlation insertion Ψ, against the inherited finite separated spectator class, defined by*

$$\Psi(z) = \lim_{r\downarrow 0} r^{-3/2}\left[\frac{r^{5/4}}{2\pi}\int_0^{2\pi} E^\circ(z)\Phi(z + re^{i\theta})\,d\theta - C_\circ\Phi(z)\right]. \tag{12.12}$$

The limit is in source distributions and has the sharper expansion

$$\frac{r^{5/4}}{2\pi}\int_0^{2\pi} E^\circ(z)\Phi(z + re^{i\theta})\,d\theta = C_\circ\Phi(z) + r^{3/2}\Psi(z) + 25C_\circ r^2\partial_z\partial_{\bar z}\Phi(z) + O_{\mathcal{D}'}(r^{2+\gamma}). \tag{12.13}$$

In particular the convergence in (12.12) is $O_{\mathcal{D}'}(r^{1/2})$. If B_r denotes the square bracket in that definition, then, uniformly for $b \in [1/2, 1]$,

$$B_r - b^{-3/2}B_{br} = 25C_\circ(1 - \sqrt{b})r^2\partial_z\partial_{\bar z}\Phi + O_{\mathcal{D}'}(r^{2+\gamma}). \tag{12.14}$$

The field regulators are removed at fixed r before this collision limit.

12.5 Conformal covariance of the extracted insertion

Theorem 12.4 (Möbius covariance and Ward action)**.** *For plane correlations and Möbius maps of the sphere, interpreted in finite source charts, the insertion Ψ has weights*

$$h_\Psi = \bar h_\Psi = \frac{77}{96}. \tag{12.15}$$

With the known spectator transformation factors understood,

$$\Psi(z) = |f'(z)|^{77/48}\Psi(f(z)). \tag{12.16}$$

In the plane, its separated stress insertion obeys

$$\langle T(w)\Psi(z)Y\rangle = \left[\frac{77/96}{(w-z)^2} + \frac{1}{w-z}\partial_z + \mathcal{D}_w^Y\right]\langle\Psi(z)Y\rangle, \tag{12.17}$$

and the conjugate identity holds as well.

The first angular modes control the change from a small circle to its conformal image and hence determine the transformation of the extracted coefficient.

Proof. Let f be a Möbius map whose pole lies outside the chosen source neighborhoods, and set $\lambda = f'(z)$, $a = f''(z)/(2f'(z))$, and $s = re^{i\theta}$. Write P' for the correlation in the transformed coordinates, with the known spectator transformation factors absorbed into it. Taylor expansion gives

$$\begin{aligned} S = f(z+s) - f(z) &= \lambda s(1 + as + O(r^2)), \\ |S| &= |\lambda| r\{1 + r\Re(ae^{i\theta}) + O(r^2)\}, \\ \arg S &= \theta + \arg\lambda + r\Im(ae^{i\theta}) + O(r^2). \end{aligned}$$

Exact covariance of the original fields gives

$$P = |\lambda|^x\{1 + (2x - y)r\Re(ae^{i\theta}) + O(r^2)\}P'(f(z), |S|, \arg S). \tag{12.18}$$

The estimates for P and its angular modes are uniform in the angle and on compact logarithmic-radius windows. They therefore also bound pairings with tests that depend smoothly on the source variables, the angle, and the logarithmic radius, with one common finite test seminorm. We use this joint topology to transport the family before taking its coefficient. Choose $\chi \in C_c^\infty(\mathbb{R})$, $\chi \geq 0$, $\int \chi = 1$, and average the raw radius as re^v against $\chi(v)\,dv$. Write $m_p = \int e^{pv}\chi(v)\,dv > 0$. Formula (12.13) implies

$$\int \chi(v)P_0(z, re^v)\,dv = C(z) + m_p r^p \Psi(z) + O_{\mathcal{D}'}(r^2). \tag{12.19}$$

All tests may now be transported jointly in the source variables, angle, and logarithmic radius. The shift $v' = v + \log|\lambda(z)|$ is a smooth diffeomorphism on the fixed compact set. It permits the transported radius to be included in the smooth test.

After the fixed rotation $\arg\lambda$ is removed, the first-order angular and radial distortion in (12.18) involves only P_1', P_{-1}' and their Euler derivatives. Explicitly, with $c = ae^{-i\arg\lambda}$ and $r' = |\lambda|r$, the first variation is

$$r\,(T_{r'} + 2x - y - 1)\,\frac{cP_{-1}' + \bar{c}P_1'}{2}.$$

The -1 is the angular integration-by-parts term. Equations (12.9)–(12.10) make this $O_{\mathcal{D}'}(r^2)$. The second-order Taylor remainder is also $O_{\mathcal{D}'}(r^2)$: move the transformation to the smooth tests and radius kernel and use the inherited bound $P = O_{\mathcal{D}'}(1)$.

To evaluate the remaining averaged leading transport, change variables from v to v' in the smooth test. The coefficient of $r^p\Psi(f(z))$ is multiplied by

$$\int \chi(v' - \log|\lambda(z)|)e^{pv'}\,dv' = m_p|\lambda(z)|^p.$$

The leading density term has its previously established factor $|\lambda|^x$. Subtract it, divide by $m_p r^p$, and use $p < 2$ in (12.19). The result is (12.16), since $x + p = 77/48$. The coefficient on the left is the original raw extraction, identified by its uniform expansion on logarithmic-radius windows.

For the Ward statement, start from the separated $TE^\circ\Phi Y$ identity and put $d = w - z$. Since $\partial_z|_{z+s} = \partial_z - \partial_s$, its normalized local part expands as

$$\begin{aligned} &\left[\frac{1}{d}\partial_z + \frac{1}{d^2}(h_\Phi + D) + \mathcal{D}_w^Y\right] P \\ &\quad + \frac{s}{d^3}\left(2h_\Phi + D - \frac{y}{2}\right)P + O(s^2 P \text{ and Euler/angular derivatives}). \end{aligned} \tag{12.20}$$

Angular averaging sends DP_0 to $T_rP_0/2$. The term with one explicit s sees only P_{-1} and its Euler derivative and is $O_{\mathcal{D}'}(r^2)$. For the remainder use the temporary logarithmic-radius averaging above and transfer derivatives to its kernel; the uniform bound on P again gives $O_{\mathcal{D}'}(r^2)$. Insert (12.13), subtract the leading density Ward identity, and take the r^p coefficient. The double-pole coefficient is $h_\Phi + p/2 = 5/96 + 3/4 = 77/96$, which proves (12.17). The same argument applies to the conjugate stress. The correlation with a separated stress is obtained by including that stress in the spectator word before extraction. □

Remark 12.5 (Testing class). The insertion constructed here acts on the fixed class $\mathscr{C}_0$ in source distributions. Section 13 gives controlled local representations for its finite separated products. Section 14 evaluates a nonzero mixed correlation from the four-point function of Section 11.

13 Joint construction of separated subleading insertions

Several pairs can approach each other at very different speeds. To control them together, we express each extracted coefficient as an integral of the original scalar, density, and stress sources inside its own region. The integral has a uniform bound after testing the source coordinate. The exterior configuration then joins these regions through the same connectivity completion used for the original fields.

We extend the one-slot limit of Theorem 12.3 from the testing class in Remark 12.5 to finitely many separated new insertions.

The exact inputs are the completion bound for finite words in $\mathscr{C}_0$ from Theorem 4.4, the leading complete-record estimate (4.12), and the null and Ward identities on $\mathscr{C}_0$. We also use weak continuity at positive displacements. For finitely many disjoint pairs this follows from Lemma 12.1 by a finite telescoping argument: put each density point at $q_i = z_i + s_i$ in the source test, then vary s_i by moving only its scalar center and the smooth test. The bound (5.15) and bounded disjoint completions apply one slot at a time on compact sets of positive displacement tuples. This proves joint weak continuity on compact sets of positive displacement tuples. Boundary-SLE fusion provides a related use of null equations and regularity [28, Sections 4–5]. Here the bounds on the complete connectivity record permit the local integral representations needed for the joint bulk limit.

13.1 Local integral representatives and their topology

Put $p = 3/2$, $y = 5/4$, and fix $0 < \gamma < 5/48$. A *source cap* is an open disk with a fixed outgoing cut, assigned to one collision and separated from all other collision regions and spectator sources. Choose nested caps $D^- \Subset D$, a compact set $K \Subset D^-$ of collision centers, and $R > 0$ such that every pair $(z, z+s)$ with $z \in K$ and $|s| \le R$ lies in D^- and stays a positive distance from its boundary. Choose a fixed positively oriented smooth Jordan contour $\Gamma \subset D \setminus \overline{D^-}$ enclosing D^-. The inner cut ∂D^- is used for the leading fusion estimate; after inserting a stress on Γ, we complete to the outer cut ∂D. Both cuts are independent of z and s. All remaining sources lie outside D.

Local packets are those of Section 4.5, with the outgoing cut of the chosen cap. All statements below are in distributions in z and the spectator coordinates. The radius R is fixed throughout the construction. Constants may depend on R, the caps, the compact source patches, the contour, and the chosen moment kernels.

An expression has *representation bound* $O(t^a)$ of differential order at most k if it is a finite sum, or an absolutely convergent integral, of controlled signed local packets and at most k

source derivatives, with the following bound: after moving the derivatives to a smooth source test, its common-cut completion is at most Ct^a times a fixed C^{k+1} seminorm of the test. The extra derivative permits convergence of parameter quadratures in this norm. Angular and contour integrals are included. The bound is uniform over common bounded outer completions of the constituent rows. Equalities between representations are identities of correlations against $\mathscr{C}_0$.

These integral representations can be defined first with every radial integral bounded away from zero and with finite quadratures, after the original mesh and source-regulator limits. Their positive-cutoff quadratures converge in the source-tested completion norm. Indeed, put $q = z + s$ in the integrated local row, so that changing s moves the scalar and the test while the density stays fixed. On a compact nonzero-displacement set, the translated-scalar bound gives

$$\left\| \int \varphi(z)[P(z, s+h) - P(z,s)]\, d^2z \right\|_{D,*} \le C_\delta \left(|h|^{44/107} \|\varphi\|_\infty + |h| \|\varphi\|_{C^1} \right).$$

Here the smooth factor $|s|^y$ is included, and $\delta > 0$ records the fixed positive separation. With k source derivatives, use C^{k+1} tests. The stress-center modulus in Section 5 gives the same conclusion for stress-contour quadratures. Uniformity along the contour and in the collision angle is established below in (13.2). Thus compact positive-radius parameter integrals are limits in this source-tested norm. Lemma 13.1 will remove the radial truncations. Throughout this construction, mesh comparisons use the same finite record space. The fixed outgoing cuts ensure that source derivatives act only on the local expression and its smooth test.

13.2 Replacing the exterior Ward operator by a local contour

For $Y \in \mathscr{C}_0$ supported outside D, write

$$P_Y(z,s) = |s|^y \langle E^\circ(z) \Phi(z+s) Y \rangle, \qquad C_Y = C_\circ \langle \Phi(z) Y \rangle,$$
$$(P_Y)_n(z,r) = \frac{1}{2\pi} \int_0^{2\pi} e^{-in\theta} P_Y(z, re^{i\theta})\, d\theta.$$

Let $\mathcal{J}$ act on a local expression in $\mathscr{C}_0$ by adding the contour source

$$(\mathcal{J}F)(z) = \frac{1}{2\pi i} \int_\Gamma \frac{T(w)F(z)}{w - z}\, dw, \qquad \mathcal{A} = 4\partial_z^2 - 6\mathcal{J}.$$

Here Γ encloses both points of the local pair. The holomorphy in a separated stress coordinate established in Section 5, after testing the scalar and density coordinates, justifies restriction of the stress correlation to this contour. The separated Ward identity gives

$$\mathcal{J} P_Y = \mathcal{W}_z^Y P_Y. \tag{13.1}$$

To verify this, the scalar self terms have zero residue. The density terms have residues $h_\Phi/s^2 - (1/s)\partial_{z+s}$ at $w = z$ and their negatives at $w = z + s$, so these residues cancel. Each exterior spectator term is analytic inside Γ before multiplication by $(w-z)^{-1}$ and contributes its value at $w = z$. This proves the identity also with stress spectators, since the central term is zero. The local representation $\mathcal{J}P$ therefore expresses the exterior Ward action using fields inside D. We apply the identity to the unnormalized pair and multiply by $|s|^y$, which is independent of the contour coordinate.

The contour remains separated from the whole collision region. Choose $d > 0$ so that every disk $B(w, 2d)$, $w \in \Gamma$, lies in $D \setminus \overline{D^-}$, and so that all local pairs with $z \in K$ and $|s| \le R$

have distance at least $2d$ from ∂D^-. Decrease R once, if necessary, so that the leading fusion estimate applies for $0 < r \le R$. The stress bound recalled in Section 4.3 gives

$$\sup_{w\in\Gamma} \|T(w)\|_{B(w,d),*} \le Cd^{-2}.$$

Apply Theorem 4.5 on the fixed inner cut, tensor its difference row with this stress row, and use the completion contraction of Lemma 4.1. This gives

$$\begin{aligned} \sup_{\substack{z\in K\\ 0\le\theta\le 2\pi}} \|P(z,re^{i\theta}) - C(z)\|_{D^-,*} &\le Cr^\gamma, \\ \sup_{\substack{z\in K,\ w\in\Gamma\\ 0\le\theta\le 2\pi}} \|T(w)[P(z,re^{i\theta}) - C(z)]\|_{D,*} &\le Cr^\gamma, \qquad 0 < r \le R. \end{aligned} \tag{13.2}$$

Here P and C denote the local packet and density row before completion by Y. The estimates use the common finite-mesh record convention before the mesh and source-radius upper limits. Their constants are independent of the contour point and collision angle. The stress Cauchy bound is uniform over $w \in \Gamma$ because the same radius d works everywhere. The stress-center modulus on finitely many overlapping neighborhoods of Γ gives norm convergence of its contour quadratures.

For $n \neq 0$, keep the leading subtraction inside the Fourier packet:

$$P_n(z,r) = \frac{1}{2\pi}\int_0^{2\pi} e^{-in\theta}[P(z,re^{i\theta}) - C(z)]\,d\theta.$$

The first line of (13.2) gives $P_n = O(r^\gamma)$ and $P_0 - C = O(r^\gamma)$ in the common-cut norm. The second gives the same bounds after adding a stress anywhere on Γ. Moreover, $|w - z| \ge d$, so for each fixed derivative order the kernel $(w-z)^{-1}$ and all its source derivatives are bounded uniformly on $\Gamma \times K$. Integrating the second bound along the finite-length contour therefore shows that $\mathcal{J}P_n$ has representation bound $O(r^\gamma)$ of order zero. Moving up to two source derivatives to the test gives the representation bound $\mathcal{A}P_n = O(r^\gamma)$ of order at most two.

At every positive radial truncation the grouped packets are finite linear combinations and angular integrals of separated words in $\mathscr{C}_0$. The grouping is preserved in estimates when the truncation is removed.

13.3 A bounded representative for the first angular mode

Set $T_r = r\partial_r$, $U = P_{-1}$, $a = 1$, and $b = 5/2$. The holomorphic null equation in mode -1 is

$$\begin{aligned} (T_r - a)(T_r - b)U &= T_r f + g, \\ f = 4r\partial_z P_{-2}, &\qquad g = -17r\partial_z P_{-2} - r^2\mathcal{A}P_{-3}. \end{aligned} \tag{13.3}$$

This is (12.6) at $n = -1$, with the exterior Ward term replaced by the contour above. It holds against every original spectator word. In particular f, g have representation bounds $O(r^{1+\gamma})$ of orders at most one and two, respectively. With upper endpoint R, the right inverses of Lemma 12.2 are

$$I_c F(r) = \begin{cases} r^c \displaystyle\int_0^r t^{-c-1}F(t)\,dt, & c < 1+\gamma, \\ -r^c \displaystyle\int_r^R t^{-c-1}F(t)\,dt, & c > 1+\gamma. \end{cases}$$

These integrals satisfy $(T_r - c)I_c F = F$, and their absolute kernel bounds give $I_c F = O(r^{1+\gamma})$ in the same representation seminorm. Put

$$v = I_b f + I_b I_a (af + g).$$

The order is as written: $(T_r - b)v = f + I_a(af + g)$, hence $(T_r - a)(T_r - b)v = T_r f + g$. Also $v, T_r v = O(r^{1+\gamma})$ of order at most two.

Choose fixed nonnegative nonzero smooth kernels $\widehat{\eta}_1, \widehat{\eta}_2$ with disjoint ordered supports in $(1/2, 1)$, put $\eta_\ell(t) = \widehat{\eta}_\ell(t/R)$, and let

$$M_{\ell 1} = \int \eta_\ell(t) t^a \, \frac{dt}{t}, \qquad M_{\ell 2} = \int \eta_\ell(t) t^b \, \frac{dt}{t}, \qquad W_\ell = \int \eta_\ell(t)[U(t) - v(t)] \, \frac{dt}{t}.$$

The matrix M is invertible: the ratios $M_{\ell 2}/M_{\ell 1}$ are weighted averages of the strictly increasing function t^{b-a} on ordered disjoint supports. The change of variables $t = Ru$ shows that $M = M_* \operatorname{diag}(R, R^{5/2})$, where M_* is the fixed invertible moment matrix of the two kernels on $(1/2, 1)$. Thus $M^{-1} = \operatorname{diag}(R^{-1}, R^{-5/2}) M_*^{-1}$. The coefficient bounds below include these factors of the fixed R. Define the local representations

$$\begin{pmatrix} A \\ B \end{pmatrix} = M^{-1} \begin{pmatrix} W_1 \\ W_2 \end{pmatrix}, \qquad \widetilde{U}(r) = Ar + Br^{5/2} + v(r).$$

The constant-coefficient distribution equation shows that $U - v = A'r + B'r^{5/2}$ against each word in $\mathscr{C}_0$. Its two window moments identify $A' = A$ and $B' = B$, so $\widetilde{U} = U$ against that word. The construction uses only original packets, at most one stress-contour insertion in each summand, and at most two source derivatives. Moreover,

$$\widetilde{U}(r) = O(r)$$

in the local representation seminorm. The equality initially follows as a distribution in $\log r$; weak continuity of the local packets and the weakly continuous integral formulas imply equality at every positive radius. The $O(r)$ bound applies to this source-tested integral representation.

13.4 The coefficient representation and a uniform tail

The zero-mode holomorphic null equation is

$$T_r(T_r - p)P_0 = -r(9 - 4T_r)\partial_z U - r^2 \mathcal{A} P_{-2}. \tag{13.4}$$

Replace U by its local representative and put

$$f_0 = 4r\partial_z \widetilde{U}, \qquad g_0 = -13r\partial_z \widetilde{U} - r^2 \mathcal{A} P_{-2}.$$

Then the right side is $T_r f_0 + g_0$. Both f_0 and g_0 have representation bounds $O(r^2)$ of order at most three. Derivatives of $\mathcal{J}$ act on the smooth kernel $(w - z)^{-1}$ and on the source expression, so each summand still contains at most one stress insertion.

For forcing of order r^2, the inverses I_0, I_p of Lemma 12.2 both integrate from zero to r. Define

$$v_0 = I_p f_0 + I_p I_0 g_0.$$

Then $T_r(T_r - p)v_0 = T_r f_0 + g_0$ and

$$v_0, T_r v_0 = O(r^2)$$

in the representation seminorm of order at most three. Consequently $P_0 - v_0 = C' + r^p \Psi'$ against each word in $\mathscr{C}_0$. The leading fusion bound identifies $C' = C$ as a functional on $\mathscr{C}_0$. Choose a nonnegative nonzero smooth $\widehat{\eta}_0$ supported in $(1/2, 1)$, put $\eta_0(t) = \widehat{\eta}_0(t/R)$, and set

$$m_p = \int \eta_0(t) t^p \, \frac{dt}{t} > 0, \qquad \mathfrak{P} = m_p^{-1} \int \eta_0(t)[P_0(t) - C - v_0(t)] \, \frac{dt}{t}.$$

Here $m_p = R^p \int \widehat{\eta}_0(u) u^p \, du/u$, so its inverse is another constant depending on the fixed R. This is a bounded local integral representation of order at most three, made from original fields and at most one stress insertion in each summand. The window identity identifies $\Psi' = \mathfrak{P}$. As before, weak continuity upgrades the equality to every positive radius. Thus, for every $Y \in \mathscr{C}_0$ supported outside D,

$$\begin{aligned} \langle r^{-p}(P_0(r) - C)Y \rangle &= \langle (\mathfrak{P} + \mathfrak{E}_r)Y \rangle, \\ \mathfrak{E}_r &= r^{-p} v_0(r) = O_{\mathrm{rep}}(r^{1/2}). \end{aligned} \tag{13.5}$$

The last bound is a local representation bound uniform over bounded outer completions of its constituent original rows. The expression on the left is schematic field notation: P_0 and C denote the corresponding local packet and density source before the exterior completion by Y. The correlation limit is the constructed one-slot Ψ, so $\mathfrak{P}$ represents that insertion against the initial class.

The radial convergence in these formulas can be stated together.

Lemma 13.1 (Absolute convergence of the radial representatives)**.** *Every radial integral defining v, $\widetilde{U}$, v_0, $\mathfrak{P}$, and $\mathfrak{E}_r$ converges absolutely in the source-tested row norm of its stated differential order. At every positive value of its radial parameters, its grouped integrand is a finite linear combination or a compact angular and contour integral of separated words in $\mathscr{C}_0$, with source derivatives moved to the test. Truncating all radial parameters away from zero and then removing the truncations gives the same representative for every order of these integrations.*

Proof. For a grouped family with representation bound $F(t) = O(t^\beta)$, the absolute kernel integrals for either right inverse satisfy

$$\begin{aligned} r^c \int_0^r t^{\beta-c-1} \, dt &= \frac{r^\beta}{\beta - c}, && \beta > c, \\ r^c \int_r^R t^{\beta-c-1} \, dt &= \frac{r^\beta - R^{\beta-c} r^c}{c - \beta} \le \frac{r^\beta}{c - \beta}, && \beta < c. \end{aligned}$$

The same inequalities hold for the source-tested row seminorm after moving the finitely many source derivatives to the test. For the first-mode forcing, $\beta = 1 + \gamma$: I_a integrates $t^{\gamma-1}$ at zero, while I_b has lower endpoint $r > 0$. These estimates also apply to $I_b I_a(af + g)$ by iteration. The window integrals for A, B stay in $(R/2, R)$ and use the finite matrix M^{-1} at this fixed R.

For f_0, g_0 the exponent is $\beta = 2$. The kernels of I_0 and I_p are integrable against these bounds; the more singular one is $t^{2-p-1} = t^{-1/2}$. Iterating the displayed inequalities therefore gives $v_0 = O(r^2)$ and $r^{-p} v_0 = O(r^{1/2})$ in the tested row norm. The window defining $\mathfrak{P}$ has positive lower endpoint and its normalization m_p^{-1} is finite for the fixed R.

In each integrand the scalar and density points have distance $t > 0$, the stress point lies on the fixed separated contour, and every exterior source lies outside D. Positive truncations consequently use the correlations of $\mathscr{C}_0$ established in Theorem 4.4. The leading subtractions stay grouped: (13.2) bounds their norms before the radial integration. These bounds give an integrable majorant for each nested integral. The tails tend to zero in the same tested norm, and the usual absolute-integrability argument proves Fubini and independence of the truncation order. The compact-parameter quadrature convergence of Section 13.1 identifies these limits with the local integral representatives. □

Auxiliary choices. The contour, R, and the moment kernels may change the representative as a formal local expression. Its pairing with every word in $\mathscr{C}_0$ is fixed by the raw extraction

limit. For products, choice independence will follow by identifying each choice with the same joint raw limit.

13.5 The local expression space and its completion

We now complete the space of source-tested local expressions in the norm supplied by the preceding construction.

Fix mutually disjoint source caps D_i and relatively compact source patches $U_i \Subset D_i$, $1 \le i \le m$. All collision pairs associated with $z_i \in U_i$ and all contours used in their representations lie in D_i. The contours are fixed curves, independent of the source coordinates and of the collision radii. They have positive distance from the source patches and from the outer cuts ∂D_i. All original spectator sources are outside these caps.

The local representatives require at most three source derivatives. Indeed, f, g in (13.3) use at most two; the radial inverses and the moment matrix act only on radial parameters and add none. The formulas for f_0, g_0 add at most one source derivative. Derivatives of the contour kernel contribute bounded smooth coefficients because the contour stays separated. The norm convergence of parameter quadratures in Section 13.1 uses one further test derivative. We therefore fix the local smooth-test order

$$q = 4. \tag{13.6}$$

Every bound below uses this same order, independently of the collision radius. Its constant depends on the fixed R and geometric choices.

A finite local original-field expression is a finite linear combination of separated words in the constructed fields inside one cap, with at most three source derivatives, optionally integrated over compact parameter sets on which all constituent insertions stay separated. Source derivatives are understood distributionally. Thus an expression of the form

$$V(z) = \sum_{|\alpha| \le 3} \partial_z^\alpha \int_{\mathcal{T}_\alpha} V_\alpha(z,t)\, d\mu_\alpha(t)$$

is evaluated against a source test φ by moving every derivative to φ and to any displayed smooth coefficient. Here a real multi-index is used for derivatives in the two source coordinates. Each $V_\alpha(z,t)$ has an outgoing row on the fixed cut, with all connectivity and parity labels retained. Additional derivatives of a completed expression are evaluated by moving them to the joint test, increasing its order by the number of derivatives.

The sufficient local bound is

$$\left\| \int_{U_i} \varphi(z) V(z)\, d^2 z \right\|_{D_i,*} \le K \|\varphi\|_{C^q(U_i)}. \tag{13.7}$$

The norm on the left is the upper completed-row norm, evaluated on the same finite-mesh label space before taking the specified upper limits. Consequently the bound controls every bounded exterior completion of the integrated row. Write $K_i(V)$ for the least constant K in (13.7); equivalently, take the supremum of its left side over all $\varphi \in C_c^\infty(U_i)$ with $\|\varphi\|_{C^q} \le 1$. The patch, cut, and order q are fixed when taking this seminorm.

We also admit limits of finite expressions that are Cauchy for the bound (13.7). First identify expressions whose difference has seminorm zero, and then take the completion. Two approximation sequences represent the same element when their difference has limiting seminorm zero. The comparisons defining this space use the common finite-mesh record convention. Absolutely convergent parameter integrals define such elements by truncation, since their tails are bounded by the corresponding integrals of the source-tested row bounds. Every bounded multilinear exterior completion extends to this space by the same estimate.

13.6 A tensor estimate

Lemma 13.2 (Disjoint local expressions)**.** *Suppose V_i obeys (13.7) with constants K_i. Fix a finite original spectator word Y and a compact set of separated source configurations. If d_Y real spectator coordinates are also tested, one may take*

$$N = 6m + d_Y + 1, \qquad p_N(\psi) = \max_{|\alpha|\le N} \|\partial^\alpha \psi\|_\infty. \tag{13.8}$$

With $d_Y = 0$ when the spectator coordinates are fixed, the estimate is

$$|\langle V_1(z_1)\cdots V_m(z_m)Y;\psi\rangle| \le C_Y \left(\prod_{i=1}^m K_i\right) p_N(\psi). \tag{13.9}$$

The same estimate holds for the completed local expressions, and their correlations are independent of the particular finite-expression approximations.

Proof. First use a product source test $\psi = \prod_i \varphi_i$ and keep all finite-expression parameters in compact separated sets. Sample the disjoint caps separately. The exterior percolation filling and the final parity rule form a multilinear completion of norm at most one. The root normalizations and the rows of the fixed original spectators give the finite factor C_Y. Integrate each local source test before gluing. Finite-mesh variation duality and (13.7) give

$$|\langle V_1\cdots V_m Y;\prod_i \varphi_i\rangle| \le C_Y \prod_i K_i \|\varphi_i\|_{C^q}.$$

The same inequality survives the regulator limits for $\mathscr{C}_0$.

For a general smooth joint test, take a finite partition of unity subordinate to products of source patches and separated spectator patches. On each product, use coordinate boxes and smooth cutoffs equal to one on the test support, and expand the extended test in a periodic Fourier series. Write n for the full frequency vector, of dimension $2m + d_Y$. A local factor of frequency n_i has C^4 norm at most $C(1 + |n_i|)^4$. Their product is bounded by $C(1 + |n|)^{4m}$.

The original spectator completion has order zero on these separated patches: disjoint root-arm extraction and the bounded scalar and stress rows give a constant times the L^1 norm of its test, by Lemma 4.1 and Theorem 4.4. Its Fourier factors thus add no derivative loss. Repeated integration by parts in a coordinate with largest $|n_j|$ bounds the Fourier coefficient by $Cp_N(\psi)(1 + |n|)^{-N}$. Hence the sum of the product estimates is bounded by

$$C_Y\Big(\prod_i K_i\Big)p_N(\psi) \sum_{n\in\mathbb{Z}^{2m+d_Y}} (1 + |n|)^{4m-N}.$$

The series converges whenever $N > 4m + 2m + d_Y$, giving (13.8) and (13.9). If an identity contains a further total of ℓ source derivatives, move them to the joint test and use $p_{N+\ell}$ instead.

Finally truncate each parameter integral and approximate each completed local expression. The multilinear telescoping identity and the bound proved show that the resulting correlations are Cauchy and do not depend on the approximations. The same argument justifies Fubini for every absolutely convergent local representation. □

Lemma 13.3 (Local decomposition and its exterior testing class)**.** *Fix the caps, source patches, contours, moment kernels, and positive radii R used above. For each patch there are*

elements V_i and $E_{i,r}$ of the completed local expression space, with local test order $q = 4$, such that

$$K_i(V_i) \le C_i, \tag{13.10}$$

$$K_i(E_{i,r}) \le C_i r^{1/2}, \qquad 0 < r < r_0, \tag{13.11}$$

where r_0 and C_i depend on the fixed choices, including R. Define

$$Q_r(z) = r^{-3/2}\left[\frac{r^{5/4}}{2\pi}\int_0^{2\pi} E^\circ(z)\Phi(z + re^{i\theta})\,d\theta - C_\circ\Phi(z)\right]. \tag{13.12}$$

Then

$$\langle Q_r(z_i)Y\rangle = \langle [V_i(z_i) + E_{i,r}(z_i)]Y\rangle \tag{13.13}$$

in source distributions for every finite separated word $Y \in \mathscr{C}_0$ outside D_i. The identity also holds for source derivatives and absolutely convergent parameter integrals of such words, with a fixed finite derivative order. Here absolute convergence means integrability of the source-tested row bounds on fixed exterior cuts; leading-subtracted packets are kept grouped in those bounds. In particular, it holds when the exterior is a finite product of completed local integral representatives in disjoint caps outside D_i, together with a finite original spectator word.

Proof. Take $V_i = \mathfrak{P}$ and $E_{i,r} = \mathfrak{E}_r$ from (13.5) in the corresponding cap. Lemma 13.1 places both in the completed expression space and gives the two bounds, with the test order derived in (13.6). Equation (13.5) gives (13.13) against each finite original word, at every positive r.

For a parameter integral of exterior words, first truncate to compact parameter sets with all constituent points separated. Linearity, finite quadrature convergence, and distributional integration by parts give the identity at this truncation. The absolute exterior row bounds, together with the fixed finite local bounds for Q_r, V_i, and $E_{i,r}$, allow the truncation to be removed. In particular, (4.12) gives

$$K_i(Q_r) \le C_i r^{\gamma - 3/2} < \infty \qquad \text{for each fixed } r > 0.$$

The bounds on $V_i, E_{i,r}$ are those above.

For several completed exterior representatives, approximate each by finite original-field integrals at positive parameter truncations. The identity holds for their product at every such approximation. Lemma 13.2, followed by the finite multilinear telescoping identity, shows that both sides converge as the approximations converge in their respective tested row seminorms. This proves the last assertion. The same argument gives the claimed extension after source derivatives are transferred to the joint test. □

13.7 Joint extraction

Theorem 13.4 (Any fixed finite number of separated new insertions)**.** *Fix $m < \infty$, separated centers $z_1, \dots, z_m$, and a finite separated original spectator word Y. Remove the mesh and all source regulators of the fields in $\mathscr{C}_0$ at fixed positive collision radii. Then*

$$\lim_{r_1,\dots,r_m \downarrow 0} \left\langle \prod_{i=1}^m Q_{r_i}(z_i)Y \right\rangle = \langle \Psi(z_1)\cdots\Psi(z_m)Y\rangle \tag{13.14}$$

exists in source distributions at arbitrary relative rates of the collision radii. On each compact separated configuration set,

$$\left\langle \prod_{i=1}^m Q_{r_i}(z_i)Y \right\rangle = \langle \Psi(z_1)\cdots\Psi(z_m)Y\rangle + O_{\mathcal{D}'}\left(\sum_{i=1}^m r_i^{1/2}\right). \tag{13.15}$$

The error is bounded using the seminorm p_N in (13.8). Its constant depends on m, the spectator word, the compact separation geometry, and the fixed auxiliary radii R and kernels. The definition agrees with the previous one-source insertion, is symmetric under permuting the new slots, and is independent of the auxiliary caps, fixed contours, radial windows, and integration cutoffs used in the local representations. All iterated limits of the disjoint collision radii have the same value.

Proof. Define the proposed right side by

$$\langle \Psi(z_1)\cdots\Psi(z_m)Y\rangle := \langle V_1(z_1)\cdots V_m(z_m)Y\rangle.$$

Lemma 13.2 makes this definition meaningful. It remains to identify it with the original joint extraction. All equalities can first be made in joint source and displacement distributions. The positive-displacement continuity established at the start of this section then gives joint weak continuity at each positive displacement tuple. The local representations inherit that continuity by compact truncation and the uniform grouped tail bounds. Hence their restrictions to the angular integrations and all positive collision radii agree with the correlations defined by the lattice prescription.

At fixed positive $r_1,\dots,r_m$, every remaining raw factor Q_{r_j} is an angular integral of a finite linear combination of separated words in $\mathscr{C}_0$ and has a finite tested row bound. Apply Lemma 13.3 to the first slot. Its exterior is a product of these finite-radius expressions and the original word Y, so the identity replaces Q_{r_1} by $V_1 + E_{1,r_1}$. For the second slot the exterior also contains this completed representative in the disjoint first cap. The last assertion of the lemma applies: truncate that representative to finite original-field integrals, use the identity on every constituent, and remove the truncation using the tensor estimate. The bound of any raw factor still present is used only at its fixed positive radius.

Repeating this operation for all m slots gives the exact identity of tested correlations

$$\left\langle \prod_{i=1}^{m} Q_{r_i}(z_i)Y \right\rangle = \left\langle \prod_{i=1}^{m} [V_i(z_i) + E_{i,r_i}(z_i)]Y \right\rangle. \tag{13.16}$$

Expand the right side by subsets. Every nonempty error subset S is bounded by

$$C_{m,Y}\left(\prod_{i\in S} r_i^{1/2}\right) p_N(\psi),$$

using (13.10), (13.11), and the tensor lemma. For $0 < r_i \le r_0$ these finitely many terms have total bound $C_{m,Y}\sum_i r_i^{1/2} p_N(\psi)$, after absorbing fixed powers of r_0 into the constant. This proves (13.15) and the unrestricted joint limit.

For $m = 1$, the limit is the previously extracted coefficient, since both are limits of the same raw Q_r. Symmetry follows from symmetry of the original separated correlations before any collision. Two choices of local representation both approximate the same raw joint correlation with an error tending to zero; their limits are therefore identical. For any fixed positive values of the other radii, the exact product representation also gives the one-radius limit by replacing its factor $V_i + E_{i,r_i}$ with V_i. Repeating this observation proves existence of every iterated limit and equality with the joint limit. □

13.8 Covariance and Ward identities of the joint fields

Corollary 13.5 (Covariance, Ward identities, and scalar null identities for the enlarged class)**.** *Let $\mathscr{C}_1$ be the class defined in (4.37). These plane correlations are jointly Möbius*

covariant in every Ψ slot, with weights $(77/96, 77/96)$. Let f be a Möbius transformation, regular at the displayed sources. With spherical charts used at infinity and the established transformation factors of the spectator word Y understood,

$$\left\langle \prod_{i=1}^{m} \Psi(z_i) Y \right\rangle = \prod_{i=1}^{m} |f'(z_i)|^{77/48} \left\langle \prod_{i=1}^{m} \Psi(f(z_i)) f_* Y \right\rangle . \tag{13.17}$$

Here f_*Y denotes the spectator word at its image points, with its primary transformation factors included. For a separated stress point w,

$$\left\langle T(w) \prod_{i=1}^{m} \Psi(z_i) Y \right\rangle = \left[\sum_{i=1}^{m} \left\{ \frac{77/96}{(w-z_i)^2} + \frac{1}{w-z_i} \partial_{z_i} \right\} + \mathcal{D}_w^Y \right] \left\langle \prod_{i=1}^{m} \Psi(z_i) Y \right\rangle , \tag{13.18}$$

where $\mathcal{D}_w^Y$ is the Ward sum over the Y slots in (4.10). The antiholomorphic identity and the finite zero-central-term Ward hierarchy hold as well. For every $Y_1 \in \mathscr{C}_1$ separated from z,

$$\langle \mathcal{N}_z E^\circ(z) Y_1 \rangle = 0, \qquad \langle \mathcal{N}_{\bar{z}} E^\circ(z) Y_1 \rangle = 0. \tag{13.19}$$

These are correlation identities in source distributions. Correlations vanish when the total number of Φ and Ψ slots is odd.

The joint construction extends the one-slot primary identities as well as the one-slot limit. Equality of local representations is preserved under disjoint gluing. If two admissible local integral representations have equal pairings with every original spectator word, then they have equal pairings with any finite collection of admissible local representations in disjoint caps. To prove this, truncate all other representations to finite original-field integrals, use the given identity for each constituent, move source derivatives to the joint test, and then remove the truncations using the absolute tensor bound. Thus equality on the initial class becomes multiplicative for these particular controlled representations. The absolute representation bounds are what permit this extension.

13.8.1 Conformal transport

Let f be a Möbius map, and choose the source caps with closures away from its pole in a fixed spherical chart. Transport a local coefficient representation term by term using the constructed covariance of the original fields. To control the radial integrals after transport, write $\lambda = f'(z)$ and $s = te^{i\theta}$. The normalized packet is transported to

$$|\lambda|^{5/48}(1 + O(t))|f(z+s) - f(z)|^{5/4} E^\circ(f(z)) \Phi(f(z+s)).$$

The target leading-row estimate is uniform in the displacement angle and in lengths comparable with t. Consequently every transported nonzero original Fourier mode is $O(t^\gamma) + O(t) = O(t^\gamma)$: the angle-independent leading density term cancels, and the smooth transport multiplier contributes only $O(t)$. This is precisely the bound needed in the radial integrals. For source derivatives, first transport the entire grouped packet and change the source variable; then transfer each derivative to the transported smooth test and its coefficients. This retains the grouped $O(t^\gamma)$ bound with a finite test order. Fixed stress contours transform to fixed separated smooth contours, whose kernels remain bounded. Hence the transported coefficient and error representations have the same finite source-test order and integrable radial bounds as before.

Theorem 12.4 identifies two local representations in the target chart: the transported representative of $\Psi(z)$ and $|f'(z)|^{77/48}\Psi(f(z))$. Their equality against words in $\mathscr{C}_0$ extends to products by the closure observation. For $Y = \prod_j X_j(\xi_j)$, with weights $(h_j, \bar{h}_j)$, this gives

$$\left\langle \prod_{i=1}^{m} \Psi(z_i) \prod_j X_j(\xi_j) \right\rangle = \prod_{i=1}^{m} |f'(z_i)|^{77/48} \prod_j f'(\xi_j)^{h_j} \overline{f'(\xi_j)}^{\bar{h}_j} \left\langle \prod_{i=1}^{m} \Psi(f(z_i)) \prod_j X_j(f(\xi_j)) \right\rangle.$$

This proves Möbius covariance of the joint plane correlations in source distributions.

13.8.2 Local conformal charges and the Ward identity

Use the proved independence of the auxiliary caps to choose nested caps $D_i^- \Subset D_i$, with the larger D_i still mutually disjoint. Construct the coefficient representative using the inner outgoing cut ∂D_i^-, and place a fixed contour Σ_i in the collar $D_i \setminus \overline{D_i^-}$. It encloses every constituent of that representative, including its first stress contour, and stays a positive distance from them. Thus $T(\zeta)$ for $\zeta \in \Sigma_i$ is an admissible exterior spectator from $\mathscr{C}_0$ for the representative identity at the inner cut. Complete the resulting local expression to the outer cut ∂D_i before the final gluing. If v is holomorphic inside Σ_i, define

$$\mathcal{Q}_v^{(i)} = \frac{1}{2\pi i} \int_{\Sigma_i} v(\zeta) T(\zeta)\, d\zeta.$$

The extra stress row is bounded on this fixed separated contour. The one-slot Ward identity, integrated in ζ, gives against every original exterior word

$$\langle \mathcal{Q}_v^{(i)} \Psi(z_i) Y \rangle = \left[h_\Psi v'(z_i) + v(z_i)\partial_{z_i} \right] \langle \Psi(z_i) Y \rangle, \qquad h_\Psi = 77/96.$$

The original exterior terms integrate to zero because they are analytic inside Σ_i. Both sides have admissible local representations; the closure observation therefore extends this local-charge identity with arbitrary finitely many other Ψ representatives outside the cap.

In the plane, for an external stress point w, use $v(\zeta) = (w - \zeta)^{-1}$ separately on all source caps. The original Ward identity expresses its action on each finite original-field approximation as the sum of these local charges and the ordinary original-spectator contributions. Absolute convergence permits the approximation limits. The local-charge formula consequently yields

$$\left\langle T(w) \prod_{i=1}^{m} \Psi(z_i) Y \right\rangle = \left[\sum_{i=1}^{m} \left\{ \frac{77/96}{(w - z_i)^2} + \frac{1}{w - z_i} \partial_{z_i} \right\} + \mathcal{D}_w^Y \right] \left\langle \prod_{i=1}^{m} \Psi(z_i) Y \right\rangle.$$

The antiholomorphic identity follows by the same argument. Additional finite stress insertions can be included in Y from the outset, so the established zero-central-term Ward hierarchy extends to the joint Ψ class. All source points remain separated in these identities.

13.8.3 The common null identity and parity

For the enlarged class $\mathscr{C}_1$ in (4.37), the existing scalar null identity extends to $Y \in \mathscr{C}_1$:

$$\langle \mathcal{N}_z E^\circ(z) Y \rangle = 0,$$

and likewise for the conjugate. Indeed, realize the stress descendant by a fixed contour in a cap around z, separated from all other caps. Both the contour and the source derivative give

controlled local source distributions. Apply the original null identity with all other coefficient representations truncated to finite original packets, and remove the truncations using the same tensor bound. The resulting identity holds in source distributions.

Every raw Q_r has one odd cluster-sign mark. Scalar and stress sources are even. The joint limit therefore preserves the rule that a correlation is zero when the total number of Φ and Ψ slots is odd. For example, pure odd-point Ψ correlations vanish, whereas the two-point function in Section 14.2 is nonzero. Together these identities and the parity rule prove Corollary 13.5.

13.9 Removing the known quadratic descendant

The raw regulator Q_r contains the descendant error $25C_\circ r^{1/2}\partial_z\partial_{\bar z}\Phi$. The same representative argument can keep this term explicit. In the first-mode construction, the conjugate null equation identifies its coefficient $A = -5\partial_{\bar z}C$ against original spectators, as in (12.10). Replace that coefficient in the representative by this original density derivative. The remaining terms satisfy

$$\widetilde{U} = -5r\partial_{\bar z}C + O_{\mathrm{rep}}(r^{1+\gamma}).$$

Substitution in the zero-mode equation and its integrable right inverse gives

$$v_0 = 25r^2\partial_z\partial_{\bar z}C + O_{\mathrm{rep}}(r^{2+\gamma}).$$

The leading terms of f_0, g_0 are respectively $-20r^2\partial_z\partial_{\bar z}C$ and $65r^2\partial_z\partial_{\bar z}C$, so $T_r f_0 + g_0$ has coefficient 25. The coefficient remains 25 after inversion because $T_r(T_r - 3/2)$ acts on r^2 by $2(2 - 3/2) = 1$. Thus the improved regulator

$$\widehat{Q}_r = Q_r - 25C_\circ r^{1/2}\partial_z\partial_{\bar z}\Phi \tag{13.20}$$

has an equivalent coefficient representative with error $O_{\mathrm{rep}}(r^{1/2+\gamma})$. Equality against words in $\mathscr{C}_0$ and the joint independence of representatives show that it defines the same joint field. This proves the sharpening in Theorem 4.11: the tensor argument improves (4.35) to $O_{\mathcal{D}'}(\sum_i r_i^{1/2+\gamma})$ for products of $\widehat{Q}_{r_i}$. The sharpened estimate uses the same source-distribution topology.

14 Nonvanishing and low-point normalizations

A local field becomes concrete when its correlations can be measured against simple configurations. The four-point formula of Section 11 gives such measurements for Ψ: first a three-point correlation that detects it, then the coefficient of its two-point function.

14.1 A finite-point detector for the extracted field

Take distinct finite points $0, w, u$ and set

$$G(s) = \langle E^\circ(w)\Phi(u)E^\circ(0)\Phi(s)\rangle.$$

The map

$$g(\zeta) = \frac{(\zeta - s)(u - w)}{(\zeta - w)(u - s)} \tag{14.1}$$

sends w, u, s to $\infty, 1, 0$ and sends zero to $t = s(u-w)/[w(u-s)]$. Covariance of the constructed scalar and density fields gives

$$G(s) = |w|^{-2y}|u - s|^{-2x}F(t, \bar t). \tag{14.2}$$

To check the pole normalization, write $a_0 = (u-w)/(u-s)$ and $g'(\zeta) = a_0(s-w)/(\zeta-w)^2$. The scalar factor at the pole w is $|a_0(w-s)|^{-y}$; its product with the factor at zero leaves $|w|^{-2y}$. The product of the two density factors is $|u-s|^{-2x}$.

Multiplying (14.2) by $|s|^y$, the first block is real analytic in $s, \bar{s}$ near zero. Its angular average contains only even integer powers of $|s|$. The second block is $|s|^{3/2}$ times a real-analytic factor whose leading coefficient is

$$-\mathfrak{k}^2 C_\circ^2 |w|^{-2y} |u|^{-2x} \left| \frac{u-w}{wu} \right|^{3/2-y}. \tag{14.3}$$

Since $3/2 - y = 1/4$, the extraction formula and translation give

$$\langle \Psi(z) E^\circ(w) \Phi(u) \rangle = -\mathfrak{k}^2 C_\circ^2 \frac{|w-u|^{1/4}}{|z-w|^{11/4} |z-u|^{11/24}}. \tag{14.4}$$

The strict positivity of $C_\circ$ makes this a nonzero matrix element. This completes the nonvanishing assertion in Theorem 4.10.

With the extraction normalization fixed in (4.33), the mixed detector coefficient satisfies

$$\frac{C_{\Psi E^\circ \Phi}}{C^2_{E^\circ \Phi\Phi}} = -\mathfrak{k}^2 = -\frac{25}{144} \left[\frac{\Gamma(1/4)}{\Gamma(3/4)} \right]^4. \tag{14.5}$$

Here the numerator denotes the coefficient in (4.32) and the denominator is $C_\circ^2$. The normalization of Ψ is fixed by the extraction, so this ratio has no remaining rescaling freedom.

14.2 The two-point normalization from two disjoint collisions

Two disjoint scalar–density pairs give the two-point correlation of Ψ. The explicit four-point formula permits both radii to tend to zero together, at arbitrary relative rates, and gives a pointwise error estimate.

Write

$$x = \frac{5}{48}, \qquad y = \frac{5}{4}, \qquad p = \frac{3}{2}, \qquad \mathfrak{k} = \frac{5}{12} \left[\frac{\Gamma(1/4)}{\Gamma(3/4)} \right]^2,$$

and retain the disk-response amplitude $C_\circ > 0$ in (4.11). For a positive collision radius r, after the mesh and original source regulators have been removed, put

$$Q_r(z) = r^{-p} \left[\frac{r^y}{2\pi} \int_0^{2\pi} E^\circ(z) \Phi(z + re^{i\theta})\, d\theta - C_\circ \Phi(z) \right]. \tag{14.6}$$

Every correlation of finitely many such expressions at positive, separated radii is a finite linear combination and angular integral of original-field correlations.

Proposition 14.1 (Two-point normalization and a joint error bound)**.** *For distinct points z, w, the two-source extraction satisfies*

$$\lim_{r,\rho \downarrow 0} \langle Q_r(z) Q_\rho(w) \rangle = \langle \Psi(z) \Psi(w) \rangle = -\mathfrak{k}^2 C_\circ^2 |z-w|^{-77/24}. \tag{14.7}$$

The limit holds at arbitrary relative rates. If $r, \rho \le c|z-w|$ for a sufficiently small fixed $c > 0$, then

$$\begin{aligned} &\left| \langle Q_r(z) Q_\rho(w) \rangle + \mathfrak{k}^2 C_\circ^2 |z-w|^{-77/24} \right| \\ &\qquad \le C |z-w|^{-77/24} \left[\frac{\sqrt{r\rho}}{|z-w|} + \frac{r^2+\rho^2}{|z-w|^2} \right]. \end{aligned} \tag{14.8}$$

Here C depends on the fixed normalization and on c, and the estimate is uniform on compact separated sets of z, w.

Proof. By translation, take $z = 0$ and write $d = w \neq 0$. Place the two density points at s and $d + t$, where $|s|, |t| \ll |d|$. In the generic cross-ratio formula (4.19), choose the density labels $u = d + t$ and $v = s$. The finite-point transport used in Theorem 4.8 then gives

$$\begin{aligned} G(s,t) &= \langle E^\circ(0)\Phi(s)E^\circ(d)\Phi(d+t)\rangle \\ &= |d|^{-2y}|d+t-s|^{-2x}F(\xi,\bar\xi), \qquad \xi = \frac{st}{d(d+t-s)}. \end{aligned} \tag{14.9}$$

The hypergeometric functions in (4.23), with the normalization established in Theorem 4.8, are

$$\begin{aligned} F(\xi,\bar\xi) &= C_\circ^2(|f_0(\xi)|^2 - \mathfrak{k}^2|f_1(\xi)|^2), \\ f_0(\xi) &= [\xi(1-\xi)]^{-5/8}U_0(\xi), & U_0(\xi) &= {}_2F_1\left(-\frac{5}{4},\frac{3}{4};\frac{1}{4};\xi\right), \\ f_1(\xi) &= [\xi(1-\xi)]^{-5/8}\xi^{3/4}U_1(\xi), & U_1(\xi) &= {}_2F_1\left(-\frac{1}{2},\frac{3}{2};\frac{7}{4};\xi\right). \end{aligned}$$

In particular $U_0(0) = U_1(0) = 1$. Analytic branches can be chosen on a fixed neighborhood of $(s,t) = (0,0)$; the absolute-value expressions below are independent of those local branch choices.

Normalize both pairs at once:

$$N(s,t) = |st|^y G(s,t).$$

Substitution gives the exact decomposition

$$N(s,t) = A(s,t) + |st|^p B(s,t), \tag{14.10}$$

where

$$A(s,t) = C_\circ^2|d|^{-y}|d+t-s|^{y-2x}|1-\xi|^{-y}|U_0(\xi)|^2, \tag{14.11}$$

$$B(s,t) = -\mathfrak{k}^2C_\circ^2|d|^{-(y+p)}|d+t-s|^{y-p-2x}|1-\xi|^{-y}|U_1(\xi)|^2. \tag{14.12}$$

Both A and B are real analytic in $(s,\bar s,t,\bar t)$ near the origin. Their relevant values are

$$\begin{aligned} A(0,t) &= C_\circ^2|d|^{-y}|d+t|^{y-2x}, \\ A(s,0) &= C_\circ^2|d|^{-y}|d-s|^{y-2x}, \\ A(0,0) &= C_\circ^2|d|^{-2x}, \\ B(0,0) &= -\mathfrak{k}^2C_\circ^2|d|^{-2(x+p)}. \end{aligned}$$

The first three expressions are the terms in the leading fusion and the density two-point normalization. Consequently, expanding the two brackets in (14.6), and using the known scalar–density three-point function for the two cross terms, gives the exact identity

$$\begin{aligned} \langle Q_r(0)Q_\rho(d)\rangle = r^{-p}\rho^{-p}\frac{1}{(2\pi)^2}\int_0^{2\pi}\int_0^{2\pi}\big[A(s,t) - A(0,t) - A(s,0) + A(0,0)\big]\,d\theta\,d\varphi \\ + \frac{1}{(2\pi)^2}\int_0^{2\pi}\int_0^{2\pi}B(s,t)\,d\theta\,d\varphi, \qquad s = re^{i\theta}, \quad t = \rho e^{i\varphi}. \end{aligned} \tag{14.13}$$

The independent angular averages are essential. A convergent real-analytic monomial $s^a\bar s^b t^c\bar t^e$ survives them only when $a = b$ and $c = e$. The four-term subtraction in the first integral also removes every monomial independent of either pair of variables. Thus its first

possible surviving term has $a = b = c = e = 1$, and that integral is $O(r^2\rho^2)$. The second integral is $B(0,0) + O(r^2 + \rho^2)$. Since $2 - p = 1/2$, division of the first integral by $r^p\rho^p$ gives $O(\sqrt{r\rho})$. This proves a joint limit, without restricting r/ρ.

For the scale-explicit estimate, apply these convergent power-series bounds to s/d and t/d on a fixed polydisk. The first integral is bounded by $C|d|^{-2x}(r/|d|)^2(\rho/|d|)^2$, and the second differs from $B(0,0)$ by at most $C|d|^{-2(x+p)}(r^2+\rho^2)/|d|^2$. Equation (14.8) follows, because $2(x+p) = 77/24$. □

Sign convention. The coefficient in (14.7) is negative. Its sign and magnitude are fixed by the specified signed disk-response extraction, with the same normalization in each new slot.

Normalization and order of limits. The mesh and the scalar and density regulators are removed at fixed nonzero s, t first. The two collision radii r, ρ then tend to zero while the centers z, w remain separated. This is the order of limits used in Theorem 13.4.

14.3 The scalar vacuum channel

The local regulators (4.2) have mean zero and depend on independent sets of Bernoulli variables when their disks are disjoint. Hence every separated scalar vacuum product vanishes, including $\langle E^\circ E^\circ\rangle$. Density spectators depend on connections through both source regions, so the mixed correlation F can be nonzero.

The two blocks exhibit the same cancellation in the $E^\circ E^\circ$ channel. Put $r_\Gamma = \Gamma(1/4)/\Gamma(3/4)$. The magnitudes of the constant leading terms of the two blocks at infinity are

$$a_0 = \frac{2r_\Gamma}{\sqrt{\pi}}, \qquad a_1 = \frac{24}{5r_\Gamma\sqrt{\pi}}, \qquad a_0 = \mathfrak{k}a_1.$$

Thus the candidate identity contribution cancels:

$$A_0a_0^2 + A_1a_1^2 = 0. \tag{14.14}$$

This agrees with the exact scalar vacuum property and checks the relative normalization of the two blocks.

14.4 Two scalar sources approach the stress channel

When two circular obstacles approach one another, their joint effect on a distant connection first records the direction between their centers. The constant term cancels, and the surviving angular dependence is that of the stress tensor. We compute its coefficient in the two-density correlations of Theorem 4.8. Keep r_Γ, a_0 and a_1 from the preceding subsection.

Proposition 14.2 (The two-scalar collision with two densities)**.** *The mixed four-point function of Theorem 4.8 satisfies*

$$F(\eta,\bar\eta) = \frac{5}{16}\left[\frac{\Gamma(1/4)}{\Gamma(3/4)}\right]^2 C_\circ^2\,\mathrm{Re}(\eta^{-2}) + O(|\eta|^{-3}), \qquad |\eta| \longrightarrow \infty. \tag{14.15}$$

The numerical coefficient is $2.735549519033\ldots$. *Consequently, as $w \to z$ with z, u, v distinct,*

$$\begin{aligned}&\langle E^\circ(z)E^\circ(w)\Phi(u)\Phi(v)\rangle\\ &\quad= 3\left[\frac{\Gamma(1/4)}{\Gamma(3/4)}\right]^2 C_\circ^2|w-z|^{-5/2}\big[(w-z)^2\langle T(z)\Phi(u)\Phi(v)\rangle\\ &\qquad\qquad + (\bar w-\bar z)^2\langle\bar T(z)\Phi(u)\Phi(v)\rangle\big] + O(|w-z|^{1/2}).\end{aligned} \tag{14.16}$$

The error is locally uniform in separated triples (z,u,v). All source regulators are removed at each fixed nonzero separation $|w-z|$ before the collision is taken.

Proof. Continue the two blocks in (4.23) from $0<\eta<1$ through the upper half-plane to the negative real axis. Their constant limits there are $e^{-5\pi i/8}a_0$ and $e^{\pi i/8}a_1$, respectively. The leading terms of the resonant hypergeometric expansion at infinity give

$$a_0=\frac{\Gamma(1/4)}{\Gamma(3/4)\Gamma(3/2)},\qquad a_1=\frac{\Gamma(7/4)}{\Gamma(3/2)\Gamma(9/4)};$$

these are the constants evaluated above. The expansion is the integer-difference case of the Gauss continuation formula [25, 15.8.8 and Section 15.12(i)]. Normalize the two solutions on this branch by

$$q_0(\eta)=e^{5\pi i/8}f_0(\eta)/a_0,\qquad q_1(\eta)=e^{-\pi i/8}f_1(\eta)/a_1.$$

Both tend to one as $\eta=-R$ with $R\to\infty$, and both are real on that ray. Since $a_0=\mathfrak{k}a_1$, the four-point formula becomes

$$F=C_\circ^2a_0^2(|q_0|^2-|q_1|^2). \tag{14.17}$$

For functions of R, write their Wronskian as $\mathcal{W}(g,h)=gh'-g'h$, where the prime is the R derivative. The differential equation (11.3), or Abel's identity applied to it, gives

$$\mathcal{W}(q_0(-R),q_1(-R))=\frac{3}{4a_0a_1}[R(1+R)]^{-3/2}. \tag{14.18}$$

The constant $3/4$ follows directly from the exponents $-5/8$ and $1/8$ and the unit leading coefficients of the blocks at zero; compare [25, 15.10.3].

The exponents of (11.3) at infinity are 0 and -2. Substituting a Frobenius expansion with constant term one shows that the coefficient of η^{-1} is zero and that the logarithmic term is $-(5/128)\eta^{-2}\log(-\eta)$. In particular, $q_j(-R)=1+O(R^{-2}\log R)$. For large R the function $q_0(-R)$ is nonzero, so integration of (14.18), with the ratio tending to one at infinity, gives

$$1-\frac{q_1(-R)}{q_0(-R)}=\frac{3}{4a_0a_1}\int_R^\infty\frac{[t(1+t)]^{-3/2}}{q_0(-t)^2}\,dt=\frac{3}{8a_0a_1}R^{-2}+O(R^{-3}).$$

The normalized constant terms, and hence the logarithmic terms, cancel in q_0-q_1. The decaying Frobenius solution therefore gives

$$q_0(\eta)-q_1(\eta)=\frac{3}{8a_0a_1}\eta^{-2}+O(|\eta|^{-3})=\frac{5\pi}{128}\eta^{-2}+O(|\eta|^{-3}).$$

These expansions hold on closed angular sectors of the chosen branch. The single-valued four-point function is covered by finitely many such sectors. Substitution in (14.17) yields

$$F=C_\circ^2\frac{3a_0}{4a_1}\operatorname{Re}(\eta^{-2})+O(|\eta|^{-3}),\qquad \frac{3a_0}{4a_1}=\frac{3}{4}\mathfrak{k}=\frac{5}{16}r_\Gamma^2,$$

which proves (14.15).

In the original coordinates use the cross ratio (4.19). Conformal covariance and the forcing identity identify the normalized mixed correlation as

$$\frac{\langle E^\circ(z)E^\circ(w)\Phi(u)\Phi(v)\rangle}{\langle\Phi(u)\Phi(v)\rangle}=|z-w|^{-5/2}F(\eta,\bar\eta).$$

As $w\to z$,

$$\eta^{-2}=(w-z)^2\frac{(u-v)^2}{(z-u)^2(z-v)^2}+O(|w-z|^3).$$

The one-stress Ward identity is

$$\frac{\langle T(z)\Phi(u)\Phi(v)\rangle}{\langle\Phi(u)\Phi(v)\rangle} = \frac{5}{96}\frac{(u-v)^2}{(z-u)^2(z-v)^2}, \tag{14.19}$$

with the conjugate formula for $\bar{T}$ [29, Appendix A.2, (A.6), and Appendix B.3, (B.4)]. Combining these equations proves (14.16), since $(5/16)/(2\cdot 5/96) = 3$. The same computation gives the stated uniformity and error on every compact set of separated triples. □

The identity contribution in this channel is zero by (14.14). Its first nonzero terms have the stress weights $(2,0)$ and $(0,2)$: after $w - z = \rho e^{i\theta}$, their angular factors are $e^{2i\theta}$ and $e^{-2i\theta}$ and their size is $\rho^{-1/2}$. Equation (14.16) identifies their action on two density insertions with the stress sources of Paper I. This exhibits the $c = 0$ structure discussed in [29, Section 2.5]: the stress source has vanishing vacuum correlations and a nonzero Ward action on density observations.

15 Two-point connections and two small obstacles

A connection can pass through two small regions in different ways. The regions may form successive bottlenecks, so that either obstacle destroys the connection, or they may provide alternative routes, so that both obstacles are needed. The mixed four-point function measures the signed balance between these two possibilities. Throughout this section, $y = 5/4$ and $x = 5/48$.

Let u, v, z, w be four distinct points of the plane. At mesh a, choose vertices u^a, v^a tending to u, v, and let

$$C = \{u^a \leftrightarrow v^a\}, \qquad p_0^a = \mathbb{P}_a(C).$$

For disjoint disks $D_z = B_\varepsilon(z)$ and $D_w = B_\delta(w)$, whose cell approximations avoid the two marked sites, write C_z, C_w, C_{zw} for the events that an open connection from u^a to v^a exists avoiding, respectively, D_z, D_w, and $D_z \cup D_w$. Define

$$q_z^a = \frac{\mathbb{P}_a(C_z)}{p_0^a}, \qquad q_w^a = \frac{\mathbb{P}_a(C_w)}{p_0^a}, \qquad q_{zw}^a = \frac{\mathbb{P}_a(C_{zw})}{p_0^a}. \tag{15.1}$$

All three are conditional probabilities given C. They concern the existence of an avoiding path in the whole cluster. Closing every site in the forbidden set gives precisely the same connection event. The forced-closed interpretation follows from the Bernoulli identity (4.3).

15.1 The one-obstacle comparison

The scalar–density three-point function gives

$$1 - q_z(\varepsilon) = C_\circ\left(\frac{\varepsilon|u-v|}{|z-u||z-v|}\right)^{5/4} + O(\varepsilon^{5/4+11/15}), \qquad q_z(\varepsilon) = \lim_{a\downarrow 0} q_z^a. \tag{15.2}$$

The constants are locally uniform on separated configurations. The quantity on the left is the probability, conditional on the two sites being connected, that every connecting path uses the small disk. Thus (15.2) measures the chance that the disk is an unavoidable bottleneck for the connection. Apply Theorems 4.3 and 4.4 to (4.3) and (4.11). The scalar Cauchy error $O(\varepsilon^{11/15})$ is multiplied by the factor $\varepsilon^{5/4}$.

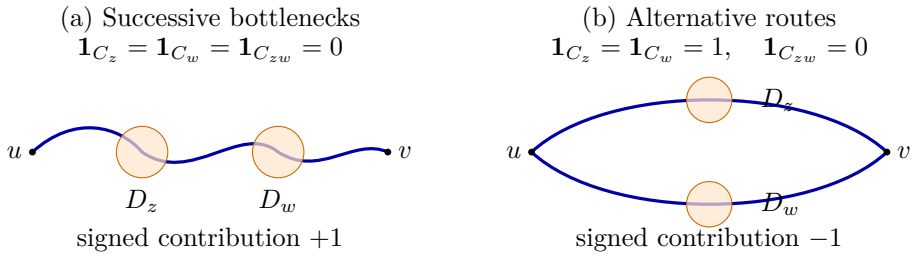


Figure 4: The two nonzero contributions to $\mathbf{1}_C - \mathbf{1}_{C_z} - \mathbf{1}_{C_w} + \mathbf{1}_{C_{zw}}$. Both panels have an open connection from u to v, so $\mathbf{1}_C = 1$. On the left every connecting path uses each obstacle; closing either disk breaks the connection. On the right each disk can be bypassed separately, while their union blocks every connecting path. The events refer to all paths in the configuration. The drawn paths show representative geometries of the two events.

15.2 The signed two-obstacle observable

Lemma 15.1 (Serial bottlenecks and alternative routes)**.** *At every mesh and for every pair of disjoint forbidden disks,*

$$1 - q_z^a - q_w^a + q_{zw}^a = \mathbb{P}_a(C \setminus (C_z \cup C_w) \mid C) - \mathbb{P}_a((C_z \cap C_w) \setminus C_{zw} \mid C). \tag{15.3}$$

The first event means that each disk separately destroys every connection. The second means that either disk can be avoided separately, but their union cannot be avoided.

Proof. The inclusions $C_{zw} \subseteq C_z \cap C_w \subseteq C$ give the pointwise indicator identity

$$\mathbf{1}_C - \mathbf{1}_{C_z} - \mathbf{1}_{C_w} + \mathbf{1}_{C_{zw}} = \mathbf{1}_{C \setminus (C_z \cup C_w)} - \mathbf{1}_{(C_z \cap C_w) \setminus C_{zw}}.$$

Take expectations and divide by p_0^a. □

Theorem 15.2 (The two-obstacle interaction)**.** *For the signed difference in Lemma 15.1, remove the mesh at fixed positive ε, δ and set*

$$\mathcal{I}_{\varepsilon,\delta}(z, w; u, v) = \varepsilon^{-5/4}\delta^{-5/4}[1 - q_z(\varepsilon) - q_w(\delta) + q_{zw}(\varepsilon, \delta)]. \tag{15.4}$$

The limit $\mathcal{I} = \lim_{\varepsilon,\delta \downarrow 0} \mathcal{I}_{\varepsilon,\delta}$ exists jointly at arbitrary relative rates. On separated compact configurations,

$$\mathcal{I}_{\varepsilon,\delta} = \mathcal{I} + O(\varepsilon^{11/15} + \delta^{11/15}). \tag{15.5}$$

With

$$\eta = \frac{(z - v)(u - w)}{(z - w)(u - v)}, \tag{15.6}$$

the exact coefficient is

$$\mathcal{I}(z, w; u, v) = C_\circ^2 |z - w|^{-5/2}(|f_0(\eta)|^2 - \mathfrak{k}^2 |f_1(\eta)|^2), \tag{15.7}$$

where

$$f_0(\eta) = [\eta(1 - \eta)]^{-5/8} {}_2F_1\left(-\frac{5}{4}, \frac{3}{4}; \frac{1}{4}; \eta\right), \tag{15.8}$$

$$f_1(\eta) = [\eta(1 - \eta)]^{-5/8} \eta^{3/4} {}_2F_1\left(-\frac{1}{2}, \frac{3}{2}; \frac{7}{4}; \eta\right), \tag{15.9}$$

$$\mathfrak{k} = \frac{5}{12}\left[\frac{\Gamma(1/4)}{\Gamma(3/4)}\right]^2. \tag{15.10}$$

The complete combination in (15.7) is independent of the choice of continuation branch.

Proof. Let $\Phi_a = g_a S$ denote the canonically normalized cluster-sign field. For two roots, averaging the cluster signs gives $\mathbb{E}[\Phi_a(u)\Phi_a(v)] = g_a^2 p_0^a$. For the two disjoint disks, the exact forcing identity gives

$$\begin{aligned}&\mathbb{E}\big[E^\circ_{a,\varepsilon}(z)E^\circ_{a,\delta}(w)\Phi_a(u)\Phi_a(v)\big]\\&\quad= g_a^2\varepsilon^{-y}\delta^{-y}\big[p_0^a - \mathbb{P}_a(C_z) - \mathbb{P}_a(C_w) + \mathbb{P}_a(C_{zw})\big].\end{aligned} \tag{15.11}$$

Here the product of the two forcing weights closes their union because their underlying sets of Bernoulli variables are disjoint. Divide (15.11) by the unforced two-point correlation. The fixed-hole mesh limits, followed by the joint two-scalar construction, then give

$$\mathcal{I}(z,w;u,v) = \frac{\langle E^\circ(z)E^\circ(w)\Phi(u)\Phi(v)\rangle}{\langle\Phi(u)\Phi(v)\rangle}. \tag{15.12}$$

Theorem 4.3, applied to the two slots by multilinear telescoping, gives (15.5). These pointwise two-root statements use the pointwise root-arm completion and source-center continuity proved in Theorem 4.4.

The map

$$g(\zeta) = \frac{(\zeta - v)(u - w)}{(\zeta - w)(u - v)}$$

sends w, u, v to $\infty, 1, 0$ and sends z to η. The covariance factors for the constructed scalar and density fields yield

$$\langle E^\circ(z)E^\circ(w)\Phi(u)\Phi(v)\rangle = |z-w|^{-2y}|u-v|^{-2x}\langle E^\circ(\infty)\Phi(1)E^\circ(\eta)\Phi(0)\rangle.$$

Divide by $|u-v|^{-2x}$ and insert the mixed four-point theorem. □

15.3 An explicit subleading connection asymptotic

The exponent $3/2$ can now be detected in an ordinary connectivity experiment with two obstacles. A single disk and two roots give the known expression (15.2); the two-obstacle formula of Theorem 15.2 supplies the additional test which detects the subleading field.

Corollary 15.3 (A hole approaches a marked endpoint)**.** *Fix three distinct points z, w, u, and put*

$$Q_\rho(z,w;u) = \frac{\rho^{5/4}}{2\pi}\int_0^{2\pi} \mathcal{I}(z,w;u,z+\rho e^{i\theta})\,d\theta, \tag{15.13}$$

$$A = C_\circ^2 \frac{|u-z|^{5/4}}{|w-z|^{5/4}|u-w|^{5/4}}, \tag{15.14}$$

$$a_* = \frac{u-w}{(w-z)(u-z)}, \qquad b_* = \frac{5}{2(u-z)} - \frac{25}{8(w-z)}. \tag{15.15}$$

Then, locally uniformly in the separated triple,

$$Q_\rho = A\left[1 - \mathfrak{k}^2|a_*|^{3/2}\rho^{3/2} + |b_*|^2\rho^2 + O(\rho^{7/2})\right]. \tag{15.16}$$

In particular, the $\rho^{3/2}$ coefficient is nonzero and negative. The limits defining $\mathcal{I}$ are taken first, at each fixed $\rho > 0$; only subsequently is ρ sent to zero.

Proof. Translate z to zero and abbreviate $U = u - z$, $W = w - z$ and $s = \rho e^{i\theta}$. Then

$$\eta(s) = \frac{a_* s}{1 - s/U}, \qquad 1 - \eta(s) = \frac{1 - s/W}{1 - s/U}, \qquad A = C_\circ^2 |W|^{-2y} |a_*|^{-y}.$$

Choose analytic powers near $s = 0$, normalized to have value one there, and define the two analytic germs

$$G_0(s) = (1 - s/U)^{5/4} (1 - s/W)^{-5/8} {}_2F_1\left(-\frac{5}{4}, \frac{3}{4}; \frac{1}{4}; \eta(s)\right), \tag{15.17}$$

$$G_1(s) = (1 - s/U)^{1/2} (1 - s/W)^{-5/8} {}_2F_1\left(-\frac{1}{2}, \frac{3}{2}; \frac{7}{4}; \eta(s)\right). \tag{15.18}$$

Both equal one at zero. Direct substitution in (15.7) gives the exact local identity

$$\frac{\rho^{5/4} \mathcal{I}(z, w; u, z + s)}{A} = |G_0(s)|^2 - \mathfrak{k}^2 |a_*|^{3/2} \rho^{3/2} |G_1(s)|^2. \tag{15.19}$$

For $G(s) = \sum_{n \geq 0} g_n s^n$ analytic in a fixed disk, orthogonality of the angular exponentials gives

$$\frac{1}{2\pi} \int_0^{2\pi} |G(\rho e^{i\theta})|^2 \, d\theta = \sum_{n \geq 0} |g_n|^2 \rho^{2n}. \tag{15.20}$$

The coefficient of s in G_0 is

$$-\frac{5}{4U} + \frac{5}{8W} - \frac{15}{4} a_* = \frac{5}{2U} - \frac{25}{8W} = b_*.$$

Consequently, the angular means of $|G_0|^2$ and $|G_1|^2$ are $1 + |b_*|^2 \rho^2 + O(\rho^4)$ and $1 + O(\rho^2)$, respectively. Applying these identities to (15.19) proves (15.16). On a compact set of separated triples (z, w, u), the denominators in G_0 and G_1 stay bounded away from zero, and the argument of each hypergeometric germ stays in one fixed disk about zero when $|s|$ is sufficiently small. Choose one such radius for the whole compact set. The germs and their prefactors are bounded on a slightly larger common disk; Cauchy's coefficient estimate then bounds the Taylor tails uniformly. The angular-average remainders $O(\rho^4)$ and $O(\rho^2)$ above consequently have constants uniform on that set. □

The exponent agrees with the one-cluster spectral description in [21, (77), p. 26]; the weight $(77/96, 77/96)$ also appeared in [20, (2.7)]. The formula above gives its coefficient for the disk-deletion connection experiment.

The quantity Q_ρ is the rescaled angular average of the signed conditional-probability difference in (15.3). Its explicit remainder follows from the analytic four-point formula. The obstacle limits are taken before the endpoint collision, as specified in Corollary 15.3.

A Monte Carlo comparison of the signed formula in Theorem 15.2 is given in Appendix B.

16 Conclusions

A circular obstacle measures where a connection is vulnerable. Retaining its full boundary record makes that response usable with other separated sources. The scalar Cauchy estimate, odd-parity screening, and positive three-point calibration yield the leading mixed fusion and the fixed-shape density-triple projection.

The six-tip calculation identifies the scalar response in each boundary-partition coordinate. Its stress variation and the eight-arm localization estimate establish the level-two null identities.

These determine the mixed scalar–density four-point function, including its signed second conformal block.

The same null equations control the local angular modes of a collision. Their second scalar coefficient defines Ψ with weights $(77/96, 77/96)$. The fixed-contour and radial integral representations give joint convergence for every fixed finite collection of separated insertions, at arbitrary relative extraction radii. The error is $O_{\mathcal{D}'}(\sum_i r_i^{1/2})$, and subtraction of the quadratic density descendant improves it to $O_{\mathcal{D}'}(\sum_i r_i^{1/2+\gamma})$ for $0 < \gamma < 5/48$.

The two-point normalization

$$\langle \Psi(z)\Psi(w)\rangle = -\mathfrak{k}^2 C_\circ^2 |z-w|^{-77/24}$$

is identified by a simultaneous two-radius calculation. The two-obstacle probability gives the same subleading coefficient a direct geometric interpretation, through the signed balance between successive bottlenecks and alternative routes. When the two scalar sources approach one another, their correlation with two density marks has a leading spin-two term. Proposition 14.2 identifies its exact coefficient and its agreement with the stress Ward correlation of Paper I.

Theorem 4.9 identifies the normalized Camia–Feng energy with the disk scalar, assuming their one-energy/two-density asymptotic (4.26). The comparison holds in the complete outgoing record and hence jointly for finitely many separated insertions with spectators in $\mathscr{C}_0$. It connects the geometric response with logarithmic density fusion and gives the energy insertion the same null identities and mixed four-point function. Proposition 10.5 explains the signs of that function through successive bottlenecks and alternative routes.

The finite-lattice experiment in Appendix B tests the disk observable and reproduces the predicted sign reversal under rotation of the obstacle pair. The amplitudes continue to change with the outer domain size; the sampled sizes do not yet show saturation at the plane predictions.

Further steps toward a percolation field algebra include a domain Ward identity incorporating boundary variation, extension of the Ψ construction to domains with holes, estimates for overlapping fusion regions, the construction and comparison of logarithmic fields, and control of complete expansions near the diagonals. A variation estimate for the untested second-mode record would give a stronger testing class than the source-distribution construction developed here. These questions connect the present local identities with the compatibility and convergence problems that arise in a full conformal field theory.

A Leading projection of three density marks

The screening argument of Section 6 also applies when three nearby density marks initially belong to three different clusters. Their odd blocks are allowed to merge during the exploration; only their total parity is relevant. At leading order, the exterior sees the total odd mark carried by the three roots. Throughout this appendix, $x = 5/48$.

Fix three distinct complex numbers $\zeta_1, \zeta_2, \zeta_3$ in a bounded set. We will show that the following limit exists:

$$\mathcal{C}(\boldsymbol{\zeta}) = \lim_{R\to\infty} R^{2x}\langle \Phi(\zeta_1)\Phi(\zeta_2)\Phi(\zeta_3)\Phi(R)\rangle. \tag{A.1}$$

The correlation at each finite R is the fixed-distinct-point density correlation constructed in [1, Theorem 1.5]. The limit will also be independent of the direction in which the fourth root tends to infinity. The proof uses its conformal covariance and the row projection (6.9).

Proposition A.1 (Leading triple projection)**.** *The limit* (A.1) *exists and is symmetric in the three arguments. For every* $0 < \gamma < x$ *and* $\rho \ll d$*,*

$$\left\| \rho^{2x} \prod_{i=1}^{3} \Phi(z + \rho\zeta_i) - \mathcal{C}(\boldsymbol{\zeta})\Phi(z) \right\|_{d,*} \le C_{\boldsymbol{\zeta},\gamma} d^{-x} (\rho/d)^{\gamma}. \tag{A.2}$$

The constants are uniform when the template stays in a bounded set and its three points have a fixed positive mutual separation. All original outgoing occupations, connections, and parity marks are retained.

Proof. Translation permits $z = 0$. Choose $s = c\rho$ large enough to contain three disjoint root disks of radii comparable with ρ, centered at $\rho\zeta_i$. Their independent normalized root arms bound the local packet row ξ^a_ρ by

$$\limsup_{a \downarrow 0} \|\xi^a_\rho\|_{\mathrm{var}} \le C\rho^{2x}\rho^{-3x} = C\rho^{-x}. \tag{A.3}$$

This is the same root-arm extraction used in (6.11), now in three disjoint disks. The packet has odd total parity, with one or three surviving odd blocks. Consequently (6.9) gives, with $R^a_{\rho,d} = \xi^a_\rho K^a_{s,d}$,

$$\limsup_{a \downarrow 0} \|R^a_{\rho,d} - b^a_{\rho,d} F^a_d\|_{\mathrm{var}} \le C d^{-x} (\rho/d)^{\gamma}, \qquad b^a_{\rho,d} = \frac{R^a_{\rho,d}(\mathbf{1})}{m^a_d}. \tag{A.4}$$

The coefficients are bounded by (6.7) and will be calibrated through their finite-mesh pairings.

For $D \ge 20d$, finite partition gluing propagates the density reference exactly: $F^a_d K^a_{d,D} = F^a_D$. Every row in the difference in (A.4) has odd total parity. Applying (6.7) and the one-arm ratio (6.8) therefore yields

$$\limsup_{a \downarrow 0} \|R^a_{\rho,D} - b^a_{\rho,d} F^a_D\|_{\mathrm{var}} \le C D^{-x} (\rho/d)^{\gamma}. \tag{A.5}$$

For a unit complex number u, test the last equation with the remote density at $2Du$, multiplied by D^x. As in (6.12), this completion has bounded supremum norm, and its pairing with F^a_D tends to $2^{-2x} D^{-x} > 0$. Denote the finite-mesh ratio of its pairings with $R^a_{\rho,D}$ and F^a_D by $A^a_D(u)$. From (A.5),

$$\limsup_{a \downarrow 0} |A^a_D(u) - b^a_{\rho,d}| \le C(\rho/d)^{\gamma}. \tag{A.6}$$

At each fixed positive geometry, Camia's density theorem gives the limit

$$A_D(u) = \rho^{2x} (2D)^{2x} \left\langle \prod_{i=1}^{3} \Phi(\rho\zeta_i)\Phi(2Du) \right\rangle. \tag{A.7}$$

For any $D, D' \ge 20d$ and any unit u, u', compare their finite-mesh ratios to the *same* $b^a_{\rho,d}$ in (A.6), and then remove the mesh. This gives

$$|A_D(u) - A_{D'}(u')| \le C(\rho/d)^{\gamma}.$$

Letting $d \to \infty$ at fixed ρ proves a common far-root limit, independent of direction. Dilation covariance of the density field [1, Theorem 1.5] rewrites (A.7) as

$$A_D(u) = (2D/\rho)^{2x} \left\langle \prod_{i=1}^{3} \Phi(\zeta_i)\Phi((2D/\rho)u) \right\rangle.$$

Thus the common limit is $\mathcal{C}(\boldsymbol{\zeta})$ in (A.1), independently of ρ.

For the fixed cut d, first fix $D \geq 20d$, take the mesh upper limit in (A.6), and then send $D \to \infty$. The triangle inequality gives

$$\limsup_{a\downarrow 0} |b^a_{\rho,d} - \mathcal{C}(\boldsymbol{\zeta})| \leq C(\rho/d)^\gamma.$$

Since $\|F^a_d\|_{\mathrm{var}} = m^a_d \to c_\Phi d^{-x}$, substitution into (A.4) proves (A.2). Symmetry follows from the finite four-density correlation. On a compact set of separated bounded templates, choose one radius smaller than a fixed fraction of the minimum distance between the three template points. The three root disks, the arm-ratio bounds, and the screening constants can then be chosen uniformly. In particular, the detector comparison has the same $C(\rho/d)^\gamma$ bound for every template in that set. Taking the far-root limit in this inequality preserves this common bound, and substituting it into the local projection proves the stated uniformity. This step uses the quantitative comparison with the same $b^a_{\rho,d}$ for all remote detectors. □

B A Monte Carlo comparison

The two-obstacle formula distinguishes two ways of keeping a connection alive. Rotating the line between the obstacles changes the balance between successive bottlenecks and alternative routes. We test this dependence directly on finite triangular lattices. The simulation samples the disk observable of Theorem 15.2. The Camia–Feng sign-pair regulator (4.24) is not sampled, so this experiment does not test the identification in Theorem 4.9.

B.1 A comparison independent of normalization

Use the connection probabilities of (15.1). Dividing the two-obstacle response of Theorem 15.2 by the product of the two one-obstacle responses in (15.2) cancels $C_\circ$ and the leading powers of the disk radii. The resulting plane prediction is

$$\lim_{\varepsilon,\delta\downarrow 0}\lim_{a\downarrow 0} \frac{1 - q^a_z - q^a_w + q^a_{zw}}{(1-q^a_z)(1-q^a_w)} = |\eta(1-\eta)|^{5/4}(|f_0(\eta)|^2 - \mathfrak{k}^2|f_1(\eta)|^2). \tag{B.1}$$

The blocks and cross ratio are those of (15.7)–(15.9) and (15.6). For marked sites $u = 1$, $v = -1$, we use two arrangements of obstacle centers:

$$(z, w) = (-1/4, 1/4), \qquad (z, w) = (-i/4, i/4).$$

Their cross ratios are $-9/16$ and $1/2 + 15i/16$, respectively. The corresponding predictions in (B.1) are 2.5130414637 and -2.9651524071.

B.2 Sampling and results

We sample independent site colors with open probability $1/2$ on the triangular lattice $\{(i + j/2, \sqrt{3}\, j/2) : i, j \in \mathbb{Z}\}$ inside a disk of radius L. Paths use only the sampled vertices inside this disk, with no boundary identifications. The marked sites are $(D, 0)$ and $(-D, 0)$; the two obstacle centers are $(\mp D/4, 0)$ or $(0, \mp D/4)$, and both obstacles have radius r. Rescaling by D gives mesh $1/D$, obstacle radius r/D, and outer radius L/D.

The two marked sites are fixed open. This conditioning multiplies all four connection probabilities by the same factor, which cancels from (B.1). Each configuration is used for the original connection and for the three disk deletions. We count the two nonzero signed events

directly using Lemma 15.1. Let n_C count original connections, let n_z, n_w count connections destroyed by the corresponding single disk, and let $n_{\mathrm{s}}, n_{\mathrm{p}}$ count successive-bottleneck and alternative-route configurations. The estimator is

$$\widehat{R} = \frac{n_C(n_{\mathrm{s}} - n_{\mathrm{p}})}{n_z n_w}. \tag{B.2}$$

The five categories of a connected configuration are survival after both deletions, loss only after the first deletion, loss only after the second, successive bottlenecks, and alternative routes. For each run, we draw n_C independent category labels with probabilities equal to their observed relative frequencies and recompute (B.2). The empirical 2.5% and 97.5% quantiles of 30 000 such resamples form the intervals in Table 1. This bootstrap calculation keeps the dependence between the numerator and denominators.

The six unstarred parameter sets in the table were fixed after a pilot run of 20 000 configurations. Two further controls were selected to examine the boundary dependence seen in those runs. The production and follow-up runs contain 3.1 million independent configurations in total, each tested in both arrangements. The pilot is excluded from Table 1. The connectivity implementation was checked on 10 000 fully sampled configurations against a separate depth-first search, including all disk deletions and the exact indicator identity (15.3).

Run	D	r	L/D	$N/10^3$	$\widehat{R}_{\parallel}$	$\widehat{R}_{\perp}$
1	24	2.75	4	500	1.816 $[1.702, 1.928]$	-1.896 $[-2.081, -1.713]$
2	24	2.75	8	500	2.182 $[2.040, 2.321]$	-2.455 $[-2.694, -2.219]$
3*	24	2.75	16	200	2.672 $[2.408, 2.928]$	-3.060 $[-3.538, -2.607]$
4	48	5.5	4	300	1.722 $[1.560, 1.880]$	-1.680 $[-1.915, -1.453]$
5	24	1.75	4	500	1.794 $[1.590, 1.994]$	-2.100 $[-2.423, -1.784]$
6	48	3.5	4	500	1.893 $[1.664, 2.122]$	-1.996 $[-2.348, -1.659]$
7	72	5.25	4	300	1.883 $[1.562, 2.201]$	-1.395 $[-1.821, -0.988]$
8*	24	1.75	8	300	2.038 $[1.697, 2.380]$	-2.297 $[-2.857, -1.754]$

Table 1: Finite-lattice ratios with 95% sampling intervals. The plane predictions are 2.5130414637 for the parallel arrangement and -2.9651524071 for the perpendicular arrangement. Stars mark the two follow-up controls.

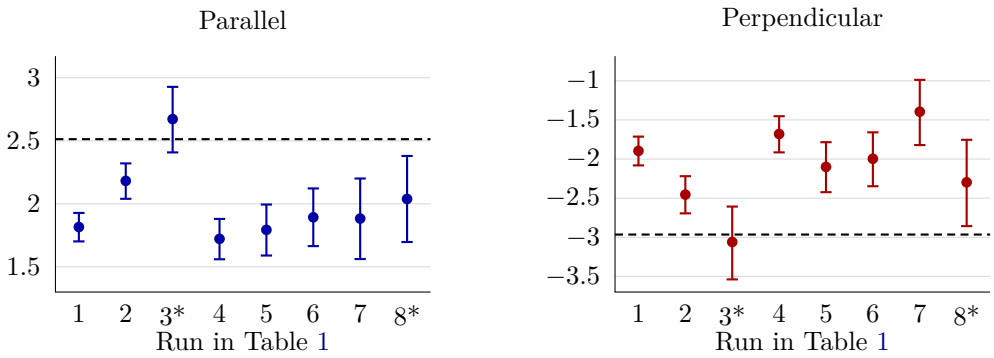


Figure 5: The signed ratios in Table 1. Error bars give the sampling intervals; dashed lines give (B.1). Runs 1–3 increase the outer radius at fixed mesh and obstacle size.

All sixteen run–arrangement estimates have the sign predicted by (B.1). The boundary comparison in runs 1–3 is particularly informative. At fixed $D = 24$ and $r = 2.75$, increasing

L/D from 4 to 8 to 16 changes the parallel estimate from 1.816 to 2.182 to 2.672, and the perpendicular estimate from -1.896 to -2.455 to -3.060. Both amplitudes continue to change substantially as the domain grows. These data show the predicted sign reversal, but not yet saturation at the plane predictions.

The smaller-obstacle and finer-mesh runs preserve the sign reversal, while their amplitudes at $L/D = 4$ show substantial finite-domain effects and a nonmonotone mesh dependence. Figure 5 displays these effects alongside the sampling intervals. These runs provide an independent finite-lattice comparison with the signed formula. A quantitative continuum extrapolation would require further control of the three scale ratios $1/r$, r/D, and D/L. The accompanying simulation archive contains the source code, all category counts, run parameters, random seeds, and analysis scripts.

Use of generative AI

The research programme was conceived by the author before generative AI was used in this project. ChatGPT 6 (OpenAI) was used extensively in proposing and developing proof strategies, mathematical arguments and calculations, and in drafting and revising the manuscript. The author takes responsibility for the content of the manuscript.

References

[1] F. Camia, *Conformal covariance of connection probabilities and fields in 2D critical percolation*, Comm. Pure Appl. Math. **77** (2024), 2138–2176. doi:10.1002/cpa.22171; arXiv:2203.08167.

[2] F. Camia and C. M. Newman, *Two-dimensional critical percolation: the full scaling limit*, Comm. Math. Phys. **268** (2006), 1–38. doi:10.1007/s00220-006-0086-1; arXiv:math/0605035.

[3] F. Camia and C. M. Newman, *Critical percolation exploration path and SLE(6): a proof of convergence*, Probab. Theory Related Fields **139** (2007), 473–519. arXiv:math/0604487v2.

[4] G. F. Lawler, O. Schramm and W. Werner, *One-arm exponent for critical 2D percolation*, Electron. J. Probab. **7** (2002), paper 2, 1–13. arXiv:math/0108211.

[5] S. Smirnov and W. Werner, *Critical exponents for two-dimensional percolation*, Math. Res. Lett. **8** (2001), 729–744. arXiv:math/0109120v2.

[6] O. Schramm and S. Smirnov, *On the scaling limits of planar percolation*, with an appendix by C. Garban, Ann. Probab. **39** (2011), 1768–1814. doi:10.1214/11-AOP659; arXiv:1101.5820v2.

[7] C. Garban, G. Pete and O. Schramm, *Pivotal, cluster, and interface measures for critical planar percolation*, J. Amer. Math. Soc. **26** (2013), 939–1024. arXiv:1008.1378v5.

[8] H. Du, Y. Gao, X. Li and Z. Zhuang, *Sharp asymptotics for arm probabilities in critical planar percolation*, Comm. Math. Phys. **405** (2024), Paper 182. arXiv:2205.15901.

[9] C. Garban, G. Pete and O. Schramm, *The scaling limits of near-critical and dynamical percolation*, J. Eur. Math. Soc. **20** (2018), 1195–1268. arXiv:1305.5526v4.

[10] M. Hillairet, *Short, Quantitative Construction of the IIC in Planar Percolation*, arXiv:2509.18852v3 (28 May 2026; first posted 23 September 2025).

[11] S. Sheffield and D. B. Wilson, *Schramm's proof of Watts' formula*, Ann. Probab. **39** (2011), 1844–1863. doi:10.1214/11-AOP652; arXiv:1003.3271v4.

[12] D. Zhan, *Two-curve Green's function for 2-SLE: the interior case*, Comm. Math. Phys. **375** (2020), 1–40. arXiv:1806.09663v2.

[13] D. Zhan, *Existence and uniqueness of nonsimple multiple SLE*, J. Stat. Phys. **191** (2024), article 101. arXiv:2308.13886v1.

[14] O. Schramm and D. B. Wilson, *SLE coordinate changes*, New York J. Math. **11** (2005), 659–669. arXiv:math/0505368v3.

[15] S. M. Flores, P. Kleban and R. M. Ziff, *Cluster pinch-point densities in polygons*, J. Phys. A: Math. Theor. **45** (2012), 505002. doi:10.1088/1751-8113/45/50/505002; arXiv:1201.6405v2.

[16] V. Olsiewski Healey and G. F. Lawler, *N-sided radial Schramm–Loewner evolution*, Probab. Theory Related Fields **181** (2021), 451–488. arXiv:2002.04128v2.

[17] E. Cépa and D. Lépingle, *No multiple collisions for mutually repelling Brownian particles*, Séminaire de Probabilités XL (2007), 241–246. arXiv:math/0511445.

[18] A. A. Belavin, A. M. Polyakov and A. B. Zamolodchikov, *Infinite conformal symmetry in two-dimensional quantum field theory*, Nucl. Phys. B **241** (1984), 333–380. doi:10.1016/0550-3213(84)90052-X.

[19] B. Doyon, V. Riva and J. Cardy, *Identification of the stress-energy tensor through conformal restriction in SLE and related processes*, Comm. Math. Phys. **268** (2006), 687–716. arXiv:math-ph/0511054v2.

[20] M. Picco, S. Ribault and R. Santachiara, *A conformal bootstrap approach to critical percolation in two dimensions*, SciPost Phys. **1** (2016), 009. arXiv:1607.07224v2.

[21] J. L. Jacobsen and H. Saleur, *Bootstrap approach to geometrical four-point functions in the two-dimensional critical Q-state Potts model: a study of the s-channel spectra*, arXiv:1809.02191v2 (2018).

[22] Y. He, J. L. Jacobsen and H. Saleur, *Geometrical four-point functions in the two-dimensional critical Q-state Potts model: the interchiral conformal bootstrap*, J. High Energy Phys. **12** (2020), 019. doi:10.1007/JHEP12(2020)019; arXiv:2005.07258.

[23] Y. He, *Logarithmic operators in $c = 0$ bulk CFTs*, SciPost Phys. **19** (2025), 008. arXiv:2411.18696v2.

[24] S. Dyatlov, *Lecture notes for 18.155: Distributions, elliptic regularity, and applications to PDEs*, MIT, version of 2 November 2026. `https://math.mit.edu/~dyatlov/18.155/155-notes.pdf`.

[25] NIST Digital Library of Mathematical Functions, Chapters 5 (*Gamma Function*) and 15 (*Hypergeometric Function*). `https://dlmf.nist.gov/`.

[26] F. Camia and Y. Feng, *Conformally covariant probabilities, operator product expansions, and logarithmic correlations in two-dimensional critical percolation*, arXiv:2407.04246v2 (26 August 2025; first posted 5 July 2024).

[27] F. Camia and Y. Feng, *The percolation energy field and its logarithmic partner*, arXiv:2508.16047v2 (1 June 2026).

[28] J. Dubédat, *SLE and Virasoro representations: Fusion*, Comm. Math. Phys. **336** (2015), 761–809. doi:10.1007/s00220-014-2283-7; arXiv:1401.1167v3.

[29] A. Gandolfi, *Towards a conformal field theory of critical percolation. I. The bulk stress tensor and Ward identities*, companion manuscript, revision of 15 November 2026.

[30] A. Karrila, *Multiple SLE type scaling limits: from local to global*, arXiv:1903.10354v1 (25 March 2019).

[31] A. Kupiainen, R. Rhodes and V. Vargas, *Local conformal structure of Liouville quantum gravity*, Comm. Math. Phys. **371** (2019), no. 3, 1005–1069. doi:10.1007/s00220-018-3260-3; arXiv:1512.01802v3.

[32] G. Baverez and B. Wu, *Irreducible Virasoro representations in Liouville conformal field theory*, Ann. Probab. **54** (2026), no. 3, 1608–1640. doi:10.1214/25-AOP1799; arXiv:2312.07344v2.

[33] C. Guillarmou, A. Kupiainen, R. Rhodes and V. Vargas, *Conformal bootstrap in Liouville theory*, Acta Math. **233** (2024), no. 1, 33–194. doi:10.4310/ACTA.2024.v233.n1.a2; arXiv:2005.11530.